UCID-20153

Helium-Cooled Molten-Salt Fusion Breeder

R. W. Moir, J. D. Lee, F. J. Fulton, F. Huegel,
W. S. Neef, Jr., A. E. Sherwood, D. H. Berwald,
R. H. Whitley, C. P. C. Wong, J. H. Devan,
W. R. Grimes, and S. K. Ghose

December 1984

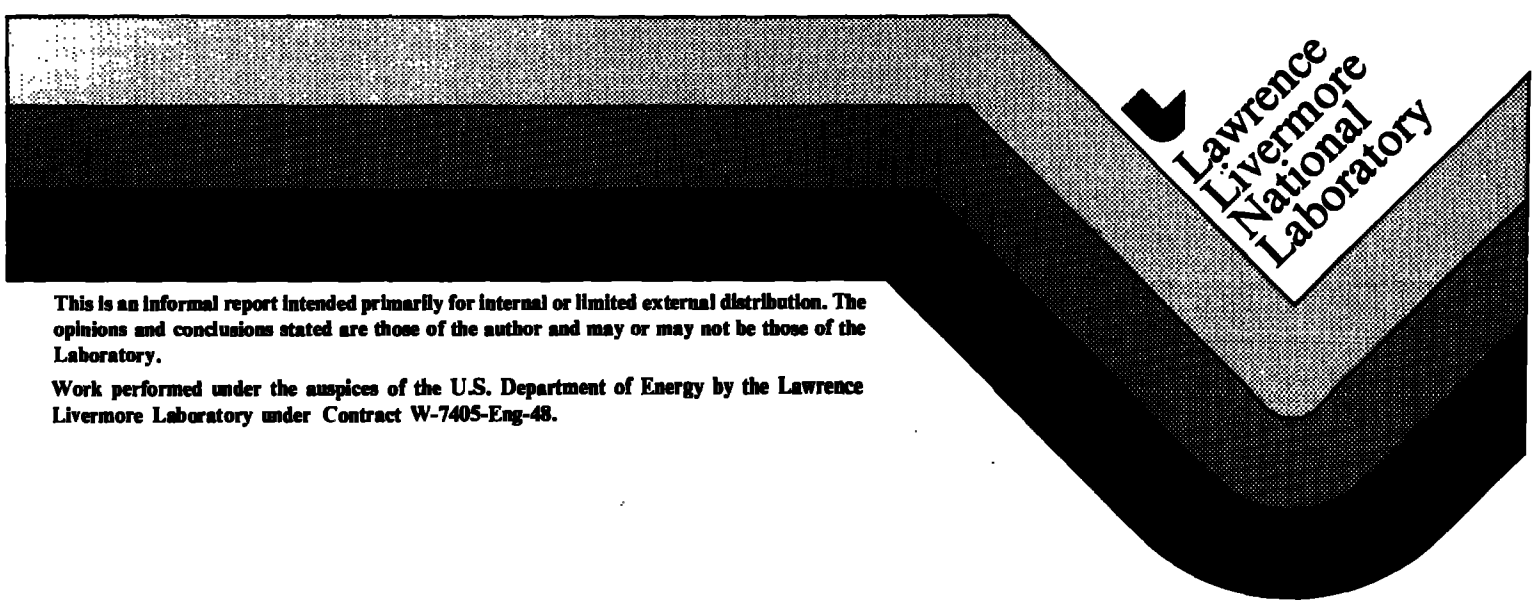

Work performed under the auspices of the U.S. Department of Energy by the Lawrence Livermore Laboratory under Contract W-7405-Eng-48.

DISCLAIMER

Printed in the United States of America
Available from
National Technical Information Service
U.S. Department of Commerce
5285 Port Royal Road
Springfield, VA 22161
Price: Printed Copy $; Microfiche $4.50

Page Range	Domestic Price	Page Range	Domestic Price
001-025	$ 7.00	326-350	$ 26.50
026-050	8.50	351-375	28.00
051-075	10.00	376-400	29.50
076-100	11.50	401-426	31.00
101-125	13.00	427-450	32.50
126-150	14.50	451-475	34.00
151-175	16.00	476-500	35.50
176-200	17.50	501-525	37.00
201-225	19.00	526-550	38.50
226-250	20.50	551-575	40.00
251-275	22.00	576-600	41.50
276-300	23.50	601-up[1]	
301-325	25.00		

[1]Add 1.50 for each additional 25 page increment, or portion thereof from 601 pages up.

HELIUM-COOLED MOLTEN-SALT FUSION BREEDER

R. W. MOIR, J. D. LEE, F. J. FULTON, F. HUEGEL,
W. S. NEEF, Jr., A. E. SHERWOOD
University of California, Lawrence Livermore National Laboratory
Livermore, CA 94550

D. H. BERWALD, R. H. WHITLEY
TRW Energy Development Group
Redondo Beach, CA 90278

C. P. C. WONG
GA Technologies, Inc.
San Diego, CA 92138

J. H. DEVAN, W. R. GRIMES
Oak Ridge National Laboratory
Oak Ridge, TN 37830

S. K. GHOSE
Bechtel Group, Inc.
San Francisco, CA 94119

December 1984

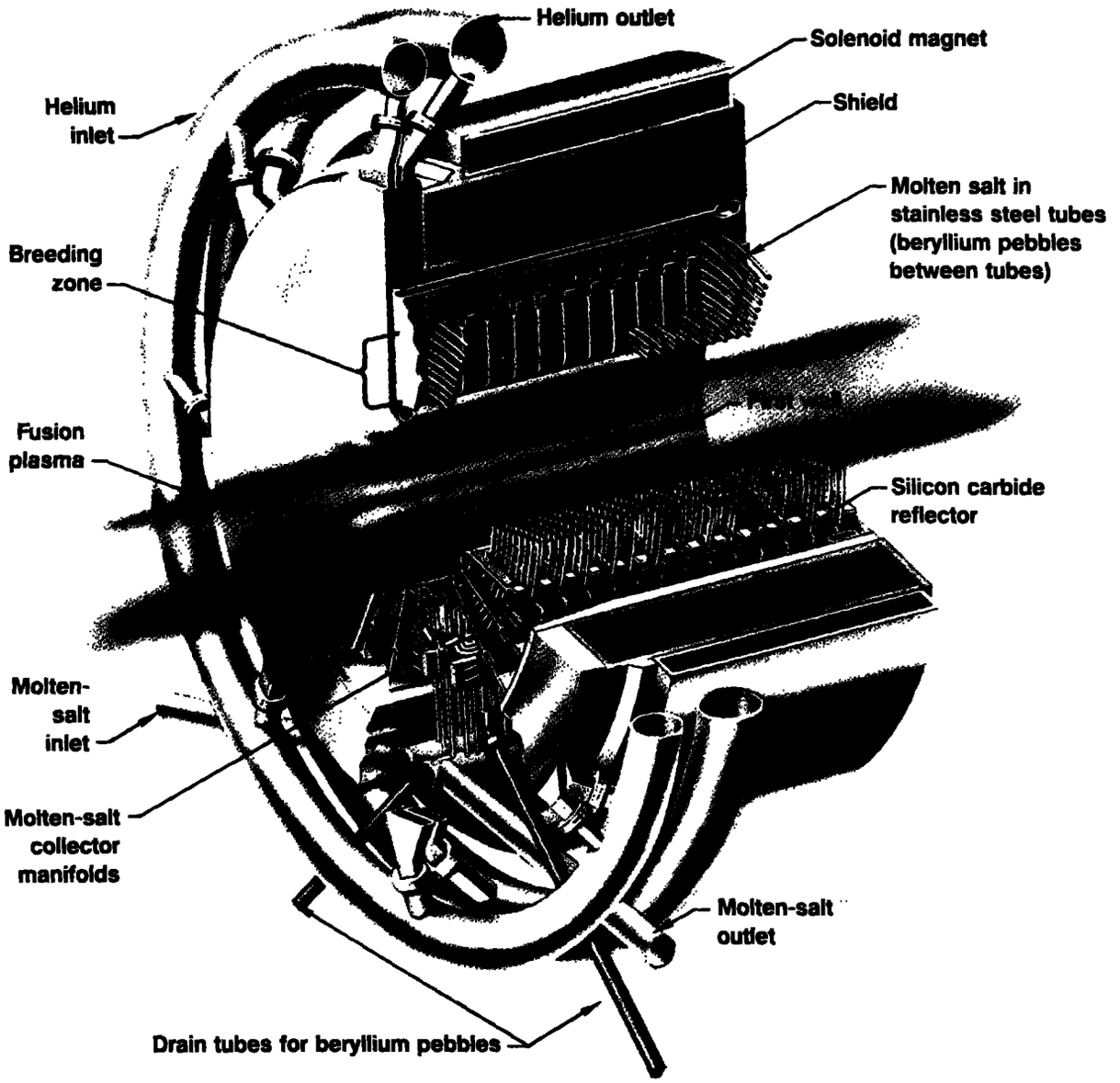

A helium-cooled molten-salt blanket.

HELIUM-COOLED MOLTEN-SALT FUSION BREEDER

CONTENTS

LIST OF FIGURES

LIST OF TABLES

HELIUM-COOLED MOLTEN-SALT FUSION BREEDER

ABSTRACT

We present a new conceptual design for a fusion reactor blanket that is intended to produce fissile material for fission power plants. Fast fission is suppressed by using beryllium instead of uranium to multiply neutrons. Thermal fission is suppressed by minimizing the fissile inventory. The molten-salt breeding medium ($LiF + BeF_2 + ThF_4$) is circulated through the blanket and to the on-line processing system where ^{233}U and tritium are continuously removed. Helium cools the blanket and the austenitic steel tubes that contain the molten salt. Austenitic steel was chosen because of its ease of fabrication, adequate radiation-damage lifetime, and low corrosion by molten salt. We estimate that a breeder having 3000 MW of fusion power will produce 6400 kg of ^{233}U per year. This amount is enough to provide makeup for 20 GWe of light-water reactors per year or twice that many high-temperature gas-cooled reactors or Canadian heavy-water reactors. Safety is enhanced because the afterheat is low and blanket materials do not react with air or water. The fusion breeder based on a pre-MARS tandem mirror is estimated to cost $4.9B or 2.35 times a light-water reactor of the same power.The estimated cost of the ^{233}U produced is $40/g for fusion plants costing 2.35 times that of a light-water reactor if utility owned or $16/g if government owned.

HELIUM-COOLED MOLTEN-SALT FUSION BREEDER

EXECUTIVE SUMMARY

In this report we describe a fusion breeder design that is based on molten-salt technology. This design evolved from earlier concepts[1-3] with design changes being incorporated to avoid prior problems. For example, steel was substituted for molybdenum and graphite coatings were eliminated. The beryllium, rather than being in large, 5-cm-diam cylindrical rods, 500 cm long, is now to be in small 1-cm-diam radiation-damage-resistant spheres. This report was summarized recently in a paper presented to the American Nuclear Society.[4] The fusion neutron source for this design is the tandem mirror, but other fusion concepts such as the tokamak could equally well have been employed. The particular tandem mirror design is based on a pre-MARS design[5]. The plant parameters are given in Table I. The technologies used are listed in Table II.

BLANKET DESIGN

The blanket concept uses high-pressure helium as the coolant and beryllium spheres as the neutron multiplier. All the fertile material for breeding both tritium and fissile fuel is in the form of molten fluoride salts of lithium and thorium that flow slowly through an array of tubes (see Figs. 1 and 2).

The molten-fluoride salt, whose composition is given in Table II, is stable to both thermal and radiation decomposition because of the rapidity of recombination. Corrosion rates of iron-based alloys are low when the salt is maintained in a reducing state. A similar salt, with somewhat differing mole fractions, was used at Oak Ridge National Laboratory in a molten-salt reactor that operated successfully for several years. The uranium produced by neutron transmutation of ThF_4 is in the form of UF_4. Upon reacting with excess fluorine in an external tank, the UF_4 is converted to UF_6, which is volatile and easily separated. This process is called fluorination. UF_6 is a standard form of uranium used in the industry.

To acquire a high enough heat capacity to cool the blanket efficiently, helium must be at a pressure of about 5 MPa (50 atmos.) Helium neither absorbs neutrons nor promotes self-welding reactions that might interfere with the free flow of the beryllium spheres as they are removed for remanufacturing

Table I. Plant parameters for the described fusion-breeder design.

$P_{nuclear}$	4440 MW
P_{fusion}	3000 MW
$P_{alpha\ particle}$	600 MW
$P_{blanket}$	3840 MW
$P_{electric}$	1380 MW_e
$P_{wall\ load}$	2 MW/m^2
Length of blanket	127 m
First wall radius	1.5 m
F_{net}	0.6[a]
M	1.6[a]
Fissile production	6380 kg ^{233}U/year at 80% capacity factor
Total cost	$4867M

[a] F_{net} is fissile atoms bred/triton consumed; M is the energy released in the blanket per triton consumed divided by 14 MeV.

Table II. Technologies employed in the fusion-breeder design.

Cooling	Helium
Structural material	316 type stainless steel
Neutron multiplier	Beryllium pebbles
Tritium and fissile breeder	Molten salt: LiF 70 mol% + BeF_2 12 mol% + ThF_4 18 mol%.
Neutron reflector	SiC

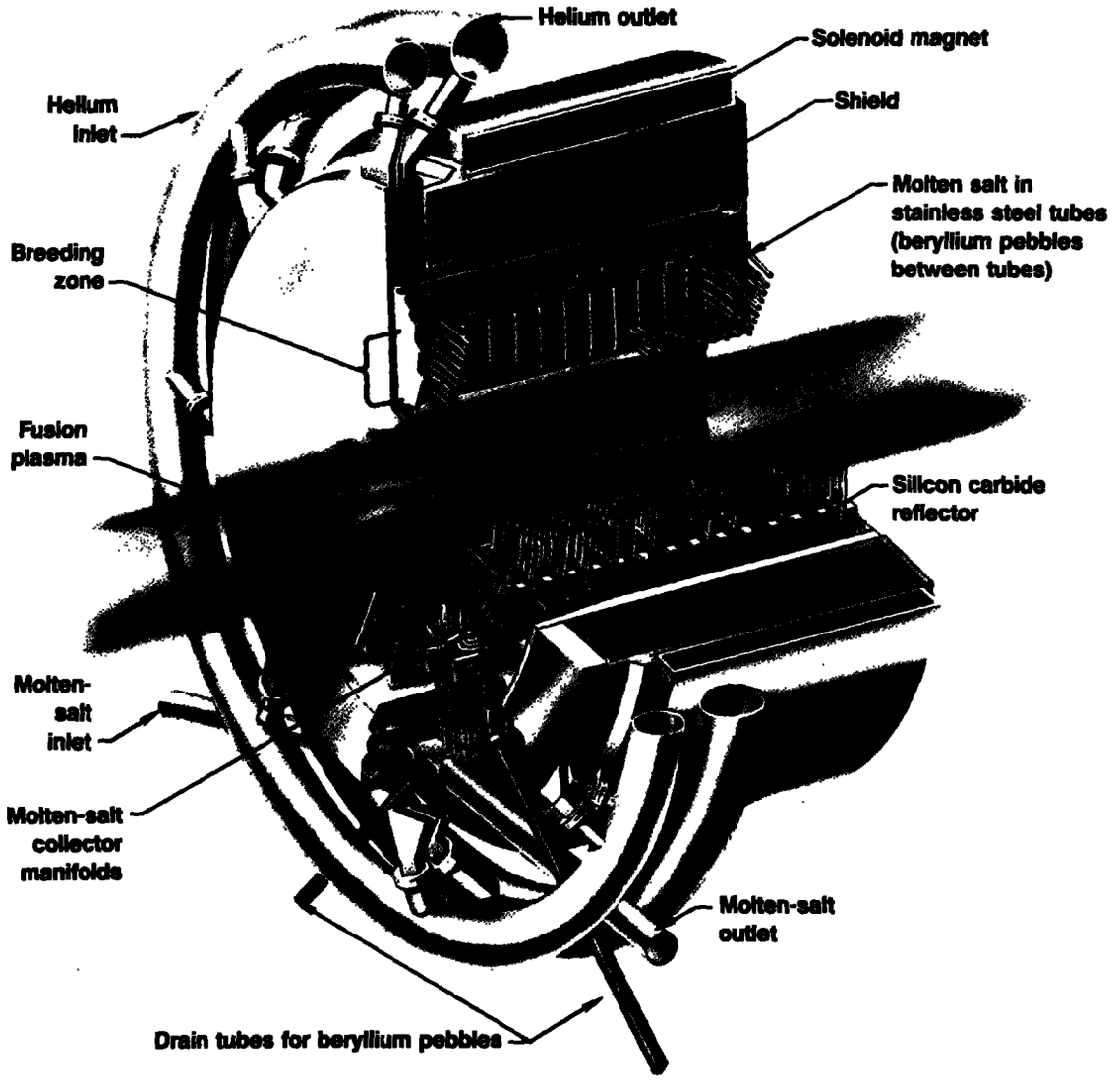

Figure 1. One module of a helium-cooled molten-salt blanket. Helium under 5-MPa pressure flows from the inlet ring header to the apex of each pod, then radially outward through the blanket to the outlet ring header, and thence to heat exchangers for generating electricity. The revenue from the sale of the electricity can be used to reduce the cost of the fissile material produced. Being a nonconductor, helium can flow unimpeded through the strong magnetic field generated in a magnetic fusion reactor.

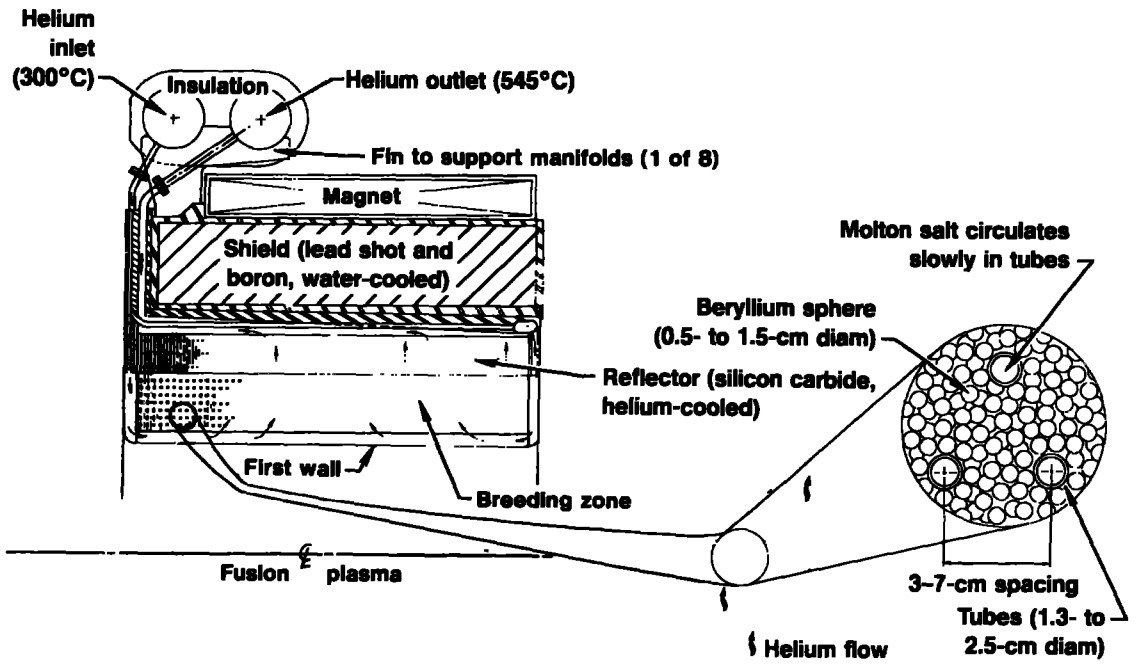

Figure 2. Cross section along the axis of one segment of a helium-cooled molten-salt blanket, showing details of the arrangement of the helium flow and the arrangement of beryllium spheres and tubing for the molten salts.

and are recycled back to the reactor. Some parameters describing the blanket and the beryllium pebbles are given in Table III.

Table III. Beryllium requirements for the molten-salt blanket.

Total blanket volume[a]	860 m^3
Pebble volume[b]	470 m^3
Pebble quantity[c]	890 x 10^6
Pebble mass	0.96 g
Beryllium mass[d]	860 tonne
Average beryllium lifetime	5 yrs.
Annual pebble throughput	180 x 10^6/yr
Annual beryllium mass throughput	170 tonne/yr

[a] 127-m central cell, 3000 MW fusion power, 0.6-m-thick blanket starting at 1.5-m radius, and a 2 MW/m^2 wall load.

[b] 10% of blanket volume is tubes; 60% packing in remainder of blanket.

[c] 1-cm-diameter pebbles.

[d] 1.84 g/cm^3 beryllium density.

Each neutron multiplication reaction in beryllium yields two neutrons and two alpha particles (helium nuclei). Most of these helium atoms remain trapped in the beryllium lattice, taking up space but not contributing to the bonding that holds the lattice together. The resulting stress that causes the beryllium spheres to expand would eventually break them apart if it were allowed to continue.

Because any break-up of the beryllium spheres would yield smaller particles that could plug the channels through which the helium flows and thus produce hot spots in the blanket, it is important to remove the beryllium spheres periodically before this can happen. We have verified experimentally that the spheres will flow freely, without bridging or blocking, if they are no larger than half the space between the tubes. To avoid any possible obstruction because of swelling of the beryllium, we made the spheres 1 cm in diameter (one-third the distance between the tubes). Figure 3 depicts the arrangements for adding and removing beryllium spheres.

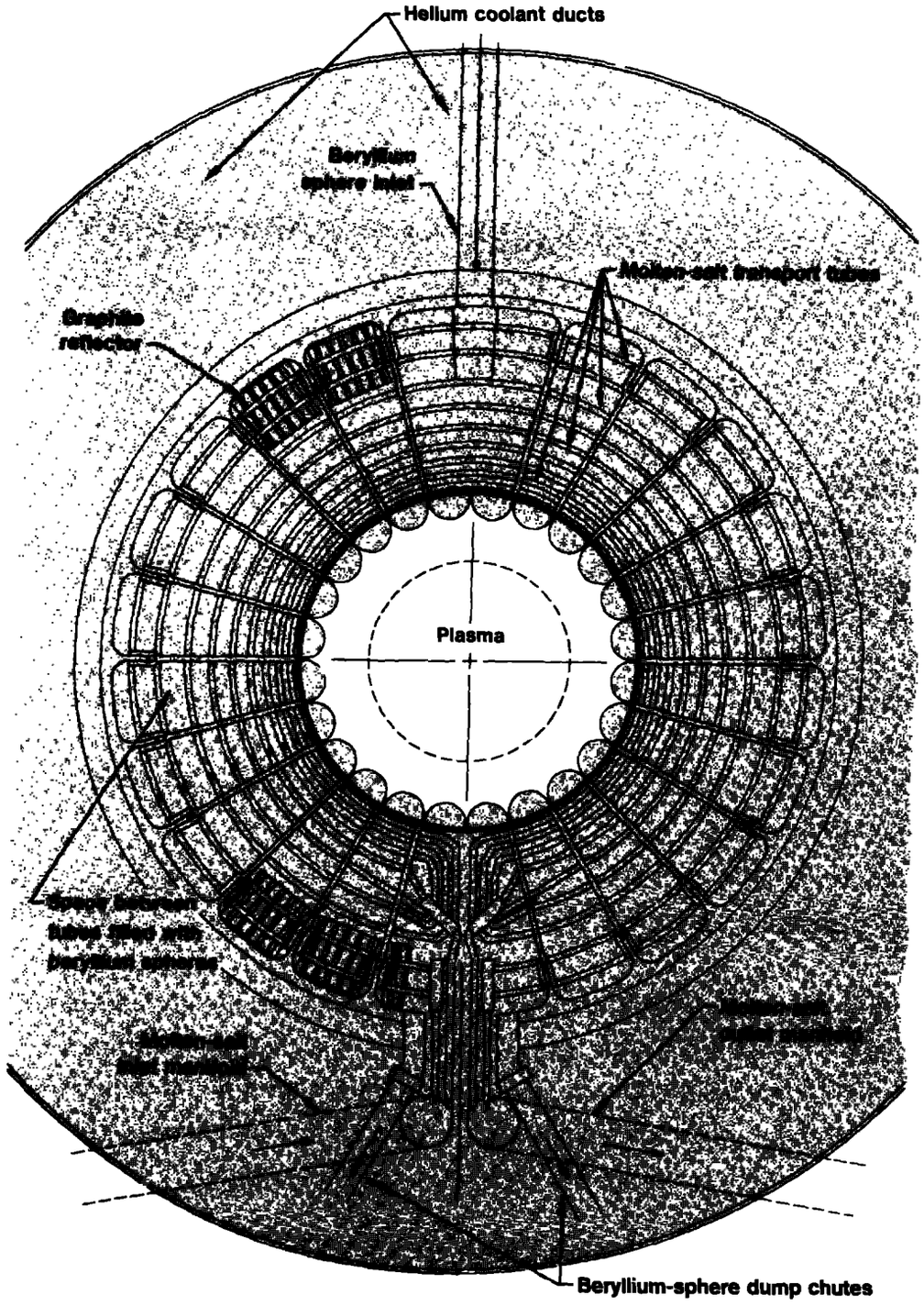

Figure 3. Cross section of the molten-salt breeding blanket. Neutron multiplication takes place in a bed of beryllium spheres. Breeding of tritium and uranium-233 takes place in the molten fluoride salts of lithium and thorium that are circulating in an array of steel tubes embedded in the beryllium spheres. The continuous flow permits continuous extraction of uranium-233 and tritium to minimize wasteful fission reactions.

Because the fertile material is constantly circulating, it is possible in this design to use a continuous processing system to recover bred tritium and uranium-233 from the molten salts. We selected fluorination, which removes uranium-233 but leaves protoactinium and many of the fission products.[6] More complex processes that do remove fission products, such as reductive extraction and metal-transfer treatments, turn out to be unnecessary.[7] Continuous processing allows the amount of uranium-233 to be kept low to minimize unwanted fission reactions.

In addition to its many advantages, this blanket design has a few disadvantages. One is that the flat side walls of each module are not made stiff enough to support the internal pressure of 5 MPa. Instead, they are made thin, each one being supported by the adjacent wall pressing in from the other side. This means that all the modules are interdependent; none can be removed for service without depressurizing the entire system. Another consequence of this enormous pressure that forces adjacent module walls together is the possibility that they may self-weld after a time. If this happened, it would be impossible to remove one module without causing damage to the other. To prevent this, it may be necessary to insert thin ceramic spacers of alumina, for example, to keep the walls apart.

NUCLEONICS

Breeding performance is predicted with the aid of Monte Carlo transport codes (see Table IV). The modeling of the blanket takes into account the heterogeneous nature of the blanket, the effect of structural material and resonant self-shielding. The uncertainty, because of the combined effects of modeling nuclear data and methods, is guessed to be as high as $\pm$25% for F_{net}. Breeding is sensitive to the amount of structural material, mostly Fe, Cr, and Ni. By increasing the steel structural fraction in the blanket from 3% to 5%, the net breeding goes from 0.65 to 0.61. Because of the low atom fraction of thorium and ^{6}Li in the blanket, parasitic neutron capture in structural material mandates low structural fraction blanket designs. Recent and ongoing work on the nuclear data on beryllium suggest that the old data resulted in an overestimate of net breeding. An experiment underway at the Idaho National Engineering Laboratory using the manganese bath method to measure neutron multiplication and an experiment recently completed at LLNL, should reduce this uncertainty substantially.

Table IV. Calculated breeding performance.

T	1.0[a]
F_{net}	0.6[a]
E (MeV)	22.4
M (E/14)	1.6

[a]Atoms bred per triton consumed.

THERMAL HYDRAULICS.

The amount of heat generated in the salt, in the tube walls, and in the beryllium is calculated by neutron and gamma-ray transport codes at several radial locations. Heat-transfer coefficients are estimated for tubes with roughened surfaces in a pebble bed, based on separate data from close-packed tubes (cross flow) and from pebble beds ($h = 0.2$ W/cm^2°C). Then the temperature of the salt-steel interface of the tubes is calculated (see Fig. 4). The inlet helium temperature is 300°C and the outlet is 545°C. The calculated maximum steel temperature is only slightly over 550°C. The concern over temperature variations around each tube and thus hot spots is largely alleviated by the averaging effect of the flowing salt. The salt is force-circulated at about 0.1 ms^{-1} and internally convects at a similar speed because of gravity and a density gradient caused by the temperature gradient in the salt. We have considered the pros and cons of having a frozen salt layer on the inside of the tube (i.e., tube temperature kept below the salt freezing point) and generally favor the no-frozen layer case. We recommend heat-transfer measurements be carried out in a pebble bed with pipes and helium crossflow to reduce the uncertainty in predicting temperatures at various places.

A start-up scenario was devised for situations where the inlet helium temperature (300°C) is substantially below the melting temperature of the salt (530°C). Before the fusion reactions are turned on, the helium is circulated through the blanket after going through a preheater, thus raising the entire blanket to the 545°C inlet temperature, which is identical to the operating outlet temperature. Preheated molten salt is then introduced into the

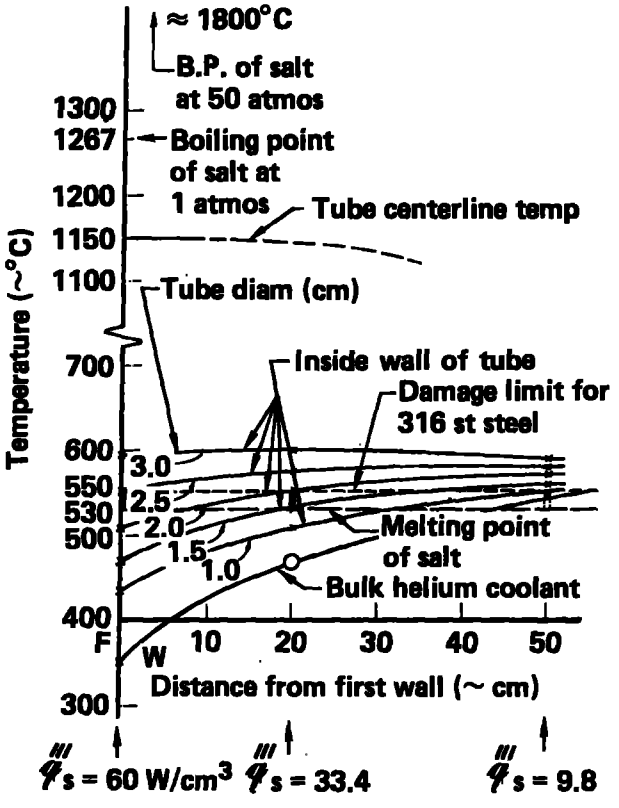

Figure 4. Helium coolant and temperature of salt tube as a function of position in blanket (Γ = 2.0 MW/m^2 at first wall.

blanket. As the fusion reaction rate is brought up, the helium circulation rate is adjusted and the preheater turned down. Figure 5 shows the start-up conditions. Shutdown is accomplished by draining the salt and reducing the helium circulation rate. Freeze-up is easily prevented by the salt's heat capacity and residual nuclear decay heat. The salt drain tanks are cooled by heat pipes; thus, the emergency cooling is accomplished entirely by passive means.

MATERIALS SELECTION AND PROPERTIES

From a neutronics point of view, we would like to maximize the ThF_4 concentration; however, higher ThF_4 concentrations raises the melting temperature. The molten-salt reactor experimental work used 12% molar ThF_4. We considered using 27% ThF_4; however, the present design uses an intermediate composition of 18% which gives a melting point of 530°C. Some properties of the salt are given in Table V.

We chose austenitic steel for this design. The maximum operating temperature is 550°C, arbitrarily chosen to avoid excess helium embrittlement. The lifetime is 100 dpa (about 8 MW•yr/m^2 or 5.7 yr at 2 MW/m^2 and 70% availability), after which time runaway swelling is predicted. There is no minimum temperature, as there is no ductile-brittle transition above room temperature. Also, no special heat treatment of welds is necessary.

Corrosion of steel is governed by reaction of the chromium of the steel with the salt and is limited by the oxidation potential of the salt and the solid state diffusion of chromium in the steel. Experiments show that for 316 type steel and a UF_4:UF_3 ratio of 10 in the salt which is a reducing state, the corrosion will only be 2 μm/yr. Steel with less chromium will corrode at a slower rate.

On the basis both of acceptable mechanical properties following high-fluence neutron exposures and of acceptable corrosion resistance, we expect the use of 316 steel in contact with uranium-fluoride salts under controlled oxidation conditions to be feasible.

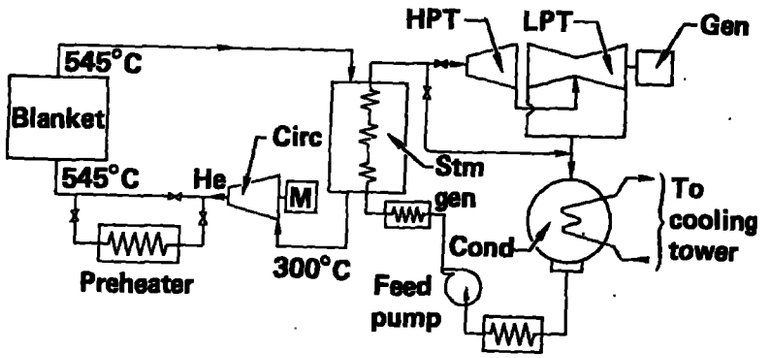

Figure 5. Start-up scenario.

Table V. Composition and properties of blanket salt.

Composition (mole %):			
LiF	72	70	71
BeF_2	16	12	2
ThF_4	12	18	27
Liquidus (°C)	500	530	565
Properties at 600°C:			
Density (g/cm^3)	3.35	3.87	4.52
Liq. heat capacity (cal/g°C)	0.33		0.23
Viscosity (centipoise)	12		15-25
Vapor pressure (torr)	<0.1		--
Thermal conductivity (W/°C cm)	0.011		0.007
Heat of fusion (cal/g)	63		54
Elec. conductivity (Ω-cm)	2.12		--
Expansion on melting (vol%)			∿5

TRITIUM PERMEATION AND RECOVERY

A study of tritium permeation and recovery from molten salt for the fusion breeder is reported in Ref. 8. This study assumes tritium to be a gas dissolved in molten salt, with TF formation suppressed. Tritium permeates readily through the hot steel tubes of the reactor and steam generator and will leak into the steam system at the rate of about 1 g/day in the absence of special permeation barriers, assuming that 1% of the helium coolant flow rate is processed for tritium recovery at 90% efficiency per pass. Tritiated water in the steam system is a personnel hazard at concentration levels well below 1 ppm and this level would soon be reached without costly isotopic processing. Alternatively, including a combination of permeation barriers on reactor and steam generator tubes and molten salt, we estimate that processing will reduce the leak rate into the steam system by over two orders of magnitude. For the option with the lowest estimated leak rate, 55 Ci/d, it may be possible to purge the steam system continuously to prevent tritiated water buildup. At best, isotopic separation of dilute tritiated water may not be necessary and for higher leak-rate options the isotopic processing rate can be reduced.

The proposed permeation barrier for the reactor tubes is a 10-μm layer of tungsten which, in principle, will reduce tritium permeation by a factor of about 300 below the bare-steel rate. The 10-μm tungsten barrier on the inside of the tubes is made by chemical vapor deposition (CVD). The reaction $WF_6 + 3H_2 \rightarrow W + 6HF$ proceeds when the temperature is raised to the range of 400 to 600° C. The amount of material is so small (65,000 lbs) that the material cost ($4M) is not important. Stainless steel will require a coating such as nickel to obtain a good bond. The techniques will require further development; however, there is quite a lot of industrial practice in CVD upon which to base this development. A relatively thick 1-mm aluminum sleeve was selected to suppress permeation through the steam generator tubes. This gave a calculated reduction of more than a factor of 500 relative to bare steel, including a factor of 30 because of an assumed oxide layer. This is essentially a brute-force approach that may well be improved upon by the development of more sophisticated permeation barriers.

To gain a better understanding of permeation effects, we derived equations describing steady-state tritium permeation for a multilayer tube wall within the blanket region. A layer of frozen salt is included, along

with fluid boundary-layer resistances. Calculations of the partial-pressure distribution show significant differences for tubes irradiated at different power densities. Molten-salt boundary-layer resistance can be important in the absence of a good permeation barrier or for a low-power tube coated with a nominal 1-μm tungsten barrier. Permeabilities of various metals are shown in Fig. 6. This nominal permeation barrier will dominate the flow resistance, however, for medium or high power density tubes closer to the first wall. Examination of the radial flux equation shows a complicated dependence on upstream partial pressure, which reduces to a linear dependence at low pressures where Henry's Law materials become flux limiters and a square-root dependence at high tritium partial pressures where Sievert's Law materials are flux limiting.

An analytical model was developed to establish the tritium split between wall permeation and reactor-tube flow. Permeation barriers are shown in Fig. 7. The barriers are shown on the outside of the tubes but could equally well be on the inside. For the molten-salt tubes, the inside barrier would greatly reduce the tritium inventory in the tube walls and further reduce the already low corrosion rate. The tritium fraction escaping through the tube walls was quantified for limiting cases of Henry's Law and Sievert's Law barriers as flux limiters. All parameters of design interest are explicitly included: tritium generation rates and solubility in salt, tube geometry, barrier permeation parameters, and molten-salt processing rate and recovery efficiency.

The tritium-recovery system flow sheet is shown in Fig. 8. Because of the low solubility of tritium in the reducing salt, a simple flash separator will allow removal of the tritium and other noncondensible gases, mainly helium. Tritium removal from helium is virtually a standard system. The bulk of the tritium is recovered as a hydride on a getter bed, with final cleanup accomplished by catalyzed oxidation and adsorption. The molten-salt system pressure (49 atm) is kept just below the helium pressure (50 atm). The flash separator will operate at below 1 atmosphere pressure. The molten-salt pump must raise the pressure back up to 49 atm. The pumping system needs more design work.

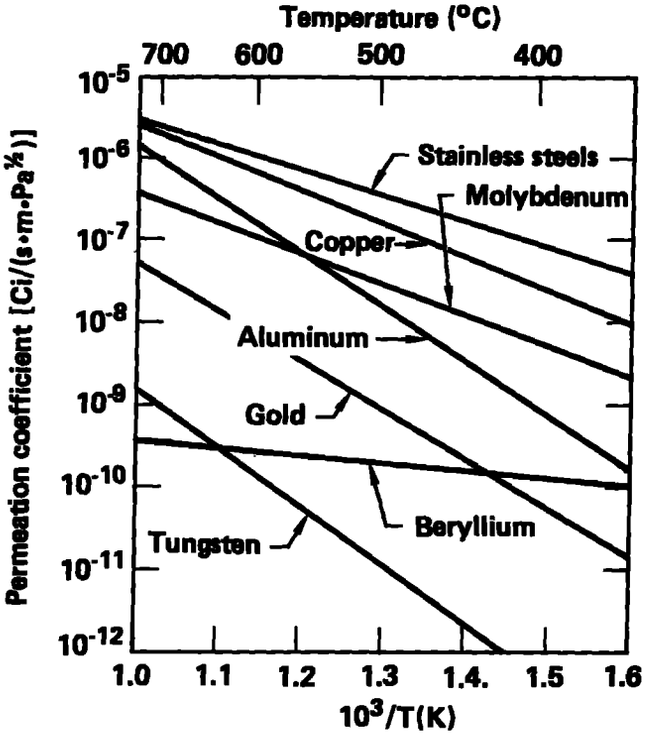

Figure 6. Permeability of various metals to tritium.

Reactor tube

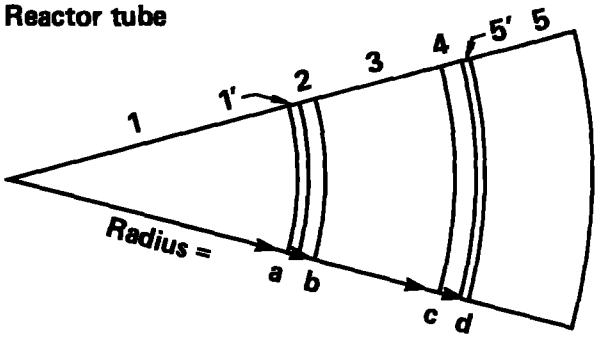

1 Molten salt
1' Molten salt boundary layer
2 Frozen salt
3 Stainless steel tube
4 Permeation barrier (tungsten)
5' Helium gas boundary layer
5 Helium gas

Steam generator tube

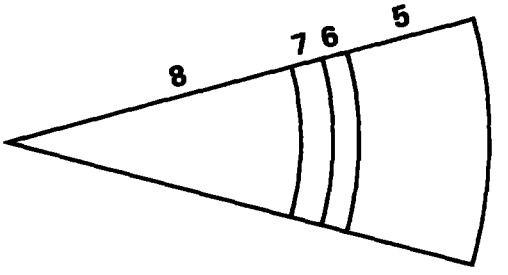

5 Helium gas
6 Permeation barrier (aluminum)
7 Stainless steel tube
8 Water/steam

Figure 7. Permeation geometry and materials.

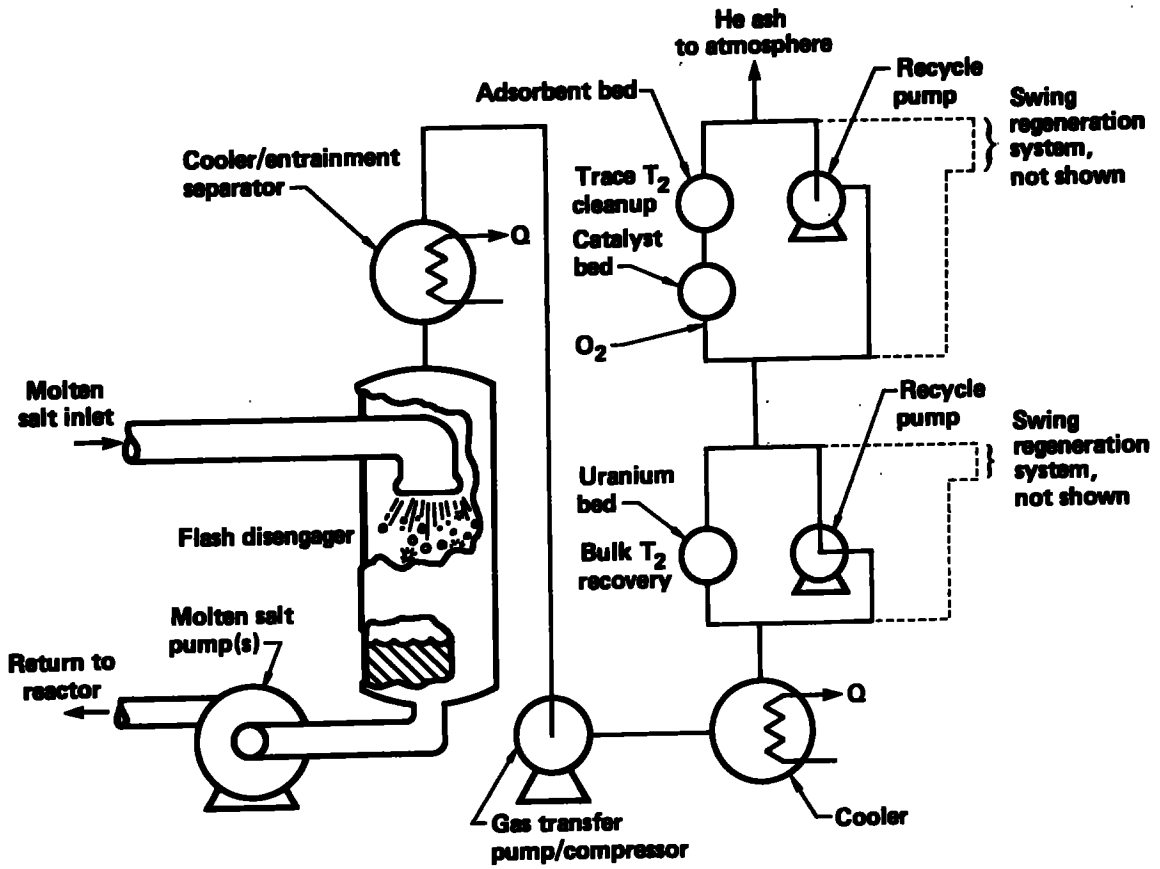

Figure 8. Tritium-recovery system flow sheet.

Finally, some definitive experimental work on the kinetics of tritium-gas conversion to tritiated water at low concentrations in helium is called for. Popular opinion has oscillated over the last decade from an initial optimism that thermodynamics would reduce the gas concentration to nil, to a current pessimism that predicts no gas conversion at all in the main helium loop. The critical experiments remain to be done, both with "clean" walls and particulate-free helium and in the presence of catalytic surfaces or other reaction promoters. The challenge is to demonstrate a method of drastically reducing tritium-gas partial pressure in the intermediate helium loop, and thus suppress permeation into the steam system.

The intermediate helium heat transfer loop has been treated as a well-mixed tank for analytical purposes, with tritium input from the molten salt tubes, with partial tritium recovery in a slipstream process loop, and with Sievert's Law tritium-permeation loss to the steam system.

A combination of effective tritium permeation barriers is required on both blanket and steam-generator tubes. Together with substantial process rates for molten salt and helium systems, the barriers hold tritium permeation into the steam system to 55 Ci/d. If this can be done, it may be feasible to simply purge the steam system of incoming tritium with only minor environmental impact and personnel hazard from steam leaks and without the costly and hazardous isotopic processing to separate tritiated and ordinary water.

Although we have focused attention on a tungsten barrier because of its remarkably low tritium permeability, we should also consider beryllium and other low-permeability materials such as ceramics and cermets in barrier development. Other materials or alloys may prove to be superior to tungsten, but probably at the price of greater thickness of coating.

The diffusivity of tritium gas dissolved in molten salt will need to be measured, especially to verify whether or not the fluid boundary-layer barrier is realistic.

BERYLLIUM-PEBBLE FABRICATION

Each beryllium pebble is a solid sphere of 1 cm nominal diameter and weighing 0.96 g. A nominal mass of 900 tonnes requires about 900 million pebbles for the initial inventory. See Table III for summary of beryllium

parameters. For an assumed average pebble lifetime of two calendar years, the annual throughput of the hot beryllium fabrication plant will be 180 x 10^6 pebbles/yr or 180 tonnes/yr. However, with efficient recycle, the actual beryllium requirement associated with beryllium pebble remanufacture might be 1 to 10%, or 2 to 20 tonne/yr.

The selected pebble fabrication process involves the development of an automated line that will cold press pebbles, vacuum sinter them, hot forge them to full density, and vacuum anneal them. To automate this process, a free flowing beryllium powder is required.

Equipment for production of spherical beryllium is simple: mechanical presses and powder feeders to make cold pressed compacts, automated vacuum sintering furnaces for pressureless sintering, mechanical presses for hot sizing the sintered compacts, and an automated vacuum furnace for annealing the forged compact.[9]

For fabrication of pebbles too damaged to reinsert into the blanket after an irradiation period, we would vacuum melt the hot pebbles and use an automated atomization process (modeled after the Brush Wellman process) to first remanufacture the beryllium powder prior to the cold-press step. We do not exclude the possibility of removing the helium gas by vacuum heating, which would result in about 30% volumetric swelling. These enlarged pebbles might then be pressed back into size possibly by pressure-less sintering. The entire process will require provision for shielding and remote maintenance. In addition, hooding requirements as per OSHA limits ($2\mu g/m^3$) must be maintained to limit airborne contamination.

Given a conservative two-year beryllium lifetime,[2,8] assuming an automated plant that operates 24 hr/da, 7 da/wk, and operates 85% of the time with no rejects, the production rate must be 110 balls per minute. While this is a high production rate for beryllium parts, it is low for some powder metal industries (e.g., tantalum capacitor manufacturers produce thousands of parts/minute). The beryllium reprocessing line is estimated to lose 7 to 10% of the beryllium throughput, so a small feedstream is required. With a free-flowing powder, the losses might be reduced below 1%.

Preliminary cost estimates for the beryllium fabrication-process required to provide beryllium pebbles for the reference tandem mirror fusion breeder[9] were developed during 1982. These cost estimates were adapted to the present case and an annual cost estimate for various assumption was made (see Fig. 9).

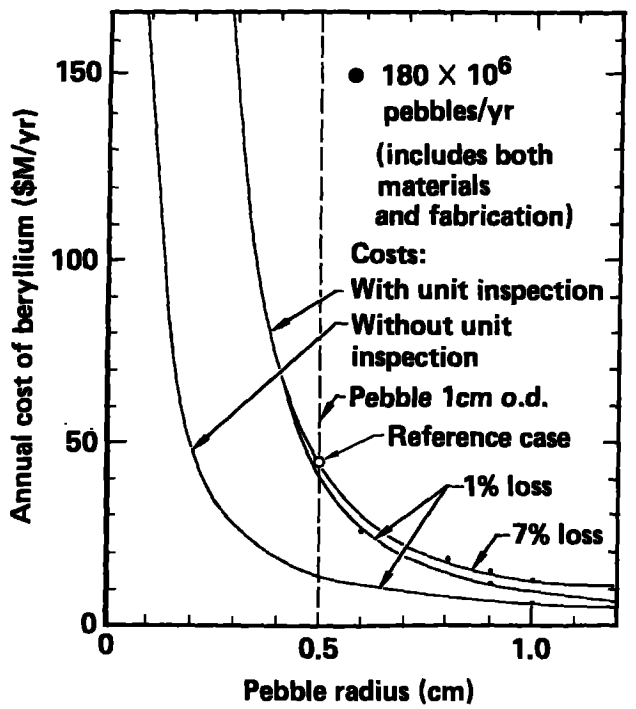

Figure 9. Cost of beryllium pebbles.

The only special equipment needed for the process line is the air handling system for containing the beryllium powder. The die life should be comparable to other powder metallurgy products (500,000 to 1,000,000 parts/die with punches redressed every ∿500,000 parts). Production of a free-flowing beryllium powder suitable for automated operations requires further development. This might be achieved by a new powder manufacturing technique at Brush Wellman (spherical powder) or the use of binders that can be totally removed during a bake-out prior to sintering. Development of a pressing technique to produce a uniform dense sphere that can be pressure-less sintered to 90 to 95% of theoretical density is also required. The pressed sphere must be strong enough to permit automated handling. We may need to develop an efficient inspection/test capability if an adequate process reliability cannot be achieved. The technology for remoting the fabrication process is expected to be straightforward, but further study is required.

MOLTEN-SALT REPROCESSING

We have selected the fluorination process to remove ^{233}U from the salt slip stream. We find it unnecessary to use the more complex reductive extraction of fission products. Molten salt reprocessing applied to the fusion breeder is well discussed in Ref. 8, therefore, we will simply add a few thoughts here.

A study[9] of three levels of molten salt reprocessing has been carried out recently. The simplest level is fluorination only, which removes ^{233}U but not protactinium or many fission products. The next level is both fluorination and reductive extraction in which both uranium and proctactinum are removed along with small amounts of fission products. The final level is the addition metal transfer treatment which removes most of the rare earth fission products.

Employing the second and third levels of reprocessing was found to have negligible effect on breeding rates and decay afterheat, except at months after reactor shut down. Therefore, our choice of employing fluorination only has been reaffirmed.

HEAT TRANSPORT AND BALANCE OF PLANT

The general arrangement or Key Plan of the plant, shown in Fig. 10, takes advantage of the linear nature of the tandem mirror. One side of the reactor building is open for rapid construction access, and the other side contains all the process and energy conversion facilities. The Key Plan emphasizes the arrangement of the Fusion Island buildings, which consist of reactor building, steam-generator building, molten-salt processing building, tritium processing building, and hot cell.

A separated construction approach is adopted where the safety-related Fusion Island buildings are built to "safety" standards and all others to commercial standards. However, in view of the unique safety features of fusion, it is proposed that new "safety" standards be developed for the fusion breeder. These safety standards need not be as stringent as the nuclear standards for fission-plant nuclear-island buildings.

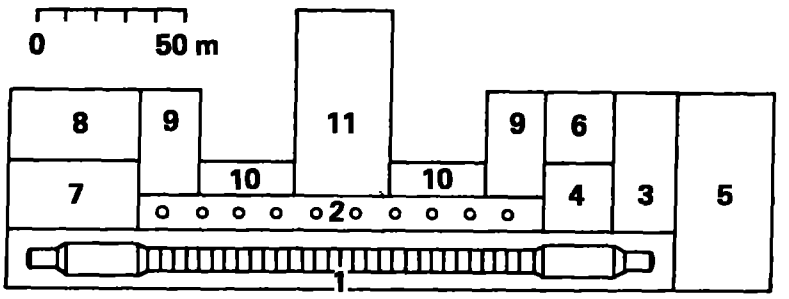

Figure 10. Diagram of plant arrangement: (1) Reactor building, (2) steam generator building, (3) tritium processing building, (4) molten salt processing building, (5) hot cell, (6) radwaste building, (7) component cooling building, (8) plant auxiliary building, (9) power supply building, (10) cryogenics building, and (11) turbine building.

The blanket heat-transport system uses helium as the coolant and transport medium. The major parameters of this system are listed in Table VI, and piping and equipment arrangement are shown in Figs. 11 and 12. The entire central cell is divided into 30 modules and ten independent heat-transport loops remove heat from the blanket (3,840 MW_t total). Each loop serves three central cell modules and consists of a steam generator and a helium circulator. The loops are not completely independent but rather must have an interconnect to equalize pressure in case one module depressurizes. The steam generators envisioned here are based upon design features similar to those currently proposed for small high-temperature gas-cooled reactors (HTGR). The features of these factory-assembled steam generators include steel pressure vessels, helical coiled water/steam tubes, and once-through steam generation (Fig. 13). Other estimated steam generator parameters include:

	Surface area (m^2)	Tube size (o.d mm)	Tube-wall thickness (mm)
Economizer	2,315	25.4	4
Evaporator	1,810	25.4	4
Superheater	1,715	25.4	5

Table VI. Heat-transport system of blanket.

Thermal power:	
Total blanket	3,840 MW_t
Added by helium circulator	110 MW_t
Blanket modules (no.)	30
Steam generators (no.)	10
Helium circulators (no.)	10
Thermal power of each steam generator	395 MW_t
Helium temperature:	
Blanket outlet/steam-generator inlet	545°C
Blanket inlet/helium-circulator outlet	300°C
Steam generator outlet/helium-circulator inlet	293°C
Helium pressure:	
At circulator outlet	5,000 kPa
At circulator inlet	4,875 kPa
Helium pressure drop:	
Blanket	55 kPa
Steam generator	50 kPa
Piping	20 kPa
Total	125 kPa
Helium pumping power:	
Total	110 MW_e
Per circulator	11 MW_e (15,000-hp motor)
Helium flow rate:	
Total	3,000 kg/s
Per module	100 kg/s
Per circulator	300 kg/s
Steam-outlet temperature	510°C
Steam-outlet pressure	16.9 MPa
Feedwater-inlet temperature	193.3°C
Feedwater-inlet pressure	19.0 MPa
Steam flow rate/steam generator	159 kg/s

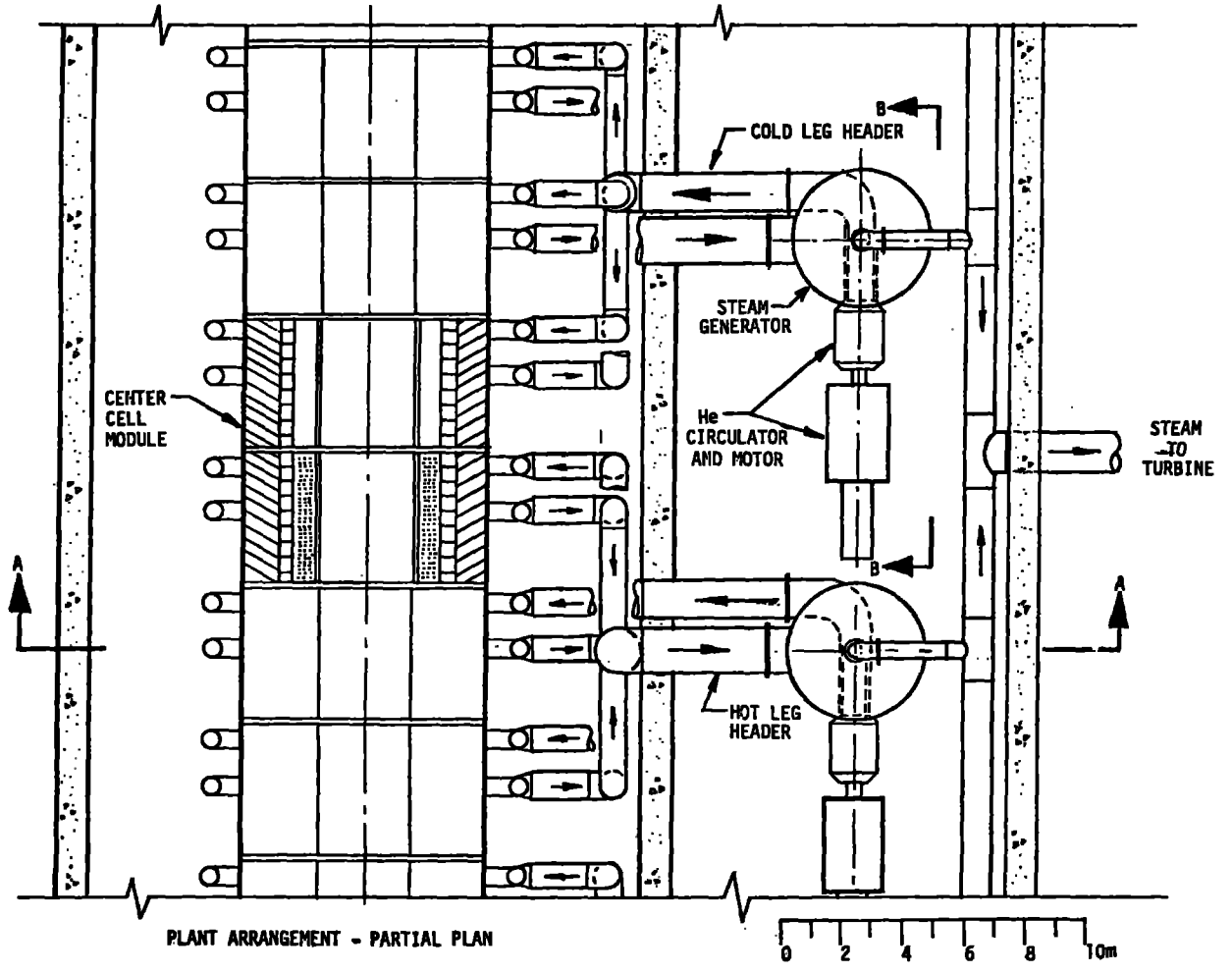

Figure 11. Heat transport system, showing piping and equipment arrangement (overhead view).

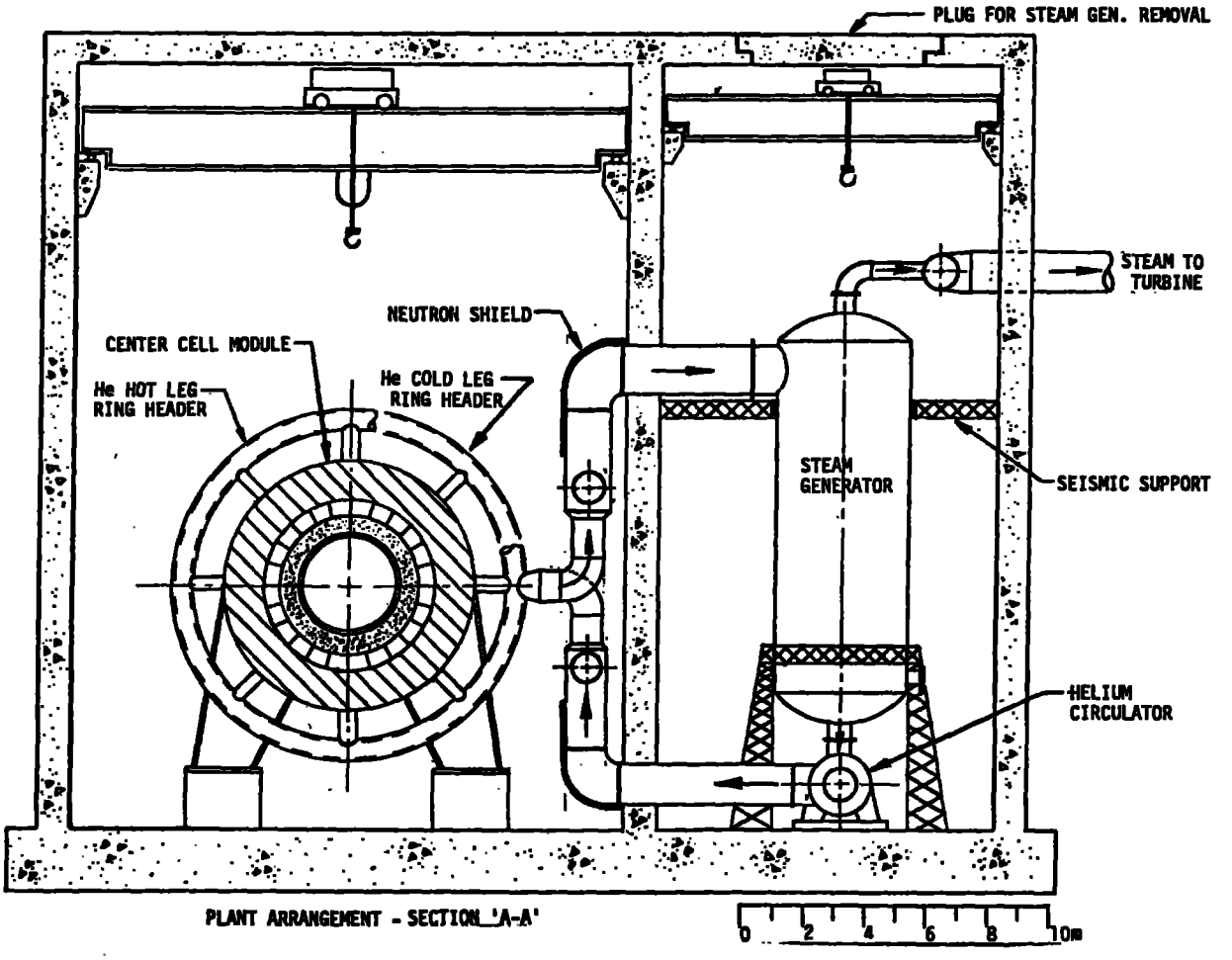

Figure 12. Heat transport system, showing piping and equipment arrangement (side view).

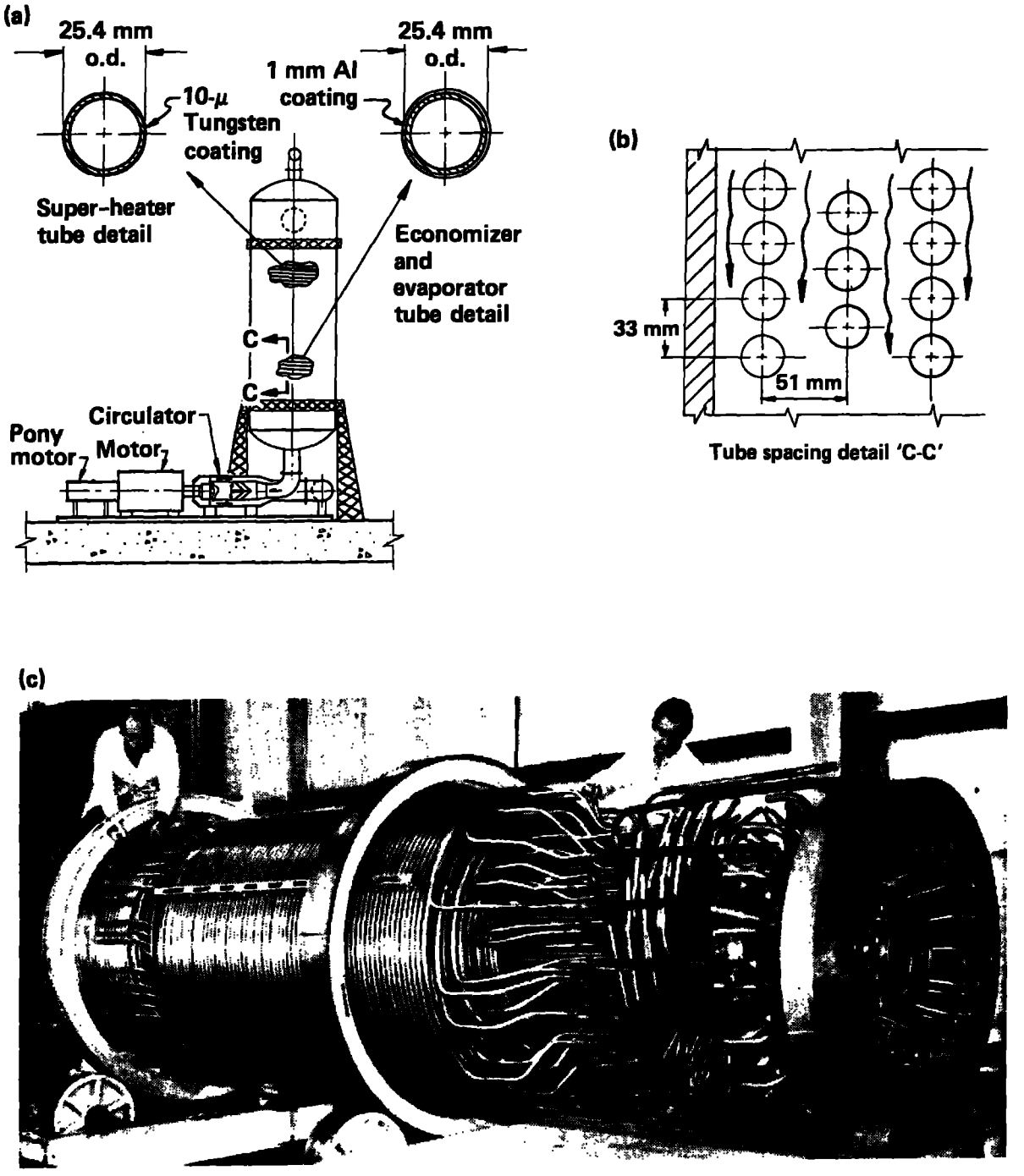

Figure 13. Steam generator arrangement. (a) Section 'B-B', (b) Typical tube sparing detail, (c) Fort Sait Vrain steam generator.

To keep the wall thickness of the steam-generator vessel low, the helium flow path may be arranged so that the cooled helium (293°C) from the economizer section exhaust is in contact with the wall. Helium piping in a helium-cooled system is a very important element because of its cost and its impact on building sizes (thermal expansion requirement) and pumping power. Because of low density of helium, large size pipes are required. In this study the largest pipe size is limited to 1.5-m o.d. To keep the wall thickness low, internal insulation is used.

Steam power-cycle parameters, listed in Table VI, are primarily based upon helium temperature and state-of-the-art steam generator technology and its cost. Without the benefits of a cost tradeoff, we assume a reasonable temperature difference (ΔT) between helium and steam and a reasonable pinch point (lowest T) at the economizer/evaporator interface. Standard steam conditions (169.9 MPa, 510°C) consistent with the current turbine-generator practice are used. Tritium permeation through steam-generator tubes is a major safety and economics concern. Two potential permeation barriers have been identified--tungsten and aluminum. When steam-generator tube surfaces are coated with either 10μm of tungsten or 1 mm of aluminum, the desired resistance to permeation is obtained. Aluminum coating on the inside surfaces is in contact with steam and may cause corrosion, while tungsten coating on the inside surfaces may exfoliate and cause damage to the turbine blades. Tungsten coating on the outside surfaces also may exfoliate and cause damage to the helium circulator impeller. Aluminum coating on the outside surfaces is not suitable in the hottest (superheater) section of the steam generator, where aluminum in contact with the hot helium (545°) is too malleable. In general, aluminum with a much higher coefficient of thermal expansion than steel may tend to separate from the steel tubes, greatly reducing the heat-transfer coefficient. Use of alonized steel (surface alloy of aluminum on steel base) may alleviate these problems; however, its permeation-resistive characteristics are not known. In addition to these potential problems, suitable methods of achieving the appropriate coating (uniform and reliable) are not available. Thus, much work, both theoretical and experimental, is needed to develop suitable permeation barriers.

INTEGRATED PERFORMANCE AND ECONOMICS

The overall performance and cost of the molten-salt fusion-breeder reactor are estimated and are combined with similar data for ^{233}U-burning LWR fission reactors to estimate the costs of electricity and bred fuel for a symbiotic electricity-generation system consisting of the fusion breeder, its LWR clients, and the associated fuel-cycle facilities. The performance parameters used to describe the molten-salt fusion breeder are given in Table I.

The results of the economics analysis for two cases are given in Table VII: utility owned and government owned. The rationale for government ownership is the precedent set by government ownership of isotope-enrichment plants (diffusion and centrifuge plants); and since the fusion breeder in effect replaces an enrichment plant, it may be treated the same. The alternate may be for a consortium of utilities to own fusion breeders in order to have fuel-supply assurance.

Table VII. Economic analysis.

Cost analysis[a]	Utility financed	Government financed
Total plant capital cost ($M)	4867	4867
Breeder/LWR cost ratio	2.35	2.35
Total fixed-charge rate (%/yr)	15.05	9.05
Effective breeder/LWR cost ratio	2.35	1.41
Year-one cost of elec. (mil/$kW_e \cdot h$)	50.8	46.9
Avg. PV cost of elec. (mil/$kW_e \cdot h$)	31.0	28.9
Year-one cost of ^{233}U ($/g)	72.5	29.2
Avg. PV cost of ^{233}U ($/g)	38.6	15.6

[a] PV = present value.

The difference in our analysis is the capital charge rate appropriate to the two cases, 9% and 15%. Another assumption is that electricity prices over the 30-year plant life are set by a fixed LWR cost but by a fuel cost whose U_3O_8 component rises 2%/yr in real terms because of resource depletion.

The average present-value cost of fuel produced is \$16/g if government owned and \$39/g if utility owned. A price for ^{233}U of \$39/g is equivalent to about \$56/kg of U_3O_8. The fusion-breeder cost estimate of \$4857M is 2.35 times an LWR cost and is based on a tandem mirror design prior to the more recent MARS[5] (Mirror Advanced Reactor) design. Design improvements may lead to lower costs and substantially reduce the sales price of ^{233}U. The following conclusions result from modeling the potential economic performance of fusion breeders:

- The molten-salt fusion breeder could be economical at today's price of uranium (55\$/kg) regardless of ownership.
- With government ownership, the molten-salt fusion breeder could break even in the first year of operation and produce a multi-billion dollar benefit over its operating lifetime.
- Bigger benefits accrue for the molten-salt fusion-breeder operation at higher breeding and/or higher blanket-energy multiplication and lower plant cost.
- A 20% breeding decrease is clearly tolerable.
- Some issues yet to be addressed include the potential impacts of lower LWR SWU costs, higher LWR fuel reprocessing costs, and the like.

TECHNICAL ISSUES

Tritium Management. Permeation barrier development and demonstration is the critical R & D need. Tritium will need to be removed from both molten salt and helium loops. Recovering tritium from molten salt has yet to be demonstrated but should be manageable since the partial pressure is high. Process technology is known for recovering tritium from helium although a large increase in scale will be required. The key is to have good permeation barriers on salt tubes and on steam generator tubes, thus easing requirements for both salt and helium process systems; single-pass process efficiencies can be moderate, and only a small fraction of the circulating helium must be

processed. Chemical vapor deposition of tungsten on steel needs development work. Failure to develop effective barriers shifts the burden of processing tritium into the steam/water system. Isotopic processing of tritiated water then becomes a high prioriity R & D requirement. Isotope separation will be more difficult and costly, and the steam system must be kept leak-free to avoid personnel hazards from tritiated water vapor. A successful barrier development effort could avoid both the need for water processing and the hazards that accompany tritiated water systems.

Beryllium Feasibility. Beryllium-beryllium self-welding and beryllium-steel welding at the contact points are issues needing experimental investigation. This is the objective of a planned set of capsule tests at ORNL. The ability of the beryllium balls to stand up under neutron radiation is maximized by design (small size), however, irradiation data are needed. Beryllium swelling--leading to jambing, cracking, chipping, and flying missiles that might damage circulars--needs investigation. Some of this can be done in fission reactors, for example, the tests carried out in EBR-II and the planned neutron radiation-induced creep tests.

Material Compatibility. We predict the steel (type 316) will have a long lifetime in contact with the salt if it is kept in a reducing state. Corrosion tests with molten salt in a flowing loop would prove the predicted compatibility. Irradiation tests in a fission reactor should be carried out to verify the chemical compatibility of salt and steel.

Reprocessing. Removal of uranium by fluorination is fairly well understood but needs demonstrating on a reasonable scale. Removal of fission products is not needed from a point of view of neutron economy. From a safety point of view, removal of fission products is desirable but only partially effective. It entails salt/metal reduction, which must be scaled up from small batch tests to larger continuous processing and requires developing refractory metal piping. We do not believe this removal processing is necessary. Therefore, development and demonstration of a continuous fluorinator is the only important reprocessing R & D need.

Neutron Economy. The breeding performance of the molten-salt design is very sensitive to parasitic absorption in structural material (principally iron, chromium, and nickel). This is due to the low concentration of thorium in the salt (only 7% of the salt atoms are thorium). It is necessary to make better calculations of the nuclear performance and to emphasize designs that minimize structural material. Alternatives to steel should be considered. Finally, experimental verification of tritium and fissile breeding should be carried out with a point 14-meV neutron source.

CONCLUSION

The molten-salt fusion breeder design appears workable if the tritium containment and recovery of multiple distributed barriers and two-stream processing works as predicted. We have identified a number of R & D items that should be studied to increase our confidence level. However, the feasibility of making tritium barriers should be given the top R & D priority. The breeding is 6400 kg/year of ^{233}U at a cost of $40/g for plants costing 2.35 times an LWR if utility owned or $16/g if government owned and supports 14 LWRs of equal thermal power. The design was carried out for a tandem mirror but should work equally well for a tokamak.

REFERENCES

1. L. M. Lidsky, "Fission Fusion Symbiosis: General Considerations and a Specific Example," Proc. Br. Nucl. Energy Soc. Nucl. Fusion Reactor Conf. (Culham Laboratory, 1969), pp. 41-53,
2. V. L. Blinkin and V. M. Novikov, "Optimal Symbiotic Molten-Salt Fission-Fusion System," IAE 2119, Kurchatov Institut, Moscow, USSR, 1977.
3. J. D. Lee, "The Beryllium/Molten Salt Blanket", Proc. Third US/USSR Symposium on Fusion-Fission, Princeton, NJ, 1979, and also in Lawrence Livermore National Laboratory, UCRL-82663 (1979); R. W. Moir et al., Tandem Mirror Hybrid Reactor Design Study, Lawrence Livermore National Laboratory, UCID-18808 (1980); also J. D. Lee et al., Feasibility Study of a Fission-Suppressed Tandem-Mirror Hybrid Reactor, Lawrence Livermore National Laboratory, UCID-19327 (1982).
4. R. W. Moir et al., Design of a Helium-Cooled Molten-Salt Fusion Breeder, Lawrence Livermore National Laboratory, UCRL-92024 (1985); Invited paper for Am. Nucl. Soc. Meeting, San Francisco, CA, March 1985 (to be published in Fusion Technology).
5. B. G. Logan et al., MARS-Mirror Advanced Reactor, Lawrence Livermore National Laboratory, UCRL-63480 (1984).
6. J. D. Lee et al., Feasibility Study of a Fission-Suppressed Tandem Mirror Hybrid Reactor, Lawrence Livermore National Laboratory, UCID-19327 (1982), Section VIIB, "Molten Salt Fuel Reprocessing" by Warren Grimes.
7. F. A. Patterson-Hine, J. W. Davidson, and D. E. Klein, "Contributions to the Thermal Power of Continuously Processed TMHR Molten Salt Blankets," Proc. 10th Symp. Fusion Engineering, Philadelphia, PA, 1983, p 988.
8. A. W. Sherwood, Tritium Permeation and Recovery for the Helium-Cooled Molten-Salt Fusion Breeder, Lawrence Livermore National Laboratory, UCID-20141 (1984).
9. D. H. Berwald et al., Fission-Suppressed Hybrid Reactor - The Fusion Breeder, Lawrence Livermore National Laboratory, UCID-19638 (1982).

1.0. INTRODUCTION

In 1969, Lidsky proposed[1-1] a fusion breeder design in which a ^{6}Li and a thorium-bearing molten salt ($LiF + BeF_2 + ThF_4$) was circulated through the blanket so that the bred material could be continuously processed from a small slip stream. He employed liquid ^{7}Li as the neutron multiplier. The thorium-bearing salt was placed behind the neutron multiplier zone with a graphite region in between to slow down the neutrons, thus suppressing fast fission. The concentration of bred ^{233}U was kept low by continuous processing so that thermal fissioning was suppressed. The predicted local breeding ratio (T + F) was 1.45, where (T + F) is defined as the number of tritons and fissile atoms produced per triton burned. The structural material was the molybednum alloy TZM, and the cooling was both by liquid lithium and by molten salt. More recent calculations[1-2] gave a breeding ratio of 1.36. Improvements to overcome the low breeding ratio and the complex and difficult-to-build design led us to the present design.

In 1977, Blinkin and Novikov[1-3] suggested replacing the ^{7}Li neutron multiplier with beryllium. This two-zone design gave a local breeding ratio of 1.63. In 1978, Lee[1-4] reported on a homogeneous one-zone design using beryllium in which the local breeding ratio was 2.2. A rather detailed study[1-5] in 1979 of this design verified the basic ideas and came up with a breeding ratio of 1.7. The study uncovered problems with fabrication of TZM, radiation damage to the beryllium and to the graphite cladding of the beryllium, as well as other problems. In 1981, a design[1-6] with steel was used to contain the molten salt. Here corrosion was predicted to be virtually eliminated by keeping the steel cool. However, ^{7}Li was used instead of beryllium to reduce excess neutrons. This fact together with the two-zone design resulted in a breeding ratio of 1.5, which was lower than desired.

DeVan in 1982 suggested using a barren salt ($LiF + BeF_2$), at a higher pressure than the fertile salt between the beryllium and its cladding, so that small inevitable leaks would not allow molten salt to contact the beryllium. This would avoid letting uranium deposit out on the beryllium, which if it could happen would lead to hot spots. Lee later suggested using helium as the coolant with the thorium-containing salt in pipes. The particular helium-cooled pipe arrangement we are now considering is similar to the design of Cheng et al.[1-7].

Corrosion is inhibited by maintaining the salt in a reducing state, where tritium is in the form of T_2 rather than TF, and the corrosion rate of steel is low. The beryllium is in the form of small (∿ 1-cm-diam) pebbles that are tolerant of radiation damage. All of these innovations, put together, eliminated the disadvantages found in the 1979 study.

The present blanket design is shown in Fig. 1-1. This design concept is promising in that it could produce a relatively low-technology, high-performing, yet economical fusion breeder, which is the subject of the following chapters of this report.

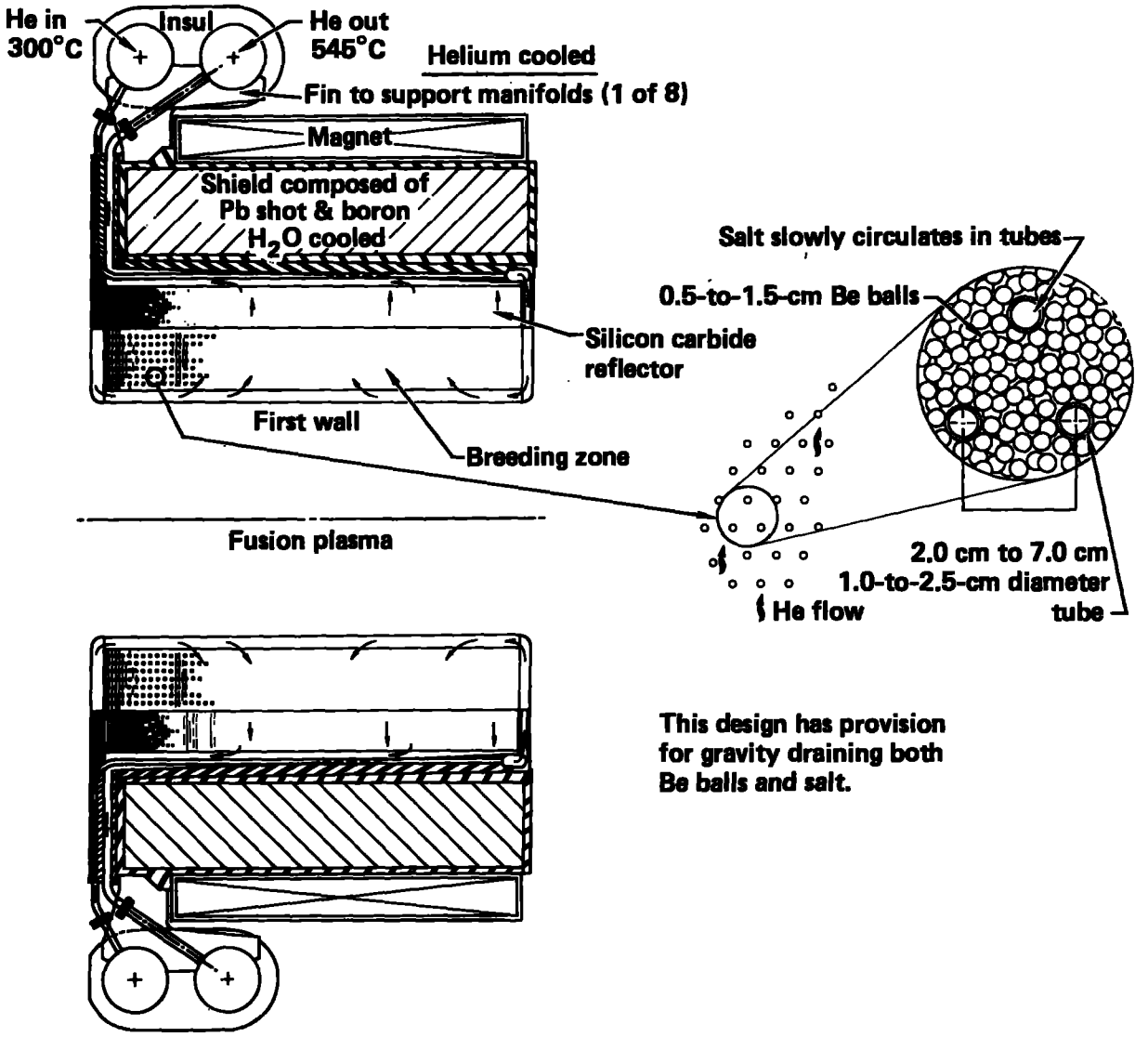

Figure 1-1. Helium-cooled molten-salt fusion breeder that uses beryllium as a neutron multiplier.

REFERENCES Section 1.0.

1-1. L. M. Lidsky, "Fission-Fusion Symbiosis: General Considerations and a Specific Example," Proc. Nucl. Fusion Reactor Conf., Culham Laboratory, 1969 (Br. Nucl. Energy Soc., Culham Laboratory, 1969), Report CLM-MFE, pp. 41-53.

1-2. A. A. Benedetti, LLNL, unpublished calculations, 1983.

1-3. V. L. Blinkin and V. M. Novikov, "Optimal Symbiotic Molten-Salt Fission-Fusion System," IAE 2119, Kurchatov Institute, Moscow (1977).

1-4. J. D. Lee, "The Beryllium/Molten Salt Blanket," Proc. Third US/USSR Symposium on Fusion-Fission, Princeton, 1979; also Lawrence Livermore National Laboratory, UCRL-82663 (January 1979).

1-5. R. W. Moir et al., Tandem Mirror Hybrid Reactor Design Study, Final Report, Lawrence Livermore National Laboratory, UCID-18808 (1980).

1-6. J. D. Lee et al., Feasibility Study of a Fission-Suppressed Tandem-Mirror Hybrid Reactor, Lawrence Livermore National Laboratory, UCID-19327 (1982).

1-7. E. T. Cheng, C. P. C. Wong, R. L. Creedon, and K. R. Schultz, "A New Fusion Breeder Blanket Design Approach Utilizing a Thorium Multiplier," summary submitted for presentation at 1983 Am. Nuclear Soc. Annual Meeting, Detroit, Michigan (June 1983).

2.0. BLANKET DESIGN

2.1. MECHANICAL DESIGN

The blanket design has several unique features. A single coolant, helium, is used. It flows axially along the first wall, having been piped there first (see Fig. 2-1). The helium then passes through a diffuser and flows radially outward through a bed of beryllium balls and salt-filled tubes, which serve as the tritium and U-233 breeding zone. Next, encountering the neutron reflector zone, the helium continues on its outward radial path through holes in the reflector and grooves in the reflector-block faces. Upon reaching the shield inner boundary, the helium is collected in ducts and carried out to a ring manifold located near one end of a blanket module (see Fig. 2-2). The shield uses water as its coolant and does not contribute its energy to the main thermodynamic cycle.

The pipes that carry molten salt through the breeding zone enter at the bottom of the blanket, go azimuthally around the plasma, and return to the bottom of the blanket where collection manifolds pass out through the shield (see Fig. 2-3). A vent valve will be included at the top of each pipe loop to aid gravity drainage of the salt tubes during reactor shutdown. The many salt tubes encircling the first wall require that the blanket modules not be separable into "pod" subassemblies but rather be assembled and leak tested as a complete unit.

The empty space between salt tubes is to be filled as completely as possible with neutron-multiplying material. Beryllium balls will be poured into the blanket from the top. The structure must be configured to allow those balls to flow freely into the breeding zone, completely filling the space between the tubes and any other structural elements. The beryllium balls are expected to swell and perhaps crack during service. The used balls can be changed by draining them by gravity through ball-exit chutes located on either side of the molten salt manifolds at the bottom of the blanket. Some balls may not exit by gravity and will be trapped in nooks and crannies inside the blanket. These can be left behind. New or reprocessed balls will replace the balls that do drain out (estimated to be over 95% of the balls). The old ones will continue to swell and crack but not to the detriment of blanket performance.

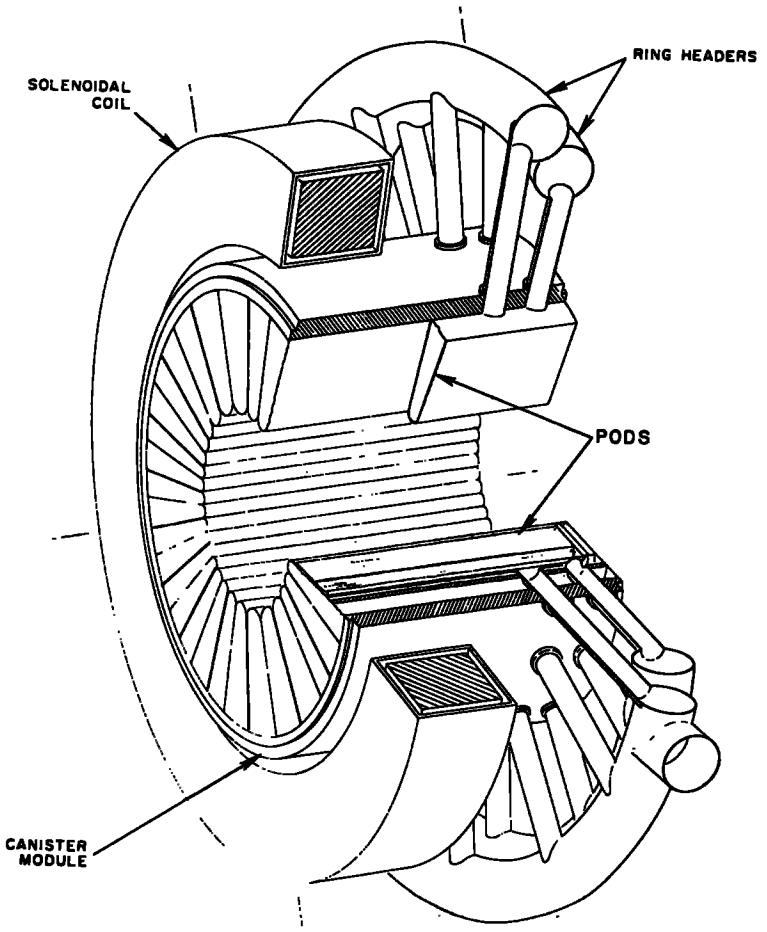

Figure 2-1. Ring headers for the supply and return helium but for a different blanket than those shown in Figs. 2-2 and 2-3.

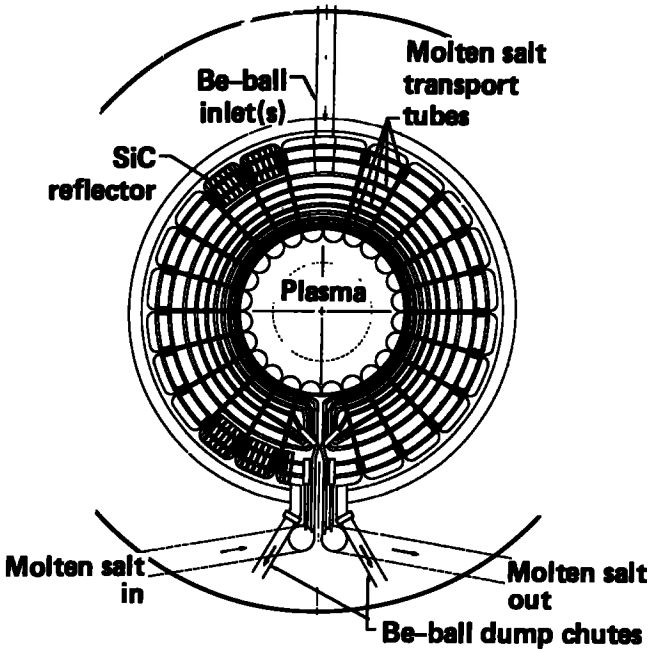

Figure 2-2. Molten-salt breeding blanket. (Cross section looking down axis of central cell.)

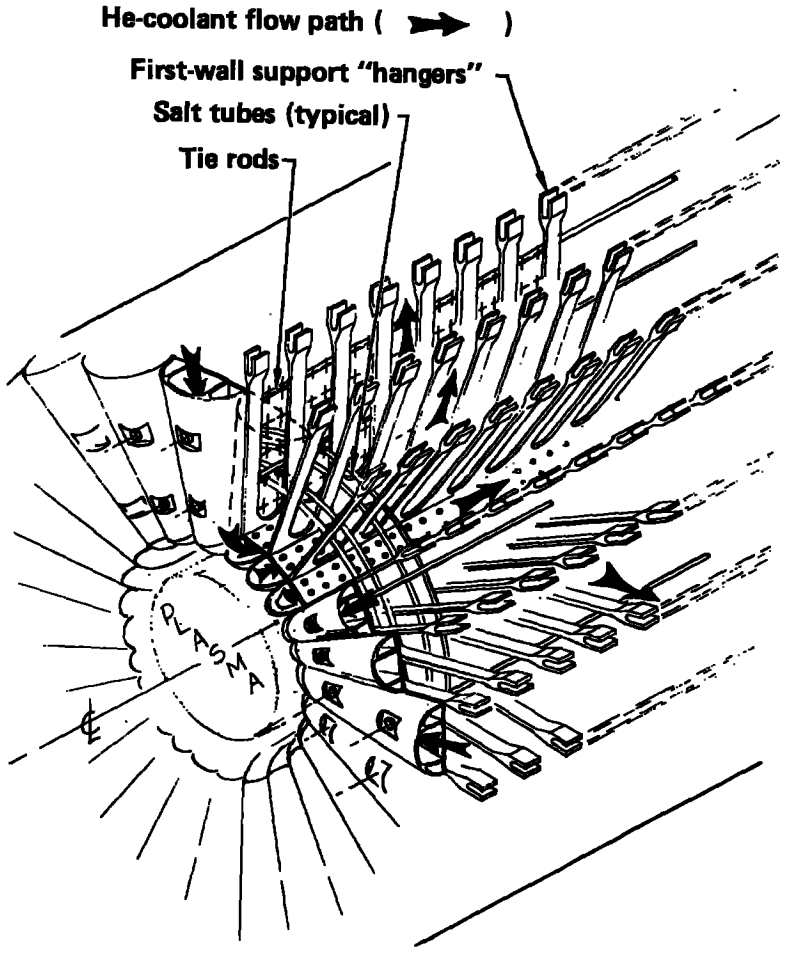

Figure 2-3. Molten-salt breeding blanket showing support hangers and salt tubes.

2.1.1. PEBBLE/TUBE SYSTEM - SALT VOLUME AND COST

The salt tubes immersed in the bed of beryllium balls must be spaced so the balls can flow either into or out of the tubed region with no bridging resulting in flow stoppage. In flow tests we found that if the balls are no larger in diameter than one-half of the free space between the tube walls, free flow will occur. Since some balls may crack or swell and develop imperfections of shape, we prefer the ball diameter to not exceed one-third of that free space. The nominal values we have chosen are given in Table 2-1.

Table 2-1. Nominal pebble/tube parameters

Tube o.d.	1.7 cm
Tube spacing	4.7 cm
Tube wall thickness	0.5 mm
Pebble diameter	1.0 cm

The tubes are held in place by clips attaching them to the radial spokes that tie the first wall to the cylinder just outside the reflector. This cylinder is the main structure preventing the first wall from buckling. Figure 2-3 shows the radial spokes and a few of the salt tubes. The width of the spokes may require some tubes to be slightly bent to get the most uniform salt distribution and also avoid the spoke.

The tube diameter is large enough so that freeze-up of the salt will not occur and small enough so that the centerline temperature will stay well below the boiling point. These limits are discussed in the thermal hydraulic section. The tube spacing is picked on the basis of nucleonics. Too large a spacing will give parasitic loss of neutrons in the beryllium and too small a spacing will displace beryllium and reduce fast neutron multiplication. The tube wall thickness is chosen to reduce parasitic absorption in the steel and

yet be thick enough to avoid the buckling caused by the helium pressure (50 atm) being higher than the salt pressure (49 atm normally but 1 atm under depressurized conditions). The pebble size is picked to be large enough to avoid excessive pumping power but small enough to freely flow between the pipes.

Axial tie rods in this design restrain the ends of the blanket module. Otherwise 50 atm of helium could not be structurally contained. These rods represent about 3.5% of the blanket volume. The salt tubes are 1% of the blanket volume and module sidewalls are about 1.5%. Salt ($LiF + BeF_2 + THF_4$) is 9.5% and beryllium balls are 53% of this breeding zone. (The region between salt tubes is assumed to be 60% beryllium and 40% helium coolant.) Table 2-2 gives typical blanket parameters emphasizing beryllium requirements.

Tube Failure Rate

With so many steel tubes in the blanket, the question of failure rate must be considered. For a triangular array having nominal spacing of 4.7 cm, there would be 80,000 tubes in the complete blanket. Each tube would be approximately 11-m long. If we can tolerate one failure in five years, the failure rate per tube per hour of operation must be less than 4×10^{-10}. The helium pressure outside the tube will be about one atmosphere higher than the salt pressure within the tubes. Small cracks (at welds for example) would allow helium to leak into the salt but would not constitute a failure. A large crack might result in excessive helium leakage and force a shutdown and module change. This would have little overall consequence other than economic if the occurrence was infrequent. An offset tube break could cause molten salt contamination of the helium-coolant loop. This would require shutdown and clean-up. Analysis should be carried out to determine tolerable crack sizes and to estimate tube failure rates. Analysis should also be carried out to determine the operational contamination limits of leaks of helium into molten salt and vice versa.

Salt Volume and Cost

The salt tubes constitute 9.1% of the 60-cm thick blanket, assuming no salt in the reflector region. The blanket volume is 860 m^3, so the salt volume will be 78 m^3 in the blanket region. The salt in the processing system and piping must be added to this. The amount of salt in the prior

Table 2-2. Beryllium requirements for the molten-salt blanket.

Total blanket volume[a]	860 m^3
Pebble volume[b]	470 m^3
Pebble quantity[c]	890 x 10^6
Pebble mass	0.96 g
Beryllium mass[d]	860 tonne
Average beryllium lifetime	5 years
Annual pebble throughput	180 x 10^6/yr
Annual beryllium mass throughput	170 tonne/yr

[a]127-m long central cell (3000 MW fusion power) with 0.6-m-thick blanket starting at 1.5-m radius. Wall load is 2 MW/m^2.
[b]Tubes represent 10% of blanket volume, with 60% packing in remainder of blanket
[c]Pebbles are 1 cm in diameter.
[d]Beryllium density is 1.84 g/cm^3.

design was 1152 m^3 or 15 times more! The present greatly reduced amount of salt should reduce the reprocessing cost and also allow removal of more fission products. Based on \$166,500/m^3 for the 12 mol% ThF_4 salt (see Ref. 2-1), the cost of the salt in the blanket would only be \$13M, implying the salt could be replaced on a fairly short interval (less than 4 years), thereby reducing the radioactive inventory.

2.1.2. MODULE END WALL

In all blanket designs difficult structural problems occur at module ends. A combination of end cover plates and coolant supply ducts is employed to minimize parasitic capture of neutrons. We bring coolant to the first wall by using the contoured end plates as coolant gas ducts (see Fig. 2-4). The coolant turns upon reaching the first wall and flows axially from each end of the module. The diffuser plate then allows the flow to turn another 90 deg and enter the pebble bed when the helium gas flows radially, thereby cooling the entire blanket.

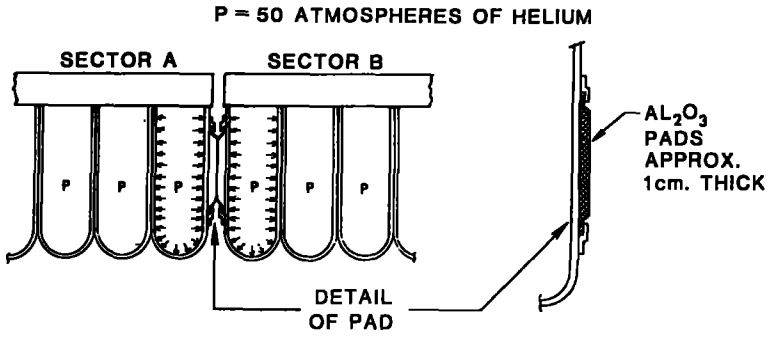

Figure 2-4. Alternate design for module end.

The large axial force on the end plates can be resisted by a combination of structural members. It must be realized that no axial force can be transmitted through the spokes. There is no web to carry axial tension in any of the 24 spoke planes.

The first wall is continuous from end to end but is subject to large pressure force radially inward. Also the first wall is thin to minimize neutron heating and is not intended to carry large axial loads. Corrugations of the first wall permit swelling as a result of neutron fluence. Those corrugations render the wall incapable of transmitting large force.

The outer cylinder to which the first-wall stabilizing spokes attach is a stout axial support that would support all of the axial pressure force if the force could be transmitted to it. Unfortunately, the bending load is very large, resulting from trying to cantilever the wedge-shaped end plates (ducts) from the outer cylinder. The metal thickness required for such attachment may cause restrictions in the coolant flow area at the duct entry. We are studying this problem. In the meantime we show two long tie rods through each end plate. These rods terminate at the corresponding end plate at the opposite end of the blanket module (see Fig. 2-4). The wedge-shaped end plate is configured with a deep bending cross section to stiffen it. This also permits it to carry the bending associated with a beam that has a rigid support at the outer one end, has two other intermediate support points (tie rods), and also has a short cantilevered segment at inner end where it joins the first wall.

An alternate module-end-support solution would allow the end modules of one sector to support those of the adjacent sector. Consideration must be given to tolerance accumulation, which can cause overstress of module sidewalls. Also unintentional "cold welding" of walls in contact could occur, which would prevent disassembly without damaging the module end-wall in contact with a neighboring sector. Both of these unpleasant effects can be overcome by the following suggestion. An aluminum oxide plate (or several smaller pads) can be mounted on the end walls of modules in adjacent sectors. The thickness of the aluminum oxide pad can be selected just before final assembly to compensate for tolerance build-up in the manufactured condition. Alternatively a pressurized cushion could be used in conjunction with the aluminum oxide plate to take up the tolerance. The ceramic pads will not weld under vacuum. Pad spacing and area must be controlled to minimize any local wall bending stresses in an unsupported area. The space occupied by these thin ceramic pads can be small. Valuable breeding volume is conserved and parasitic neutron capture minimized. This alternate design is shown schematicaly as Fig. 2-5. Further work is needed on design of the module end support.

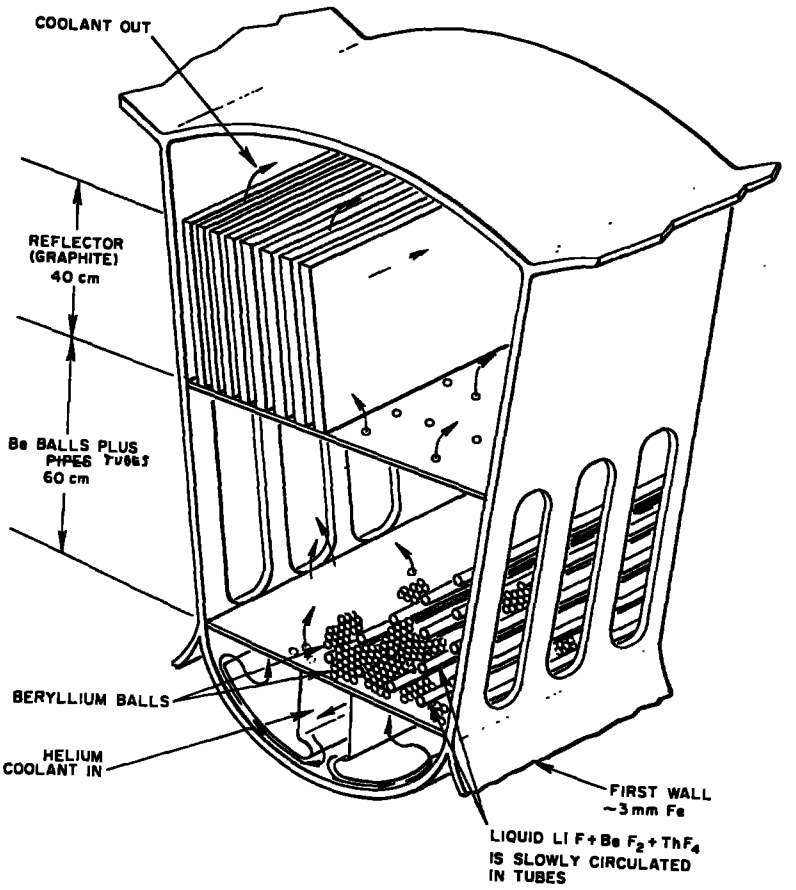

Figure 2-5. Axially oriented salt pipes.

2.1.3. TANDEM MIRROR ALTERNATE BLANKET DESIGNS

Several variations of this blanket and first-wall design should be examined. Instead of the lobed first wall with helium ducted separately to each axial lobe, it might be less costly to have two concentric cylinders spaced apart by periodic axial fins. The inner cylinder faces the plasma. Helium coolant flows in the space between the cylinders. The outer cylinder is perforated to permit flow of coolant into the pebble bed. The axial fins, which tie together the inner and outer cylinders, provide buckling stiffness to the assembly. It is still likely that some radial support from the shield will be required, probably by radial tie rods.

Another interesting concept is the variant of the double first wall, already described, in which the coolant is fed to the wall in a different fashion. If radial support rods are necessary for buckling stability of the double first wall, why not flow coolant to the first wall through tubes that replace those rods? The design at the first-wall connection for such a tube was studied and appears quite feasible, permitting a reliable structural connection and well distributed coolant. Instead of an end plate that doubles as a coolant inlet duct, we would need an end plate whose only function is to restrain coolant pressure. As noted previously, the axial load transfer and distribution will certainly affect the shape of the end plate, and it is not clear whether its mass, hence parasitic capture, will be any lower than the design that doubles as a coolant duct. We still do not expect the first wall to carry axial load because of provisions for neutron-induced swelling.

Alternate Tube Arrangement

For some alternate designs, we handle the salt tubes quite differently. If the tubes tend to run axially (rather than azimuthally), then the blanket can be segmented into identical wedge-shaped pods (see Fig. 2-5). The end-plate problem benefits from the pod side plates, which now can carry tensile load. The neutronics of the blanket will show parasitic capture because of the many pod boundary plates. We doubt there are advantages to such tube orientation. One clear disadvantage is the tube-draining requirement. The orientation of some of the tubes will prevent simple gravity draining. A more complex purging method using pressurized gas blow-down would be necessary.

2.1.4. TOKAMAK BLANKETS

For the tokamak configuration, the pods can have orientations related to the above, namely running toroidally (similar to axially in a mirror) or poloidally (similar to azimuthally in a mirror). The toroidal pod orientation is shown in Fig. 2-6.

If the salt tubes run poloidally around the torus (as in Fig. 2-3), disassembly of the torus into wedge segments or modules would be possible. The blanket sections would be very large and difficult to handle. They would completely encircle one segment of the plasma. In top view the module would be wedge shaped. The poloidal direction for the salt tubes does permit gravity drain of the salt.

The poloidal pod orientation - salt tubes also running poloidally - is shown in Figs. 2-7 to 2-9. Very large modules are required since the plasma must be completely encircled, as before. Each module would be 13-m tall, as shown in Fig. 2-7. The first wall can be well cooled as shown in Fig. 2-8. A separate feed tube at the top of each pod provides for beryllium pebble filling. A similar but larger drain tube at the bottom of each pod would be joined to a large manifold to permit pebble extraction. The module must be continuous from top to bottom of the reactor to allow beryllium pebble addition and removal. Horizontal divisions preclude draining pebbles from a "flat floor".

If the tubes carrying salt run in the toroidal direction, a tube drainage problem must be solved. Some pods will be oriented so gravity aids salt drainage. Those on the upper portion of the blanket will have to be drained by some gas blow-down procedure, because their tube feed lines point upward to varying degrees.

Toroidal salt tubes are limited in length to a pod that can be assembled between toroidal field coils. Depending on design details, this toroidal tube length cannot exceed 30 deg of arc for a twelve-magnet system. More realistically, the angle will probably be 15 to 20 deg.

The preferred tokamak configuration is toroidal pods and poloidal tubes (see Fig. 2-6).

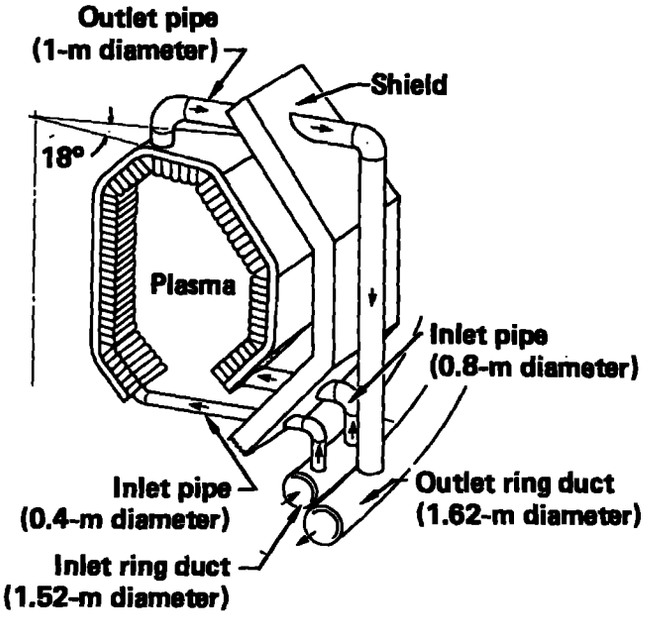

Figure 2-6. Tokamak module and piping arrangements.

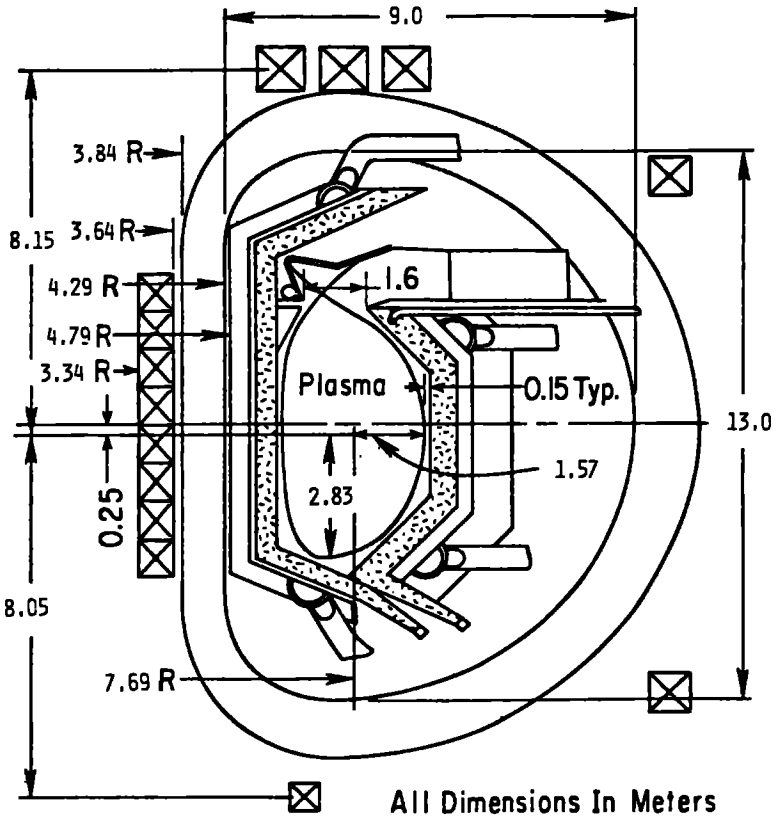

Figure 2-7. Poloidal pod orientation.

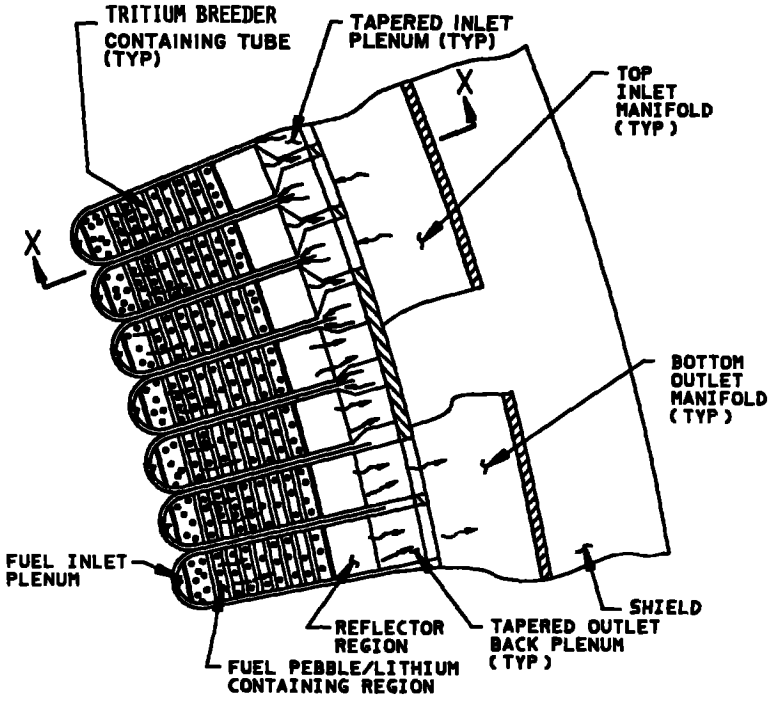

Figure 2-8. Poloidal pod orientation - blanket cross section enlarged to show lobe detail (not to scale).

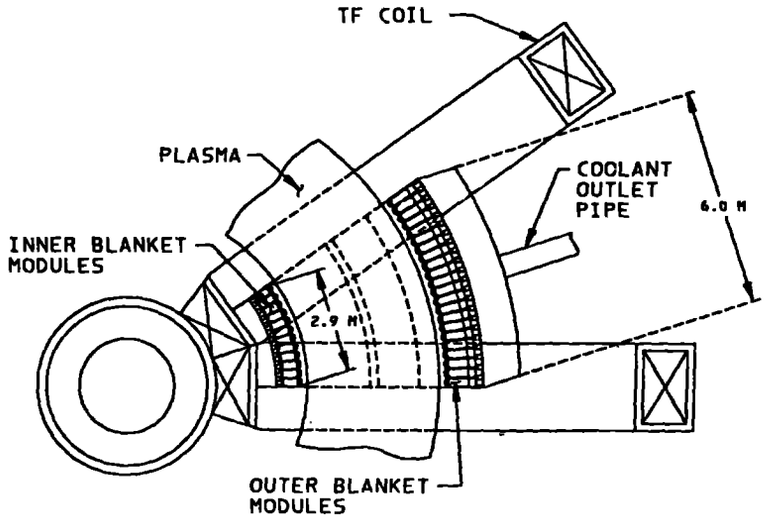

Figure 2-9. Blanket cross section (A-A of Fig. 2-8) of poloidal pod orientation.

2.1.5. BERYLLIUM PEBBLE FABRICATION TECHNOLOGIES

In this section, the technology required to produce and recycle beryllium pebbles for the fusion breeder blanket is described. Beryllium availability is reviewed, a production process is proposed, its cost is estimated, and process development issues are discussed. The beryllium pebble design and lifetime considerations are discussed in Refs. 2-2 and 2-3. The lifetime of the beryllium pebbles is presently quite uncertain (five years assumed in this analysis which is 7 MW·y/m^2, but is, to a large extent, dependent on the fabricated properties described below.

Requirements

As described in Section 2.1., each beryllium pebble is a solid, 1-cm-diam sphere. The pebbles occupy one fuel zone 60 cm in thickness. The volume of this zone, for a 127-m central-cell length, is 860 m^3. For an approximate 60% pebble-packing fraction outside of the tubes that occupy 10% of the volume, the pebble volume is 470 m^3. Therefore, 890 x 10^6 pebbles will be required for the initial inventory. The net beryllium mass is 860 tonne (1.84 g/cm^3). For an assumed average pebble lifetime of five calendar years, the annual throughput of the hot beryllium fabrication plant will be 180 x 10^6 pebbles/yr or 170 tonne/yr. The above quantities were summarized in Table 2-2.

Beryllium Availability

Our FY81 assessment of long-term beryllium availability[2-1] indicated that the amount of beryllium required for the reference blanket would represent about 3% of the known beryllium reserves in the U.S. (Bureau of Mines estimate). Similarly, the same 860 tonne requirement represents about 1% of the total estimated U.S. beryllium resource, about 0.24% of the known world beryllium reserves, and about 0.07% of the total estimated world beryllium resource. A more recent assessment was provided in Ref. 2-4.

Our energy growth projections of the same study[2-1] indicated that on the order of 40 fusion breeders might eventually be built prior to 2050. On this basis, we conclude that the U.S. beryllium resource will be marginally adequate for this application without a definitive requirement for imported beryllium.

Currently, the only source of beryllium metal in the free world is Brush Wellman, Inc. They produce $Be(OH)_2$ at a mill in Delta, Utah. The beryllium source is bertrandite ore, which contains ∿4 lb/tonne of beryllium per year. They are planning to increase production by about 60%, using Chinese ore (40 to 50 lb/tonne of beryllium) to satisfy their projected needs for BeO and Cu-Be alloys.

In 1982, Brush Wellman converted ∿27 tonne/yr of the beryllium from the mill in Delta, Utah, to beryllium metal in a plant at Elmore, Ohio. They estimate the maximum capacity of the metal production capability of the plant to be ∿115 tonne/yr.

Recognizing the current production capability, it is of interest to consider Brush's capability to expand capacity. To produce one entire beryllium inventory during a four-year period (i.e., for the first commercially sized fusion breeder), a beryllium requirement of 215 tonne/yr would require Brush to expand operations as follows:

1. Develop a source of high-grade ore (perhaps Chinese).
2. Expand the mill at Delta, Utah, by about 70%.
3. Increase the metal production capability at Elmore by 2.6 fold.

It is quite clear that the beryllium-production capacity would have to be carefully coordinated with fusion-breeder development to assure that a supply bottleneck does not occur.

Fabrication Process

The selected pebble-fabrication process involves the development of an automated line that will cold press pebbles, vacuum sinter them, hot forge them essentially to 100% of theoretical density, and vacuum anneal them. Brush currently uses the first three steps of this process to produce aircraft brake segments - the only difference is that the present process is manually operated because current beryllium powder is not free flowing and not amenable to automated operations. In order to automate this process, a free flowing beryllium powder is required.

The brake parts produced by Brush have properties as good or better than S-200-E.

Ultimate tensile strength	40 ksi
Yield strength	30 ksi
Elongation	1%
Density	1.84 g/cm^3

We do not expect a free flowing powder to degrade these mechanical properties. In fact, some of the manufacturing processes currently being discussed with Brush would be expected to increase both the tensile strength and elongation.

The equipment needed for production is simple: mechanical presses and powder feeders to make cold-pressed compacts, automated vacuum sintering furnaces for pressureless sintering, mechanical presses for hot sizing the sintered compacts, and an automated vacuum furnace for annealing the forged compact.

For fabrication of pebbles too damaged to reinsert into the blanket after an irradiation period, we would vacuum melt the hot pebbles and use an automated atomization process (modeled after the Brush Wellman process) to first remanufacture the beryllium powder prior to the cold-press step.* The entire process will require provision for shielding and remote maintainability. In addition, hooding requirements as per OSHA limits (2 $\mu g/m^3$) must be maintained to limit airborne contamination. A beryllium decontamination step (e.g., electro-refining) is not assumed but might simplify the shielding and remoting requirements.

Given a five-year beryllium lifetime and assuming an automated plant that operates 24 hours/day and 7 days/week and operates 85% of the time with no rejects, we must have a production rate of 400 balls per minute. While this is a high production rate for beryllium parts, it is low for some powder metal industries (e.g., tantalum capacitor manufacturers produce thousands of parts/per minute). The beryllium reprocessing line is estimated to lose 7 to 10% of the beryllium throughput, so a small feedstream is required. With a free-flowing powder, the losses might be reduced perhaps as low as 1%.

As an alternative, lower density parts can be made by cold pressing and sintering. If the parts are sintered to 90% of the theoretical density, they are predicted to have 70 to 80% of their full density conductivity. Some 90%-dense beryllium parts made in this manner have been tested at LLNL. These were characterized with respect to mechanical properties, porosity, etc. It is possible that the lower density parts will swell less and, consequently, have longer life.

*We do not exclude the possibility of removing the helium gas by vacuum heating, which would result in about 30% volumetric swelling. These enlarged pebbles could then be pressed back into size.

Process Cost Estimate

The beryllium fabrication-process components and their estimated costs were developed in the 1982 tandem mirror fusion breeder-design study[2-2]. These costs, corrected for inflation to 1984 dollars, are listed in Table 2-3. The listed equipment is sufficient to produce or recycle 18 million pebbles per year, 3-cm o.d., or the entire beryllium inventory in two years. The cost attributed to remoting the process is a guess.

These costs were adapted to the present blanket requirements (180 million pebbles per year, 1 cm o.d.) by scaling the above component costs by throughput and by the characteristic parameter of the pebble (diameter, area, or volume) that drives the magnitude of a specific process and/or cost. For example, the amount of beryllium makeup and the cost of volumetric furnaces is assumed to scale directly with the pebble volume at a fixed process rate (pebbles/yr). Similarly, the cost of pressing, air-handling systems, and plant staff (assumed to be $2M/yr for the 1982 blanket requirements) is assumed to scale as the pebble area at a fixed process rate. The cost of transfer lines is assumed to scale as the pebble diameter, and the cost of inspection is assumed to scale directly as the process rate (pebbles/yr). For the newer analysis, the cost of milling machines (which would scale as the pebble diameter) was deleted as the pebbles for the molten-salt blankets do not have the cut groove of the beryllium/thorium snap ring design of Ref. 2-2. A new cost, inspection, was introduced. We assumed that an inspection test assembly, performing a relatively simple mechanical operation (e.g., a compression test) could be developed to test one pebble per 15-second interval for a capital equipment cost of $400,000. Approximately 100 such assemblies ($40 million) would be required for the molten-salt blanket.

Table 2-3. Estimated costs of components for processing beryllium pebbles.

No. of units	Process Components		Cost
8	Presses with feeders		$ 3.4 M
4	Sintering furnaces		1.7
4	Sizing presses		1.7
4	Annealing furnaces		1.7
4	Milling machines		1.7
1	Transfer line		2.5
12	Inspection lines		4.8
	Air handling, filters, etc.		4.3
		Subtotal	$21.8 M
		Remoting (100%)	21.8
		TOTAL	$43.6 M

The cost of beryllium fabrication as a function of the blanket pebble inventory (I,grams), lifetime (L,years), and radius (r,cm) is estimated to be

$$\text{Cost(\$M/yr)} = 0.13 \frac{I}{L} \left[0.221 + \frac{0.184}{r} + \frac{0.054}{r^2} + \frac{0.153}{r^3} \right] .$$

This cost estimate, shown graphically in Figure 2-10., assumes a capital cost of 15%/yr and includes makeup of 7% of the beryllium throughput at $350/kg. If the loss can be reduced from 7% to 1%, the leading term of the sum (0.221) is reduced to 0.059 . For the molten-salt blanket (I = 860 tonne, L = 5 yr, r = 0.5 cm), the annual cost becomes $45M/yr. This relatively large cost represents roughly 6% of the overall annual cost. It is dominated by inspection and would be reduced to less than $18M/yr if the inspection lines can be eliminated.

Development Issues

The only special equipment needed for the process line is the air-handling system needed to contain the beryllium powder. The die life should be comparable to other powder metallurgy products (500,000 to 1,000,000 parts/die, with punches redressed every $\sim$ 50,000 parts).

Production of a free-flowing beryllium powder suitable for automated operations requires further development. This might be achieved by a new powder manufacturing technique at Brush Wellman (spherical powder) or the use of binders that can be totally removed during a bake-out prior to sintering.

Development of a pressing technique to produce a uniformly dense sphere that can be pressurelessly sintered to 90 to 95% of theoretical density is also required. The pressed sphere must be strong enough to permit automated handling. An efficient inspection test capability may need to be developed if an adequate process reliability cannot be achieved.

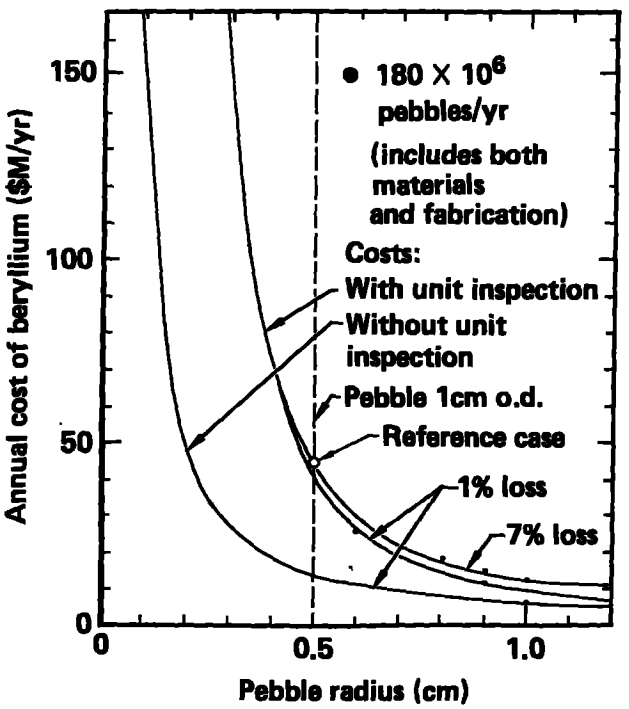

Figure 2-10. Annual beryllium cost versus pebble size.

2.2. NUCLEONICS

2.2.1. INTRODUCTION AND SUMMARY

In this section we describe the nucleonic appraisal of this blanket concept (helium-cooled beryllium-pebbled, fertile molten salt in tubes) as an aid in determining its potential and if future work is justified.

The first step in this appraisal, we will calculate the nuclear parameters of a representative unit cell and compare results with the lithium-cooled beryllium thorium pebble-bed reference blanket of last year. The unit cell model is an infinite assembly and contains no structure other than the tubes containing the molten salt. Thus the results represent an upper limit of performance. To appraise the effects of finite thickness and first wall and other structures on performance, a cylindrical model is used. The cylindrical model is also used to estimate energy deposition versus radius.

The Monte Carlo neutron-transport codes TART and ALICE with ENDL nuclear data are used for this analysis. ALICE is a version of TART that uses the Probability Table Method to treat resonance effects.

Results indicate that the neutronic performance of this blanket concept should be good. Total tritium + net fissile breeding ($T + F_{net}$) in the unit cell is 2.16 compared to 2.32 for the reference blanket. Net fissile breeding (F_{net}) equals Th(n,γ) - U(n, fiss) - U(n,γ) reactions per source 14-MeV neutrons; and T is defined as the number of tritons produced per 14-MeV neutrons. Energy multiplication (m) is 1.95 versus 2.32. The cylindrical model has a $T + F_{net}$ of 1.85 compared to 1.83 for the reference case. On correcting the cylindrical model results for heterogenous effects, we find $T + F_{net}$ is 1.75. When T (1.06 as in reference case) is subtracted, the blanket fissile-breeding ratio (F_{net}) is 0.69 compared to 0.62 for the reference case. When additional structure and other effects are considered F_{net} may drop to about that of the reference case. Energy multiplication M of this blanket is estimated to be 1.6 compared to 1.8 for the reference case. The nuclear design and analysis of this blanket concept has just begun and much needs to be done to optimize the design and improve the analysis. Integration of heat transfer and structural requirements must also be undertaken. Resonance, as well as heterogeneous effects, appears significant and needs to be included in the analysis.

The results given above are for a 27 mol% ThF_4 salt. Replacing it in the unit cell with a 12 mol% ThF_4 salt results in an 8% drop in $T + F_{net}$. If blanket $T + F_{net}$ drops 8% to 1.62, F_{net} drops 20% to 0.56. Increasing the molten-salt volume fraction may reduce the effect of changing salt composition.

While these initial results are encouraging, more rigorous analysis and optimization are needed before we can say with reasonable assurance that this blanket concept has good nuclear performance potential.

The following subsections describe the analysis in more detail.

2.2.2. UNIT CELL

The blanket interior consists of a bed of beryllium pebbles plus molten salt in tubes. The unit cell model shown in Fig. 2-11 is used to assess the nuclear potential of this configuration. The cell is driven by a xy-planar, isotropic, 14-MeV neutron source located at z = 0+. All exterior planes of the cell are reflecting, therefore, the cell is in effect an infinite assembly of unit cells. Results with this model give an upper limit because finite thickness, first walls, and other structures are not included. Results of the various cases calculated with this model are given in Table 2-4. Most calculations were done with the TART code and 175 group nuclear data. Two cases (7a and 8) were run with ALICE to estimate the importance of resonances. The parameter 'pitch' is the x and z separation of the molten-salt tube center lines. Cell x and z dimensions are one-half the pitch. The beryllium contains 0.1 at.% Fe impurity. The standard deviation is less than 2%. Some general observations: As the ^6Li amount drops (cases 1 to 3) so does total breeding ($T + F_N$) because parasitic captures increase. As the pitch is decreased (cases 4 to 4b), neutron multiplication, represented by total captures, decreases but breeding increases. A 7-by-7 cm pitch was chosen as a preliminary design point, but further optimization is needed.

The effects of resonance self shielding was important, reducing F while increasing T by about the same amount. Since T should stay constant, the ^6Li amount must be reduced, which will reduce $T + F_N$ because of increased parasitic capture. Obviously, resonance self shielding must be included when pitch optimization is done. Tube size should be varied as well. Tube size and pitch may also need to be varied to achieve the correct interface temperatures between the molten salt and tube wall. In Table 2-5, results are

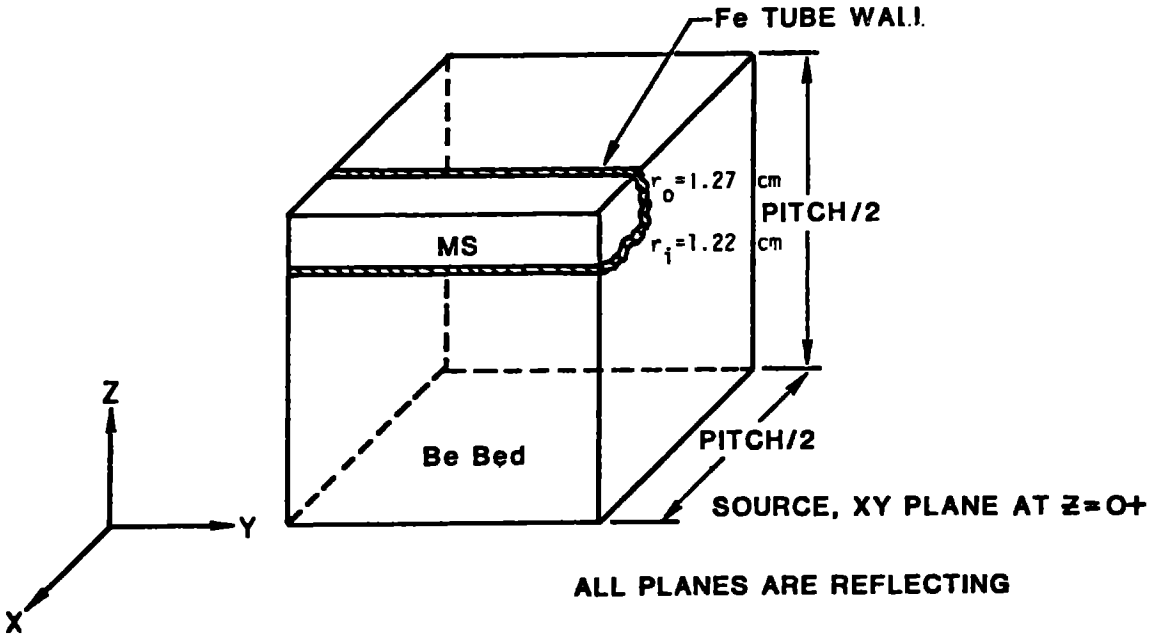

MS Composition (ρ = 4.5 g/cc)

LiF	71 m/o
BeF_2	2 m/o
ThF_4	27 m/o

BE Bed Composition

Be	50 v/o
Fe	0.1 v/o

Figure 2-11. Unit cell calculational model for molten salt (MS in Fe) + beryllium + helium blanket.

Table 2-4. Nuclear performance of the unit cell (MSHE series).[a,b,c]

Case No.	Pitch (xz) (cm)	$^6Li/Li$	U/Th	T	F	T + F_{net}	Total captures	E(M)
1	14 x 14	0.10	0.01	2.15	0.267	2.34	2.86	33.1 (2.36)
2	14 x 14	0.05	0.005	1.98	0.325	2.25	2.79	30.7 (2.18)
3	14 x 14	0.02	0.005	1.77	0.477	2.13	2.87	--
4	14 x 14	0	0	0.006	1.31	1.31	2.68	--
4a	3.74 x 14	0	0	0.021	1.71	1.73	2.49	--
4b	3.74 x 7	0	0	0.038	1.75	1.79	2.25	--
5a	3.74 x 14	0.01	0	1.16	0.94	2.10	2.51	--
6	7 x 7	0.01	0	1.08	0.99	2.07	2.45	21.4 (1.52)
7	7 x 7	0.013	0.0011	1.22	0.97	2.16	2.56	27.4 (1.95)
7a (ALICE)	7 x 7	0.013	0.0011	1.50	0.69	2.15	--	28.7 (2.04)
7HO	7 x 7	0.013	0.0011	0.967	1.34	2.28	2.59	26.2 (1.86)
8 (ALICE)	7 x 7	0.0059	0.0011	1.43	0.59	1.98	--	27.0 (1.92)

[a]Abbreviations: MSHE = Molten-salt/beryllium/helium; T = tritons bred/triton consumed; F = fissile atoms bred/triton consumed; E = energy released in blanket (MeV)/triton consumed; M = E/14; 7HO = homogenized version of Case 7.

[b]Low-temperature molten salt is 71.7 mol% LiF + 16 mol% BeF_2 + 12.3 mol% ThF_4.

[c]Standard deviation <2%.

Table 2-5. Comparison of the molten-salt/beryllium/helium unit cell values with those for the reference beryllium/thorium/lithium unit cell (values in parentheses).[a,b]

				Partitioning of energy in		
				MS		Fe tube
T	F	T + F_{net}	M	(or Th)	Be	(or Li)
1.22	0.97	2.16	1.95	72%	23%	4%[c]
(1.28)	(1.11)	(2.32)	(2.32)	(47%)	(26%)	(27%)

[a] U/Th = 0.11% (0.25%).

[b] Abbreviations: T = tritons bred/tritons consumed; F = fissile atoms bred/triton consumed; MS = molten salt.

[c] Neutron transport only.

compared for the 7-by-7 pitch case (#7) and the unit cell of last year's reference blanket. Also listed in Table 2-5 is the partitioning of energy in the various materials. The molten-salt values may change somewhat when gamma transport is included. Also activation-product decay heating is not yet included. Th-233 and Pa-233 should be the major contributors. Case 7HO is a homogenized version of Case 7. Comparing the two cases (7 and 7HO) gives an estimate of the error introduced by homogenizing the blanket for calculational simplification. The homogenized case over-predicts T + F by 6%.

Case 8 is the same as Case 7a except the 27 mol% ThF_4 salt is replaced by the lower melting point 71.7 mol% LiF + 16 mol% BeF_2 + 12.3 mol% ThF_4 salt. This change results in an 8% drop in T + F.

2.2.3. CYLINDRICAL MODEL

We initially used a simple radial-zoned cylindrical model to study the effects on performance of a finite-thickness blanket and first-wall structure. The model consists of an iron (Fe) first wall (1-cm thick and an inner radius of 150 cm) that is followed by a 59-cm-thick zone containing a homogenized mixture of the bed materials, as did Unit Cell 7HO. The outer radius of the bed (at 210 cm) is a radial leakage boundary. The DT plasma is modeled as a volumetric, cylindrical, isotropic, 14-MeV neutron source with a radius of 60 cm. Results of a TART calculation with this model are listed in Table 2-6. These results show that the ^6Li concentration must be increased to increase tritium breeding (T). This should also increase T + F.

The homogenized bed of the cylindrical model includes 0.8 vol% Fe to account for the molten-salt-containing tube walls. The few additional structure required for structural support and for helium ducting is not expected to reduce breeding (T + F) by more than a few percent, and its effect will be partially compensated for by reducing first-wall thickness, from the 1.0 cm assumed to a more reasonable value. These assumptions will be tested with a more exact model that will include the heterogeneous nature of the structure as well as the tubes.

It is also apparent that a thicker blanket including a moderator and/or reflector is needed to utilize the rather large radial leakage found in this case. For estimating T + F with this case, it is assumed that 80% of the leakage can be utilized.

Table 2-6. Cylindrical-model TART calculations.[a]

T	0.62
Th (n,γ)	1.04
Leakage (radial)	0.26
U (n, fission)	0.016
Th (n, fission)	0.008
U (n,γ)	0.0021
Total captures in bed	1.87
Energy (MeV)	21.6 (M = 1.54)
Total captures in first wall	0.122
$T + F_{net} \sim 0.62 + 1.02 + (0.8)\ (0.26)$	1.85

[a]All values are per 14 MeV source neutron. Standard deviation < 2%.

2.2.4. BLANKET PERFORMANCE ESTIMATE

A preliminary estimate of performance is made by combining results from the unit cell and the cylindrical models. This is done by weighting the cylindrical $T + F_{net}$ results by the T + F ratio from the heterogeneous (HET) unit-cell calculation and from the homogeneous (HOM) unit-cell calculation.

$$(T + F_{net})_{blanket} = (T + F_{net})_{cyl} \frac{(T + F_n)_{HET}}{(T + F_n)_{HOM}} = 1.85 \times \frac{2.16}{2.28} = 1.75\ (\pm 10\%) \quad .$$

Net fissile breeding can now be estimated by subtracting the required tritium breeding (T_{req}), assuming T_{req} is 1.06,

$$F_{net} = (T + F_{net})_{blanket} - T_{req} = 0.69\ (\pm 25\%) \quad .$$

The percent uncertainties listed are only a crude estimate and are not based on uncertainty analysis. Performing a similar exercise for blanket energy multiplication M resulted in an estimate for (M) of 1.60.

The next round of performance estimates for this blanket will be made with a more rigorous model that incorporates the heterogeneous nature of the molten salt in tubes and in a finite-thickness model that includes first walls, structure, moderators, and/or reflectors.

2.2.5. HEATING PROFILES

The cylindrical model was also used with TART to estimate the $(n + \gamma)$ heating profiles in the blanket. The profiles are tabulated in Table 2-7 and displayed in Fig. 2-12. For this case, the tubes have a 2.54 cm (o.d.) with a 7-by-7-cm pitch, thus the molten salt-containing tubes occupy 10% of the volume. The curve labeled P_{avg} is the result of a homogeneous calculation in cylindrical geometry. The curves labeled P_{tube} and P_{Be} are estimates of volumetric heating profiles in the tubes and the beryllium pebbles. They are calculated by weighting P_{avg} by unit-cell derived energy partitioning and volume fractions. Volume fraction of the beryllium is 45%. The fourth curve on the figure is the integrated energy deposition vs r in kilowatts per centimeter (kW/cm) of module length. This can be used to determine bulk temperature rise in the helium coolant. All curves are normalized to 1.0 MW/m^2 wall loading. The dashed portions of the curves are estimates of what will happen when the blanket is made thicker and a reflector is added. When doing the initial cut at the thermal hydraulics (TH), the dashed part of the curves were followed out to 210 cm.

The rigorous model will also be used to accurately determine the heating profiles.

Table 2-7. Power density in new Be-MS-Fe blanket at unit first-wall (FW) loading (first estimate)

$$PD = \frac{E}{V} \cdot \frac{1}{14.06} \cdot A_{FW} \cdot \Gamma^{a}$$

Zone No.	RI (cm)	E (MeV)	V (10^{-5} cm^3)	PD_{avg} (W/cm^3)	PD^{b}_{tube} (W/cm^3)	PD^{c}_{Be} (W/cm^3)	$\int_{Rfw}^{R} PD^{d}$ (kW/cm)
4 (FW)	150	1.46	3.78	10.4			
5	151	0.638	3.81	4.49	30.4	2.99	9.79
6	152	3.65					1.41
7	158	0.571	3.98	3.85	26.0	2.57	3.85
8		3.19					42.4
9	165	0.492	4.16	3.17	21.5	2.11	63.7
10		2.69					67.0
11	172	0.406	4.34	2.51	17.0	1.67	85.1
12		2.17					87.8
13	179	0.322	4.51	1.91	13.0	1.27	102.3
14		1.72					104.5
15	186	0.249	4.69	1.42	9.63	.95	116.0
16		3.13					117.7
17	209	0.628	5.27	0.143	0.96	--	138.7
18(leakage)	210	1.04					138.9
		21.8					145.8
		(M = 1.55)					

[a] $A_{FW} \cdot \Gamma = (2\pi\ 150 \times 400)\ 100 = 3.77 \times 10^{7}$.

[b] $PD_{tube} = PD_{avg} \times EF_{tube}/VF_{tube} = PD_{avg} \times 0.7/0.103 = PD_{avg} \times 6.77$.

[c] $P_{Be} = P_{avg} \times EF_{Be}/VF_{Be} = P_{avg} \times 0.3/0.45$.

[d] (4) $$\int_{R_{FW}}^{R} PD = \frac{\sum_{R_{FW}}^{R} E}{14.06} A_{FW} \cdot \Gamma = \sum^{R} E \frac{2\pi 150}{14.06} \times 1 \times 100 = \sum^{R} E\ 0.6703.$$

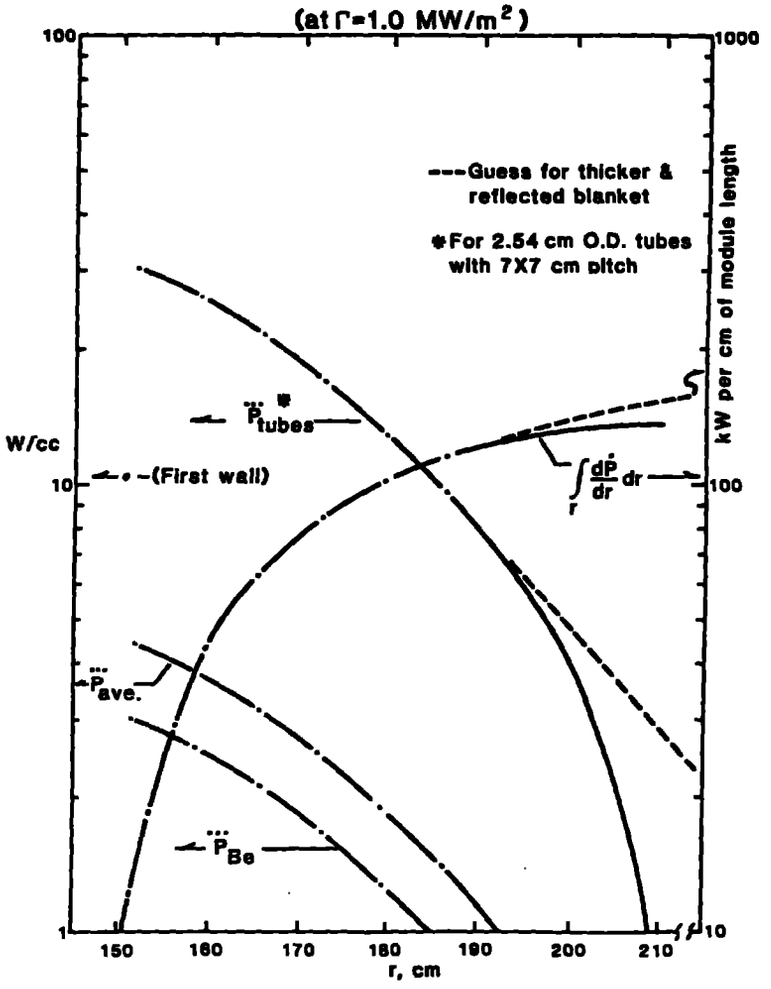

Figure 2-12. First estimate of power densities in beryllium/molten-salt blanket.

2.3. THERMAL HYDRAULICS

2.3.1. SALT IN MOLTEN STATE (NO FROZEN LAYER)

It is possible to arrange the chemical constituency of the molten salt (LiF 70 m/o + BeF_2 12 m/o + ThF_4 18 m/o) so that its melting point is 530°C. This may permit operation of the salt-tube in beryllium-pebbles blanket at conditions where no frozen salt layer exists on the inside surface of the salt tubes.

The variation of volumetric power generation with distance from the first wall is shown for a 1 MW/m^2 first-wall flux in Fig. 2-13. Because our design is for 2 MW/m^2, all values read from this curve must be doubled.

Estimation of temperatures in the blanket involves the following relationships:

- How much of the total blanket energy is deposited in the coolant when it reaches the radial location of interest? This allows calculation of the coolant temperature at that point.
- What is the film coefficient of heat transfer on the outside of the tube? This permits calculation of the film temperature drop corresponding to the rate of energy deposited in the salt ($\dddot{q}_s$).
- What thermal resistance does the tube wall offer? This allows calculation of the wall drop corresponding to the same $\dddot{q}_s$ as in the foregoing .
- What temperature difference develops from the tube centerline to the tube wall? This permits estimation of the maximum salt temperature for a given $\dddot{q}_s$. This salt temperature should be at a safe margin from the boiling point. The boiling point of flibe at atmospheric pressure is 1267°C. At 50 atm it is about 1810°C. We assume our salt composition has similar boiling points.

The temperature difference through the helium-coolant film on the outside of the steel tube varies with the tube diameter, so long as the film coefficient may be assumed constant in the tube size range of interest -- namely 0.5 to 2.0 cm in diameter. We believe this assumption is valid, since the independently calculated h_c values for balls and for tubes in that size range are very close, 0.2 ($\pm$ 20%) $W/cm^2 \cdot °C$ when surface roughening is taken into account. There is significant variation of h_c around each tube;

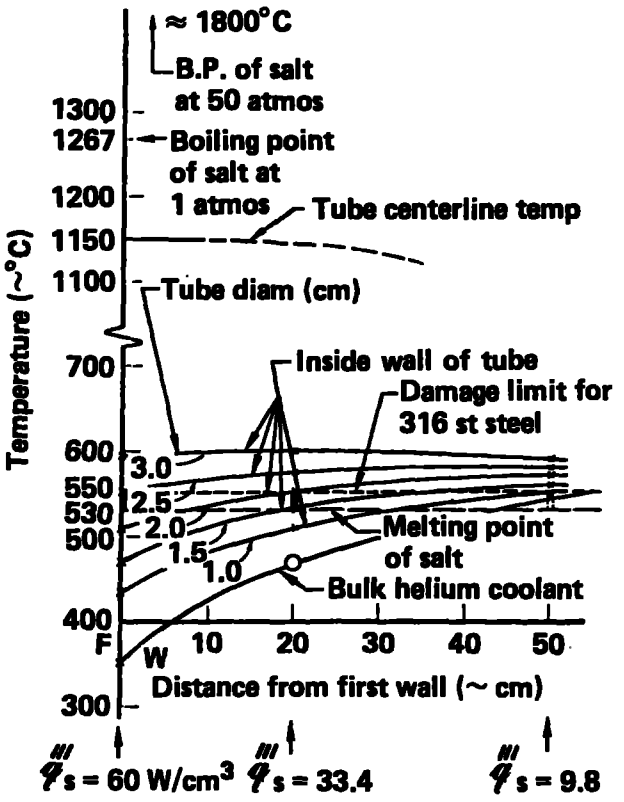

Figure 2.13. Helium coolant and salt-tube temperature versus position in blanket.

however, the slowly flowing salt will average this variation. Since our packed bed is a mixture of balls and tubes of comparable size we believe that the same surface heat-transfer coefficient should apply to all surfaces in the bed.

Heat removed from the salt crosses four thermal resistances: (1) conductive resistance of the salt, (2) the tube wall, and (3) two film drops (one outside and one inside the tube). If the salt were in the solid state, its own low thermal conductivity would result in large temperature differences between the salt near the tube centerline and the salt near the wall. But our salt is liquid, hence mobile. Its density varies approximately as

$$\rho \left(\frac{g}{cm^3}\right) = 3.87 - 8(10^{-4})\, T(^{o}C) \quad .$$

We have calculated the expected rate of circulation within the salt tubes. If one assumes a temperature difference from tube centerline to wall of 500°C -- a tolerable number to stay far from the salt's boiling point -- it can be shown that circulation rates across the tube have characteristic velocities of 30 to 40 cm/s. These flows will be somewhat suppressed by MHD forces since the salt is an electrical conductor. Even if the true circulation rates are one-tenth those calculated, i.e., 4 cm/s, this rate of circulation inside a 1- to 2-cm-diam tube represents a substantial mixing mechanism. We believe temperature differentials within the molten salt can be maintained under 500°C by this natural convection process.

Salt throughput velocity is 10 cm/s. The vortex velocity because of density difference is approximately 15 cm/sec perpendicular to the tube axis. Total velocity near the tube wall is then about 17.5 cm/s. With laminar boundary-layer theory, we calculate a surface coefficient of about 0.22 W/cm^2-°C. Near the first wall this converts to 67°C film drop for a 1-cm-diam tube and 135°C for a 2-cm-diam tube. The relationship is linear between tube diameter and film ΔT for a given volumetric heating rate in the salt.

If the salt internal temperature difference is less than 500°C, the circulation rate will be smaller. That will cause a lower surface film coefficient and a higher film temperature drop at the tube's inside surface. These opposing effects lead us to conclude that 600 °C is a high (conservative) estimate of the temperature difference between salt at the tube

centerline to that at the tube inner surface, for tubes near the first wall. As tubes further back in the blanket are considered, the free convection velocity within a tube will probably be lower, since the volumetric power into the salt is less. This reduces the film coefficient at the tube's inner surface, but since fewer watts per unit area need be transmitted, the film temperature drop will be little changed.

We have assumed coolant inlet temperature at 300°C and have estimated that in flowing radially inward to the first wall and in cooling that first wall the bulk coolant temperature increases 55°C.

The expression for the average temperature drop in the coolant film on the outside of the salt tube becomes

$$\Delta T_f = 75d \ (^{o}C) \ ,$$

where d is the salt tube diameter in centimeters. Similarly the tube-wall temperature drop is expressed as

$$\Delta T_t = 3.7d \ .$$

This assumes constant wall thickness of 0.05 cm and thermal conductivity for the Type 316 stainless steel at 0.21 W/cm°C.

When all the temperature differences are summed, a plot such as that shown in Fig. 2-13 results. On this plot, we show points for a range of tube diameters at various depths into the blanket. The shaded area defines a "window" of acceptable tube sizes, bounded by the melting temperature of the salt (530°C) and the acceptable operating temperature for the stainless steel as a result of neutron-induced damage effects that are a function of temperature. That temperature of 550°C is not a "sharp" limit. Temperatures as high as 600°C may be tolerated.

The power per unit volume ($\dddot{q}_s$) deposited in the salt can be obtained from Fig. 2-14, remembering that our first-wall flux is 2 MW/m^2 and that values read from the curve must be doubled. At the first-wall, $\dddot{q}_s$ is 60 W/cm^3; at 20 cm from the first wall, it is 33.4 W/cm^3; and at 50 cm, it is 9.8 W/cm^3.

Figure 2-13 is interpreted as follows: just behind the first wall, the tube diameter must be between 2.2 and 2.4 cm. Twenty centimeters further back in the blanket, the tube size must lie between 1.4 and 1.9 cm. Near the back of the blanket, the tubes must be quite small -- no larger than 1 cm. A practical lower limit is from 0.5 to 0.8 cm in diameter.

At the back of the blanket, the present design restricts the temperature of the bulk coolant entering the return plenum to 545°C. Reduction in film

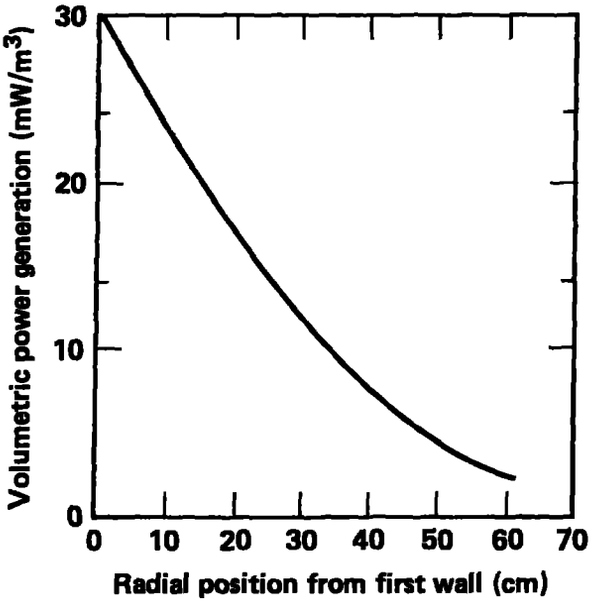

Figure 2.14. Spatial volumetric power generation in molten-salt tube at neutron wall loading of 1 MW/m^3.

temperature drop would allow higher-bulk coolant temperature without exceeding tube material temperature limits. This larger coolant temperature rise equates to lower coolant flow rate. Both effects promote higher plant electrical output. Higher temperature improves cycle efficiency. Lower flow rates reduce coolant pumping power ($MW = k \times Q^3$!).

The film temperature drop inside and outside the tubes can be reduced by decreasing the power density in the salt. This can be simply accomplished by increasing the fraction of salt in the desired zone. Virtually the same total amount of energy would be deposited in the zone, so that the $\dddot{q}_s$ would be inversely proportional to the amount of salt present. Larger diameter tubes at a greater grid spacing (to maintain free beryllium pebble flow) accomplishes this. More salt results in less beryllium in a specified zone. Breeding will be slightly reduced because of lower neutron multiplication.

The tube diameters probably need not exceed 3 to 4 cm so as not to experience excessive temperature difference from tube centerline to wall. As previously discussed, a strong convective mixing will be caused by temperature-induced density difference. The salt electrical conductivity is quite low. If the convection is greatly reduced by MHD effects, the temperature difference determined only by thermal conductivity might exceed 700 or 800°C between a tube centerline and the steel wall. We have not yet attempted to include MHD effects in our thermal-hydraulic calculations.

2.3.2. THERMAL HYDRAULICS FOR CASE OF FROZEN SALT LAYER

Early in this study we chose a 27 mol% ThF_4 salt with a melting point of 565°C because of high breeding as a result of less parasitic neutron capture. Later, to get a lower melting-point salt, we compromised and chose the 18% salt. The thermal hydraulic analysis for the frozen salt layer case is included here, because we may wish to return to the frozen layer concept.

The volumetric power generation in a molten-salt tube as a function of radial position from the first wall is given in Fig. 2-14, which is a replot of Fig. 2-12, for a neutron-wall loading of 1 MW/m^2. (Note: the design value is 2 MW/m^2.)

Using this power generation distribution, we give in Fig. 2-15 the temperature of the molten-salt centerline and of the tube wall at the hottest

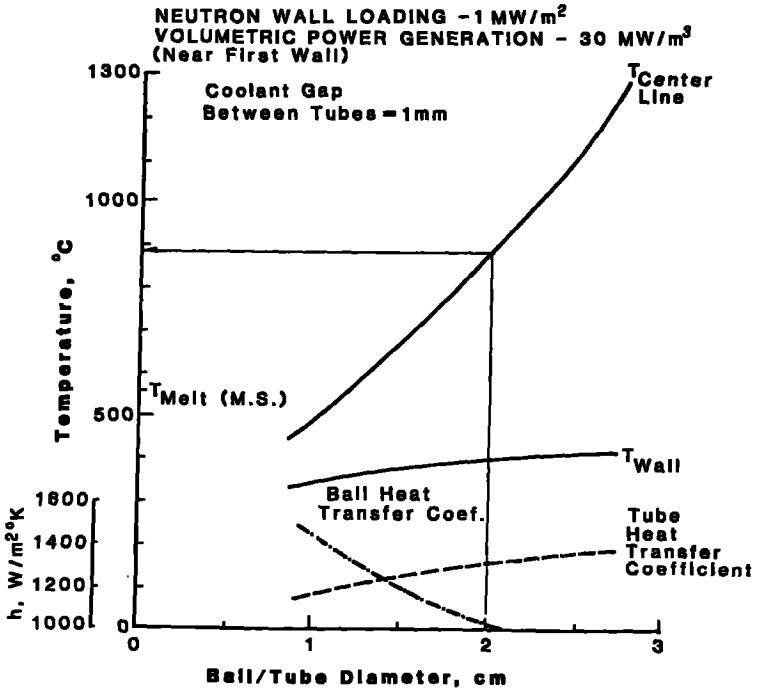

Figure 2.15. Tube wall and centerline temperatures as a function of tube diameter.

location near the first wall as a function of tube diameter. The heat-transfer coefficient for a single row of tubes spaced 1 mm apart is used for the calculation. The dimension of 1 mm is selected as a reasonable minimum gap that can be maintained by wire-wrap. The coolant used for this calculation is helium at 50 atmospheres, with an inlet/outlet temperature of 285/550°C, which can give a thermal cycle efficiency of 39%.[2-5] As indicated in Fig. 2-15, the average tube-heat transfer coefficient is similar to that of a packed bed of 1.3-cm diam balls. Fig. 2-15 shows that at a neutron wall loading of 1 MW/m^2, the tube wall temperature is well below the melting point of molten salt at 565°C, indicating a frozen salt layer on the wall, which may help to protect the wall from corrosion. In this and the following calculations, the corresponding thermal conductivities used for beryllium, molten-salt (71 LiF-2 BeF_2-27 ThF_4) and tube-wall (2-1/4 Cr-1 Mo) are 75.0, 0.7, and 33.0 W/m•K, respectively. Elsewhere we have chosen type 316 stainless steel for the tubes. Perhaps the choice should be given more thought.

As indicated in Fig. 2-15, at a fixed gap width of 1 mm, the cross-flow packed-tube heat-transfer coefficient[2-6] increases as a function of tube diameter and for a packed bed of fixed void fraction of 0.4, its heat-transfer coefficient[2-5] decreases as a function of ball diameter.

For a tube diameter of 2 cm, the temperature distribution of the molten-salt tube is given in Fig. 2-16 as a function of blanket radial position. The tube centerline temperature decreases as a function of distance from the first wall because of the decrease in volumetric power generation. The wall temperature increases toward the back of the blanket and is less than 10°C above the helium outlet temperature at the exit. At a coolant outlet temperature of 550°C the molten-salt tube at the back of the blanket will exceed 550°C. To reduce this temperature, the helium outlet temperature can be reduced to somewhat below 550°C without severely impacting the thermal cycle efficiency. To reduce the reactor size, it is also of interest to increase the neutron wall loading. At a wall loading of 2 MW/m^2, Fig. 2-17 shows the molten-salt tube temperature at the centerline and wall as a function of tube diameter and tube radial position. As indicated in Fig. 2-17, with the tube sizes considered and a coolant outlet temperature of 500°C, the tube wall temperature always stays below the melting temperature of the molten salt.

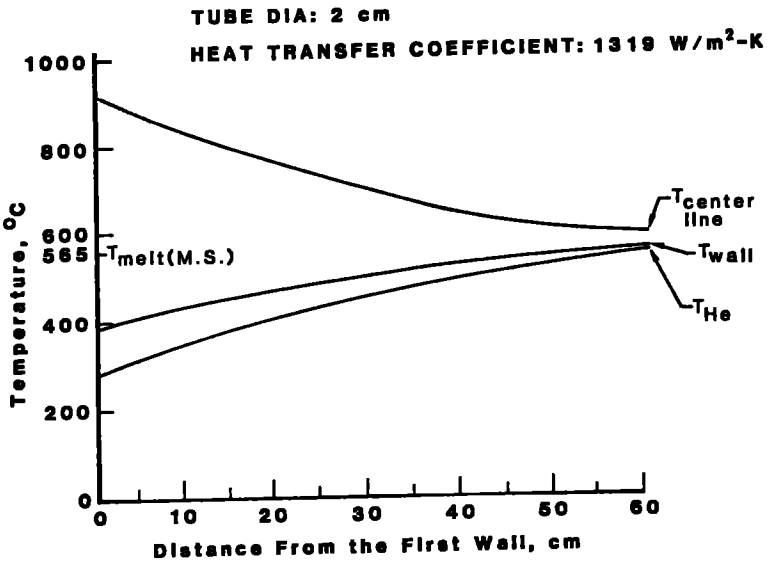

Figure 2-16. Temperature distribution for molten-salt tube at a neutron wall loading of 1 MW/m^2.

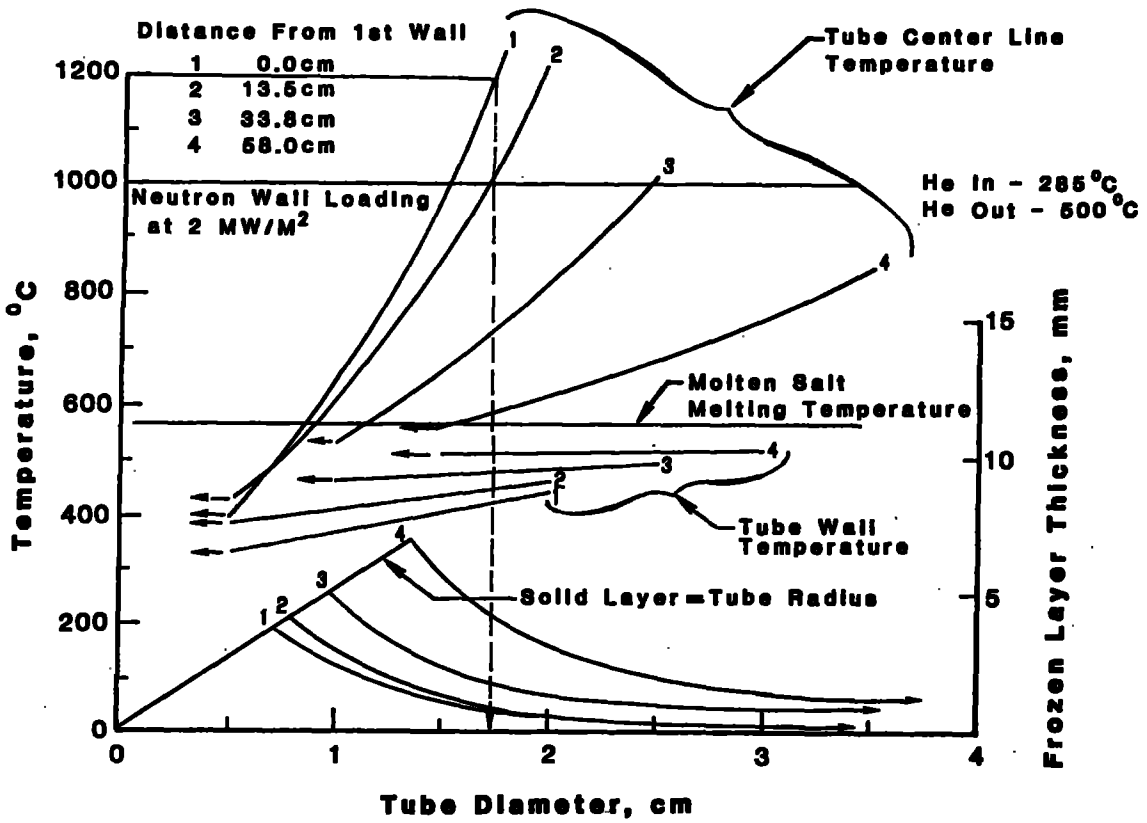

Figure 2-17. Temperature of molten-salt tube and thickness of molten layer as functions of tube diameter.

This means that a solid layer of the salt would be formed on the inside of the tube. The thickness of the molten-salt solid layer inside the tube as a function tube diameter and radial position is also indicated in Fig. 2-17.

In calculating the solid layer thickness, we approximated the natural convective heat transfer of electrically conducting fluid in a magnetic field by assuming a magnetic-laminar-flow Nusselt number of 8.23.[2-8] Convection would enhance the fluid heat transfer by a factor of 2 over purely conductive heat transfer. This interpretation was compared by calculating the modified Peclet number Pe[2-9], which gives the ratio of convective to conductive heat transfer in a uniform magnetic field. At a magnetic field of 4 T and a characteristic dimension of 2 cm, Pe = 2.15 was calculated for FLiBe, which agrees well with the above model. Note from Fig. 2-17 that with a tube diameter of 1.75 cm, the maximum molten-salt temperature is 1200°C, the maximum tube-wall temperature is less than 550°C, and the solid layer maximum thickness is 4 mm.

A potential heat-transfer problem for this design is that hot spots may be generated near or at the contacts between the balls and tubes. A possible way of relieving the problem is by ribbing the tubes as shown in Fig. 2-18. This can reduce the solid-contact area and at the same time increase the heat-transfer surface area of the molten-salt tubes.

For the blanket configuration considered here, the pumping power for the helium blanket loop, including the steam generator side, can amount to $\sim$ 4% of the reactor thermal power. This would give a net thermal-cycle efficiency greater than 36%.[2-5] The estimated percentage of pumping power fraction breakdown of the helium power conversion loop is given in Table 2-8. The blanket pumping power dominates the total helium loop pumping power.

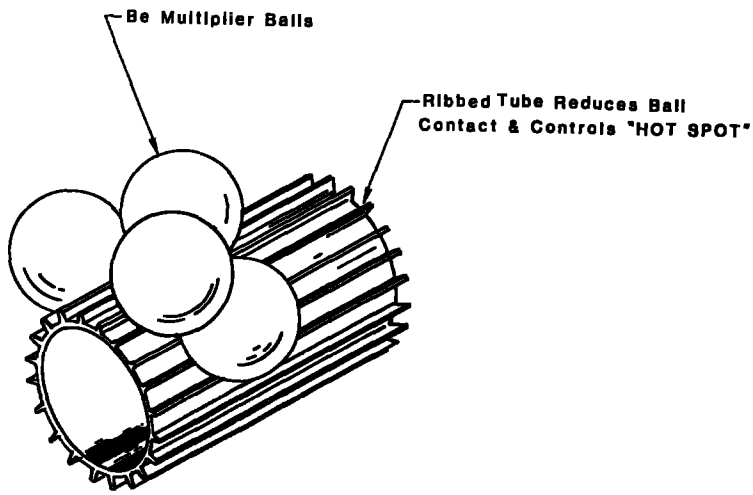

Figure 2-18. Ribbed-tube design.

Table 2-8. Estimated helium-loop pumping-power distribution.

Components		Pumping-power fraction[a] (%)
Blanket		3.1
Friction	1.4%	
Turning, joining, and dividing	1.3%	
Expansion and contraction	0.4%	
Sector lines; collection-ring ducts		0.1
Steam-generator piping		0.2
Steam generator		0.7
TOTAL		4.1

[a]Pumping-power fraction = pumping power/reactor thermal power.

2.4. SELECTION AND PROPERTIES OF MATERIALS

2.4.1. SALT COMPOSITION AND PROPERTIES

From a neutronics point of view we would like to maximize the ThF_4 concentration; however, higher ThF_4 concentrations raises the melting temperature (see Table 2-9). The Molten Salt Reactor Experiment work was all with 12% (molar). We have considered using 27% ThF_4. The present design uses an intermediate composition of 18% which gives a melting point of 530°C.

Table 2-9. Composition and properties of the blanket salt, using three concentrations of ThF_4.

Composition (mol%):	LiF	72	70	71
	BeF_2	16	12	2
	ThF_4	12	18	27
Liquidus (°C)		500	530	565 ± 5
Properties at 600°C:				
Density (g/cm^3)		3.35	3.87	5.04 minus 8×10^{-4} T, where T is in °C
Liquid heatcapacity (cal/g·°C)		0.33	-	0.23 ± 5%
Viscosity (centipoise)		12		15 to 25
Vapor pressure (torr)		< 0.1		-
Thermal conductivity (W/cm·°)		0.011		0.007 ± 25%
Heat of fusion(cal/g)		63		54
Electrical conductivity(Ω·cm)		2.12		--
Expansion on melting (vol%)				∿ 5

2.4.2. RADIATION DAMAGE AS BASIS FOR CHOICE OF AUSTENITIC STEEL

Austenitic steel was chosen for this design. The arguments are discussed in 1983 by Abdou et al.[2-4] The maximum operating temperature is 550°C, which is somewhat arbitrarily chosen to avoid excess helium embrittlement. The lifetime is 100 dpa (about 8 MW•y/m^2 or 5.7 years at 2 MW/m^2 and 70% availability), after which time runaway swelling is predicted. With the austenitic steel there is no minimum temperature and no ductile-brittle transition above room temperature. Also, no special heat treatment of welds is necessary. The corrosion aspects are discussed in the next two sections.

2.4.3. ANALYSIS OF RELEVANT CORROSION DATA

The first nuclear reactor fueled by a molten salt, the Aircraft Reactor Experiment, was operated in 1954. The reactor circulated a molten mixture of NaF, ZrF_4, and UF_4, using Inconel 600 as the containment material. Further development led to the operation of the Molten Salt Reactor Experiment (MSRE) in 1965. This reactor was fueled with the molten salt mixture ^7LiF-BeF_2-ZrF_4-UF_4, was moderated with graphite, and used Hastelloy N as the containment material. In the period between 1965 and the termination of the project in 1973, development studies were aimed at a molten salt breeder reactor (MSBR) based on a Li_2BeF_4 solvent containing 0.3 mol% UF_4 and 12 mol% ThF_4. Hastelloy N, the reference material for the MSBR, was used for constructing the supporting engineering and fuel-reprocessing test assemblies. This latter testing experience, combined with four years of operational experience in the MSRE and some eight years of developmental testing prior to the MSRE, provides one of the largest data bases ever assembled for a reactor material ahead of commercialization.

The suitability of Hastelloy N for MSBR service largely pre-empted the testing of alternative alloy systems. Limited irradiation tests of type 316 stainless steel were completed to compare the degree of embrittlement induced by thermal neutrons with that induced in Hastelloy N. A type 316 stainless steel thermal-convection loop (TCL), discussed below, was operated with Li_2BeF_4 to determine the suitability of stainless steels for containment of nonfuel-containing salt. Two other stainless steel TCLs, one of 304L and the other of 316, were operated with UF_4-containing salt to provide a

baseline corrosion rate for iron-based alloys under nominal MSBR operating conditions. The latter loops provide a relevant, if limited, set of corrosion experiments from which to assess the potential of austenitic stainless steels as containment materials for the molten-salt fusion reactor blanket. However, even more important is the detailed understanding of the corrosion mechanisms and kinetics acquired in the testing of Hastelloy N, which can be used to predict the corrosion behavior of alternative alloy chemistries.

The selection of a practical containment material for molten fluoride salts begins with a consideration of the reduction-oxidation potentials of the component elements of the container with respect to components of the salt. Table 2-10 shows the electrode potentials of relevant alloying elements compared against a standard $HF(g)/H_2$ electrode. We see that molybdenum and nickel each have lower oxidation potentials than iron and that all three of the latter elements have considerably lower potentials than chromium. Thus, in the absence of passivation, chromium will be the most reactive toward fluoride ions among the major alloying elements used commercially for high temperature alloys. The electrode potentials of various couples of thorium, protactinium, uranium, and plutonium in molten Li_2BeF_4 are indicated in Fig. 2-19.[2-10] The salt oxidation potential for which Hastelloy N was developed (and that maintained in the MSRE) is shown by the shaded region in Fig. 2-19. Under the latter condition, the predominant ionic species are Th^{4+}, Pa^{4+}, U^{4+}, with some U^{3+} and Pu^{3+}. Figure 2-20[2-10] shows a Pourbaix diagram in which solubilities of Cr, Fe, and Ni in $LiF-BeF_2-ThF_4$ (72 Nb-12 mol%) are shown as a function of the redox potential of the salt, expressed as the U^{4+}/U^{3+} molar ratio. Also shown are the oxygen solubility limits for the formation of oxides of Cr, Fe, Ni, Th, and U, respectively. Note that only chromium can exist at measurable concentrations in the melt when the U^{4+}/U^{3+} ratio is below about 100. Note also that precipitation of structural metal or fuel component oxides is not significant at U^{4+}/U^{3+} ratios below 100 unless the oxide mole fraction exceeds 10^{-3}.

The chemistry of Hastelloy N has been tailored to achieve compatibility with UF_4- and ThF_4-containing salt mixtures by simply allowing the salt to "equilibrate" with the alloy. In any heat transfer system, true equilibrium between the salt and the alloy can never be attained because of temperature differences in the system. Nevertheless, in a Hastelloy N closed-loop system

Table 2-10. Electrode potentials[a] of container materials in Li_2BeF_4 (600°C).

	Cr^{2+}/Cr^0	Fe^{2+}/Fe^0	Mo^{3+}/Mo^0	Ni^{2+}/Ni^0
Potential (V)	-0.45	-0.08	∿ 0	0.37

[a] $HF(g)/H_2$ = zero volts.

charged with UF_4-containing salt at 600 to 700°C, a steady-state U^{4+}/U^{3+} ratio (shown experimentally to be in the range 100 to 350 is attained within a few hundred hours. Under these conditions, corrosion proceeds by the selective oxidation of chromium at the hottest loop surfaces and by reduction and deposition of chromium at the colder loop surfaces as a consequence of the redox reaction

$$2\ UF_4 + Cr \rightleftharpoons 2\ UF_3 + CrF_2\ .$$

In the case of the MSRE and MSBR fuel salts, the resultant maximum corrosion rate of Hastelloy N is well below 2 μm/year at 704°C (1300°F).

If a 300-series austenitic stainless steel is exposed to UF_4-containing salts under the same closed-system conditions described above, corrosion again is manifested by the selective removal of chromium from hot-leg surfaces and concommitant chromium deposition at cooler surfaces. However, because of the much higher chromium activity in the stainless steel compared with that in Hastelloy N, the extent of chromium mass transport for stainless steels is considerably greater than for Hastelloy N. Table 2-11 lists the operating conditions of two stainless steel thermal-convection loops[2-6] that circulated lithium-beryllium salts containing 1 mol% and 0.3 mol% UF_4, respectively. The former loop was constructed of type 304L stainless steel and yielded corrosion data over a nine-year period. Corrosion was selected toward chromium and was controlled by the solid-state diffusion rate of

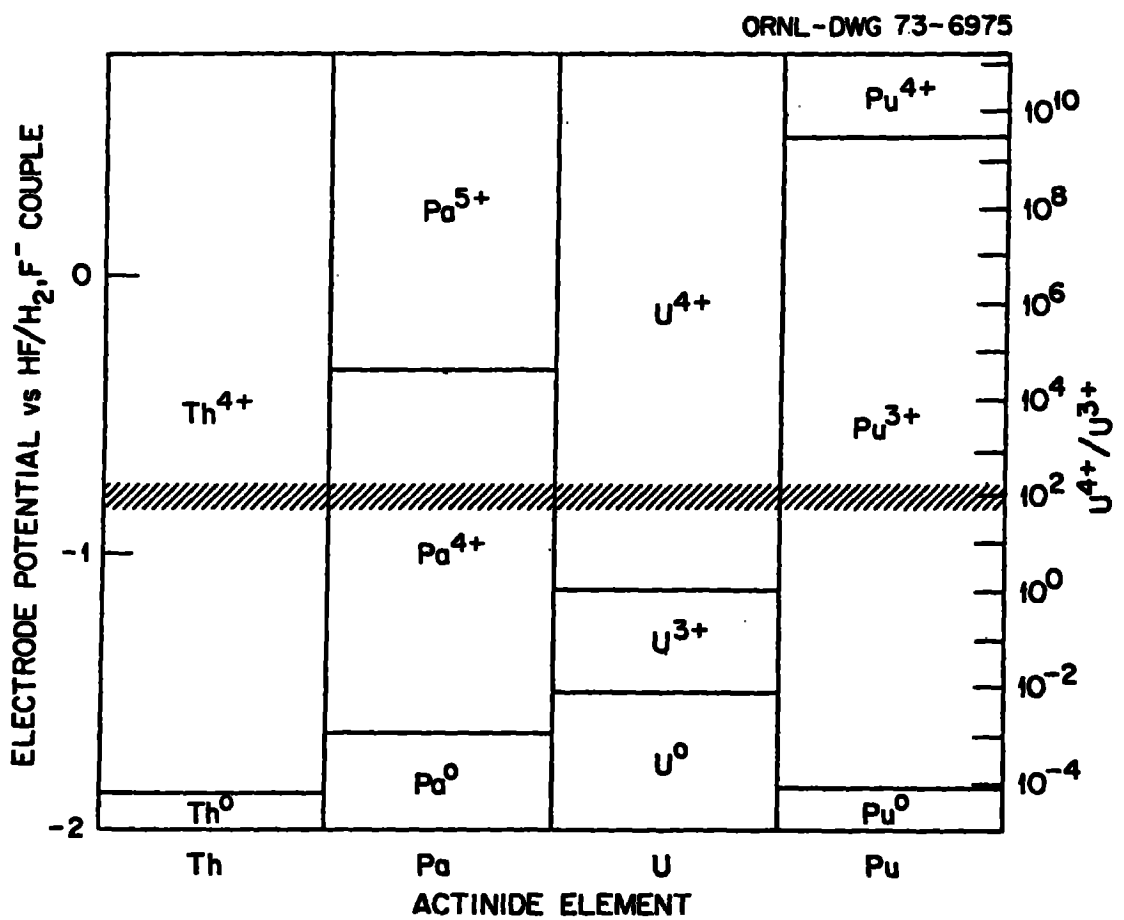

Fig. 2-19. Oxidation states of the actinides in Li_2BeF_4 at 600°C. (Ref. 2-10).

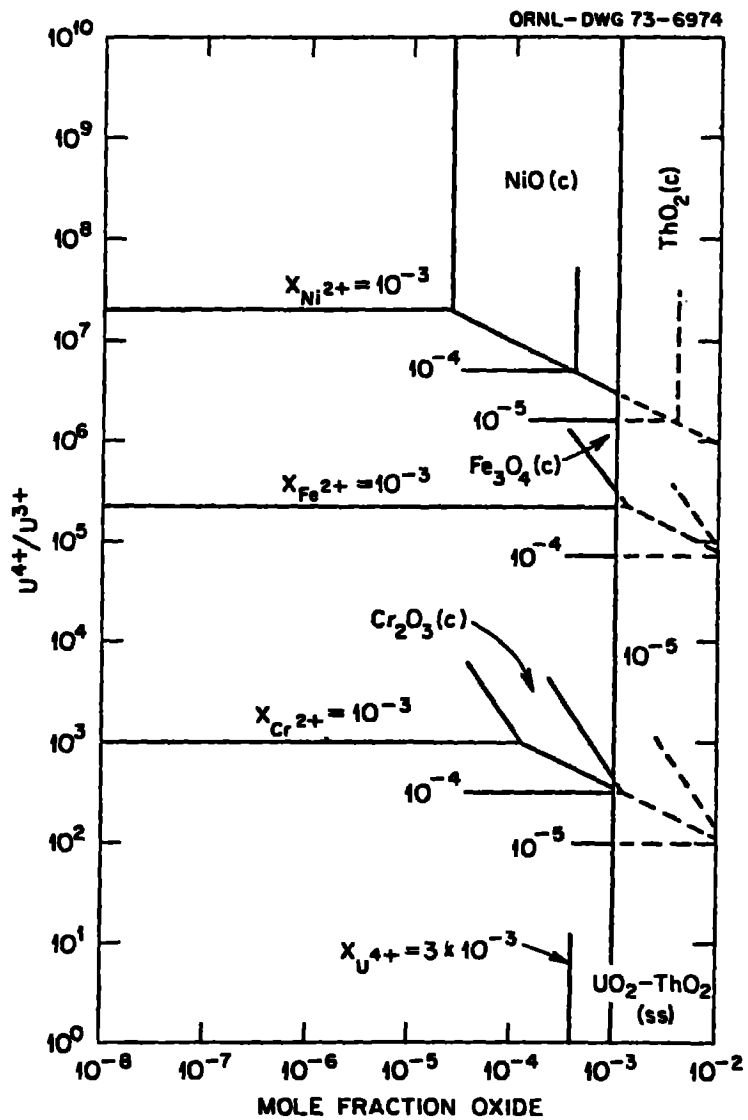

Fig. 2-20. Pourbaix diagram for structural metals in LiF-BeF_2-ThF_4 (72-16-12 mol%) at 600°C (Ref. 2-10).

Table 2-11. Operating conditions of stainless steel thermal-convection loops involving LiF-BeF_2-based molten salts (Refs. 2-11 and 2-12).

Loop material	Salt composition (mol%)	Temperature Maximum (°C)	Temperature ΔT (°C)	Time (h)
304L SS	LiF-BeF_2-ZrF_4-ThF_4-UF_4 (70-23-5-1-1)	688	100	83,520
316 SS	LiF-BeF_2-ThF_4-UF_4 (68-20-11.7-0.3)	650	110	4,490
316 SS	LiF-BeF_2 (66-34)	650	125	25,100

chromium (parabolic time dependence). Although the weight loss over the nine-year period was relatively small (equivalent to an average uniform corrosion rate of 21.8 μm/year at 688°C), corrosion was manifested as subsurface voids that extended several millimeters below the surface. The second loop shown in Table 2-11 was constructed of type 316 stainless steel and operated for 4490 hours. The corrosion rate of this loop was slightly lower than the 304L stainless steel loop during the equivalent time period. However, corrosion again was manifested by subsurface voids, in this case to a depth of 26 μm at 650°C.

2.4.4. CORROSION PROPERTIES OF THE TMHR BLANKET

The corrosion data discussed above indicate that the rate of thermal gradient mass transport of austenitic stainless steels caused by the Cr-UF_4 redox reaction is solid-state diffusion limited and, therefore, is relatively

slow. Nevertheless, the depletion of chromium at the hotter surfaces can be expected to degrade the mechanical properties of the steels as the operating period exceeds about one year. It is possible, however, to significantly lower these rates by (1) reducing the chromium concentration of the steel and (2) reducing the redox potential (i.e., U^{4+}/U^{3+} ion activity ratio) in the salt. The effectiveness of the first approach can be seen by examining the corrosion rate of a maraging steel (12% Ni, 5% Cr, 3% Mo, balance Fe) that was tested[2-6] as a coupon in the 304L loop listed in Table 2-11. The average corrosion rate of this steel during a 5700 h exposure at 662°C was a factor of 2 lower than that of 304L stainless steel at the same loop position. The effectiveness of controlling the redox potential of the salt is illustrated by corrosion-rate data obtained from the third stainless steel loop[2-12] with operating conditions listed in Table 2-11. In this latter type 316 stainless steel loop, no uranium was contained in the salt, and the redox potential was adjusted by buffering the salt with metallic beryllium. Before adding the beryllium, the corrosion rate of the 316 stainless steel under closed system conditions averaged 8 μm/year at 650°C. After contacting the salt with a small metallic beryllium rod, the corrosion rate was lowered to 2 μm/year over a 2000-h test period.

Corrosion may also be induced by the intense radiation fields within the blanket (e.g., through radiolytic decomposition of the fluoride salts) or by neutronic transmutations involving lithium, beryllium, and fluorine. Fortunately, $LiF\text{-}BeF_2$ based salts appear to have good radiation stability provided the salts are kept at temperatures in excess of 150°C, and it has been shown by means of extensive in-reactor testing that under these conditions radiolytic decomposition processes do not lead to enhanced corrosion of structural metals.[2-13] Chemical transmutations lead to production of excess fluorine in the molten salt (thereby rendering it more oxidizing towards its container), however this increase in corrosion potential can be avoided by inclusion of a suitable redox buffer (e.g., C_e^{3+}/C_e^{4+}) in the melt.[2-14]

The selection of type 316 stainless steel as the reference material for the TMHR piping is predicated (1) on acceptable mechanical properties following high-fluence neutron exposures and (2) on acceptable corrosion resistance in $LiF\text{-}BeF_2$ salts containing uranium under controlled oxidation conditions. Based on the corrosion studies discussed above, the UF_4:UF_3

molar ratio in the salt must be maintained at a somewhat lower value than that which occurs naturally in a closed system charged with UF_4-containing salt. This can be accomplished by chemical buffering, e.g., contacting the salt with a reactive metal such as chromium. (Such a buffering step is also required to control the buildup of oxidants in the salt that accrues from transmutation reactions, as discussed in Section 2.2.) There is, however, a lower limit on the UF_4:UF_3 ratio that is set by the disproportionation of UF_3 through the reaction $3\ UF_3 \rightarrow 4\ UF_4 + U^0$. The lowest UF_4:UF_3 ratios attained during sustained exposures of Li_2BeF_4 salts have been on the order of 10, and no measurable UF_3 disproportionation has occurred under these conditions. Lower ratios may, therefore, be feasible; however, a ratio of 10 represents a relatively reducing condition from the standpoint of UF_4-316 stainless steel chemical interactions (see, for example, Fig. 2-20) and is considered adequate for TMHR at the proposed time and temperature conditions.

In summary, corrosion tests of 316 stainless steel have not yet been conducted under the exact conditions and salt chemistries specified for the TMHR. Nevertheless, there is an extensive background of relevant information, concerning molten-fluoride salt-corrosion mechanisms and operating requirements, that provides a rational basis for the TMHR blanket design.

2.5. START-UP SCENARIO

The problem of start-up of molten-salt systems results from the large difference between the inlet helium coolant temperature of around 300°C and the melting point of the salt at 530°C (490 to 565°C for the range of compositions under consideration). If the molten salt were pumped into the blanket with the fusion neutron source off, the salt would freeze in the pipes. Later melting could break the steel pipes because of the 5% volumetric expansion upon melting. Once the reactor is operating, the nuclear heat generation in the salt keeps its temperature above the melting point. At the front of the blanket where the helium is coldest (300°C) the heat generation is highest, and we predict helium film drops (not to mention the film drop in the salt) of over 200°C. So, in principle, if one can start up, there is no problem under normal conditions. At shut down the problem is fundamentally easier to handle than start-up because of the decay nuclear heating. However, freeze-up still can occur.

Two possible approaches to start-up will be discussed. The first (reference case) is to raise the helium inlet temperature to just over 530°C, introduce the salt and then program the inlet temperature down as the neutron source is brought on. The second case (backup) requires introducing the salt at the same time as the neutron source is brought on. In either start-up approach, the salt would be drained at shut down. If the salt will gravity drain at 0.1 m/s and the mean pipe length is 20 m, then the entire blanket can be drained in 200 s. We propose to force circulate the salt with pumps at over 0.1 m/s to process out the tritium; hence the pipe system will be so constructed as to allow rapid circulation and drainage. The important point seems to be to keep the steam generator operating near its design point (∿ 500°C helium inlet and ∿ 300°C helium outlet). This can be done with a helium preheater as shown in Fig. 2-21, which is valved out of the circuit after start-up.

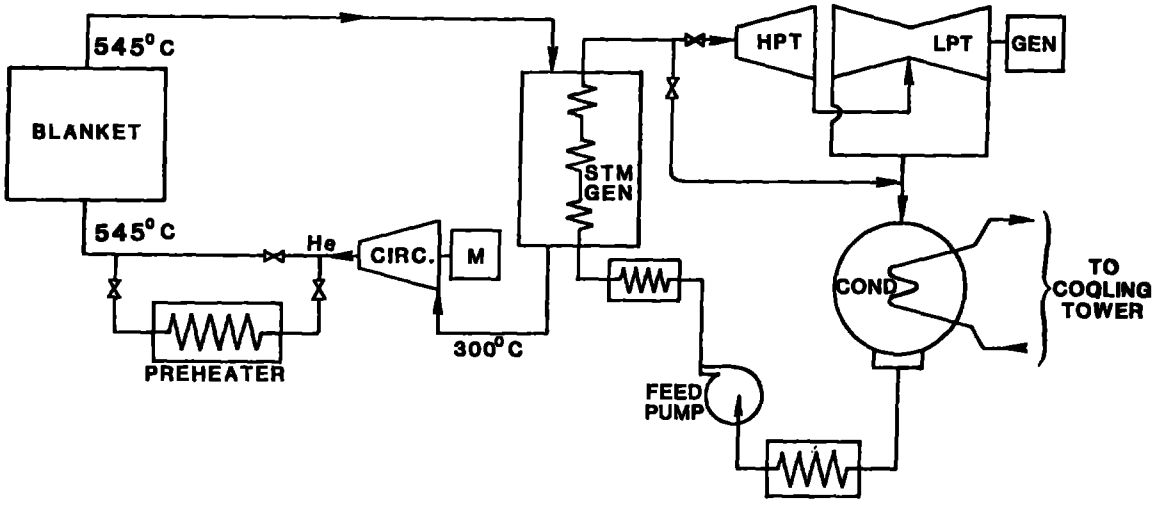

Figure 2-21. Start-up scenario.

Reference Start-Up Method

This method involves preheating the entire blanket to a temperature 15°C above the melting point of the salt (530°C + 15° = 545°C, for example). The sequence is as follows:

1. The blanket is preheated (over a period of hours) by circulating helium through a preheater: The helium inlet temperature is 545°C and finally the outlet will be 545°C. Steam is generated in the steam generator at a low rate to reduce the helium temperature to 300°C at the circulator inlet.
2. The preheated salt is introduced into the blanket and continues to circulate.
3. The neutron source is brought on slowly.
4. Simultaneously, the inlet temperature of the helium is lowered by controlling the amount of helium preheat.
5. The helium circulator speed is controlled to keep the outlet temperature of the helium at 545°C.
6. For planned shutdown the salt would be drained and the helium circulators slowed down to remove decay heat from structural material.
7. Steam generated in the steam generator would be condensed in the condenser.

Backup Method for Start-Up

In this method we simultaneously introduce the salt as the neutron source is brought on. The sequence is as follows:

1. The blanket is preheated over hours by circulating helium. Friction losses will be sufficient to warm up the helium and blanket mass to 300°C. No steam would be generated in the steam generator.
2. The neutron source is slowly brought on, perhaps by starting up the plasma to a fraction of full density and temperature and raising the ratio of deuterium to tritium.
3. The preheated salt is introduced into the blanket at a temperature 20°C or so above the melting point.
4. The helium circulators are speeded up as the power increases, keeping the outlet helium temperature close to the 545°C design value.
5. For planned shut down, the salt would be drained and the helium circulators slowed down to remove decay heat from structural material.

Rapid Shutdown

1. Begin salt draining.
2. Slow down circulators. (Some salt freezes on walls while the neutron source is off, and cool helium is circulated).
3. Allow any frozen layer to melt and drain.

2.6. SAFETY

In the molten-salt fusion-breeder, we have come very close to achieving a design that can be completely and passively cooled during an accident, without any damage occurring to the reactor.

A predominant safety concern in fusion breeders has been the accident where loss of cooling causes melting and release of radioactive nuclides. Suppression of fission greatly reduces the production rate of fission products. With the molten-salt fusion breeder, we have a design wherein the salt will drain into holding tanks and can be cooled passively by, for example, heat-pipes, which dump the heat into the atmosphere. After an accident or off-normal situation occurs and the neutron source is turned off, the reactor can cool itself by passive means. For this to be true, we must show that the blanket will not melt because of induced radioactivity of the steel structure alone.

Some of the fission products and actinides in the salt are continuously removed and, hence, their inventory quickly reaches a steady-state value. Other fission products are not removed and their inventory increases linearly with time; the only loss being radioactive decay. Since there is so little salt in the reactor, it can be disposed of every few years, thus limiting the inventory of the few radionuclides that are hard to extract.

2.7. FROZEN SALT-LAYER ISSUES

At one point in the design iterations of the helium-cooled molten-salt blanket, the design called for steel tubes cooled to a temperature somewhat below the salt melting point. It was felt this would help reduce corrosion. The 27-mol% ThF_4 salt melted at 565°C. Later in the design cycle, we realized the corrosion with 316 stainless steel was low if the salt is kept reducing. Further, we were concerned that even if we wanted a frozen layer,

some places would be under-cooled and these walls would not have a frozen layer. To keep the wall temperature down, we lowered the melting point to 530°C by going to the 18-mol% ThF_4 salt and selected a no-frozen-layer design.

Even so, some areas will be over-cooled, so we will likely have a frozen layer in a few places. To cover the case where some frozen layers exist and the case where we might want to go back to a full-coverage frozen layer, we will discuss some of the issues on frozen-salt layers.

SOME THOUGHTS ABOUT A TMHR WITH FROZEN-SALT WALLS

The question "How often do you need to thaw the frozen layer?" involves many complexities and, in our view, not completely answerable without a great deal of experimentation. The question of fluorine generation is not the only issue involved, and it may very well not be the most important one.

The MSR salt (69 LiF, 29.1 BeF_2, 5 ZrF_4, zero UF_x) did not generate F_2 while molten and under its (relatively low) full fission power. And it did not generate F_2 when solid and above about 150°C while exposed to the radiations from fission product decay. The fact that it did generate F_2 at temperatures below about 150°C under fission-product-decay energy may well have been due to the presence of a complex and exotic crystalline $LiF\text{-}BeF_s\text{-}ZrF_4$ compound, and the MSRE fuel be a special case. But we do not know whether MSRE fuel or any other fluoride - would generate and release fluorine when solid and under very high radiation levels. This must be tested; we did not test this because we had no need to do so.

The proposed Tandem Mirror Hybrid Reactor (TMHR) is to generate 5.4×10^{-3} g/s of T, essentially all by reaction of neutrons with ^6Li. After the reaction products equilibrate with a well stirred melt (which the TMHR blanket fluid may not be) the overall reaction (in the absence of reducing agents) presumably is as follows:

$$n + {}^6LiF \rightarrow {}^4He + T^+ + F^-,$$

with TF dissolved in the molten salt. We propose to keep the TF reduced to T_2 (in the molten portion of the blanket) by

$$2\ UF_3 + 2\ TF \rightarrow 2(UF_4) + T_2\ .$$

Generation of 5.4×10^{-3} g/s of T is equivalent to generation of 2.77×10^{-11} g-mol/s·cm^{-3} TF of the 65 m^3 of TMHR salt along with an equal quantity of He. If all 65 m^3 of active salt were molten, reduction of TF at this generation rate (with 6% of the U as UF_3 entering the system and 5% as UF_3 leaving the system) would require some 820 litres/min to the reducer and a reducer cycle time of about 1.4 h. This is probably all right. The generated T_2 (1.385×10^{-11} mol/s·cm^{-3}) must be removed, along with the He, at a more rapid rate, because in 1.4 h (5040 s) the effective pressure of T_2 would be about 1.93 atm and that of He would be near 1.6 atm at 600°C. The TMHR salt will be under 500 psi or greater, so there should be no gas bubbles until the salt is depressurized.

None of this seems out of the question. Stripping of the T_2, He, and Kr + Xe on 8000 litres/min (8.13-min residence time) would be at effective dT_2 pressure of 145 torr, He pressure of 117 torr, and Kr + Xe at about 40 torr. One should be able to add 1 vol% of He (before pressurizing the salt) and have no bubbles in the 500 psa system. All of this may be feasible.

The discussion immediately above is based on the assumption that the frozen-salt film effectively prevents diffusion of tritium into the coolant helium. We doubt seriously whether this will prove to be the case in any realistic system such as that with an 8-min tritium cycle time.

What sort of flow rate does this imply in the tubes? We cannot answer this without some further assumptions. To confine 65 m^3 of salt within 0.5-in.-diam tubes requires 5.13×110^7 cm (5.13×10^5 m) of tubing. These are presumably distributed equally among 40 to 50 modules, so each module contains at least 1.030×10^4 m of tubing. If we assume the average tube length is 100 m (which may well be awkwardly long) we have a total of 5130 entrances and exits (ca. 100 each per module).

To flow 8000 litres/min, therefore, presumes a flow rate of about 0.2 m/s in each of the tubes. [We have for the moment ignored the frozen film.] This sluggish flow will almost certainly mean that the salt in some tubes will be stagnant. Faster flow with the same number of tube sections (perhaps with only an 8000 litre/min slipstream through the stripper) may be feasible, as may longer and fewer tubes. There are obviously difficult design questions here that can be addressed only after detailed analysis and modeling of the system.

The proposed TMHR is to generate about 0.25 g/s of ^{233}Th. After equilibration, the 65 m^3 of active salt will contain some 3612 g-mol of ^{233}Pa; if the salt is 71 LiF, 2 BeF_2, 27 ThF_4, the ^{233}Pa concentration will be about 0.125 mol%. If the uranium content is to be 1.1×10^{-3} times the thorium content, the salt carries about 0.03 mol% U, corresponding to 858 mol/65,000 litres of uranium or some 3.08 g of ^{233}U/litre. If we assume that a fluorinator of reasonable size can remove 75% of the uranium, we need to process about 0.108 litres/s (about 1.75 gal/min) of salt to remove 0.25 g ^{233}U/s. This corresponds to a U-cycle time of about 7 days and represents a tiny fraction of the stream to be stripped of T_2. Such a continuous fluorinator must be developed and demonstrated, but all in all the uranium removal should be feasible.

Note that, for the liquid portion of the blanket salt, the rate of generation of ^{233}U per unit volume will be nearly uniform throughout the blanket. This uniformity is due to the 27-day half-life of the ^{233}Pa plus the fact that, at least in the discussion above, sparging of the tritium entails mixing of the liquid blanket (on the average) every 8 min or so. Since the liquid portion of the blanket is maintained at a constant ^{6}Li concentration, the rate of tritium generation per unit volume of liquid will be a function of the neutron flux and will presumably diminish with distance from the front wall. Presumably, to the extent practicable, the path length of the liquid could be made shorter for tubes near the first wall so that tritium concentrations in the exit salt would be reasonably uniform.

Again, there are serious design questions (problems) that must be modeled and addressed before one can say anything for sure about the system.

Assuming a uniform, frozen, 0.5-mm thick layer of salt on the walls of the 0.5-inch (1.27-cm) pipes means that about 15% of the 65 m^3 of salt is to be solid. Presumably this considerable fraction of the total volume is to be maintained in the solid state for long times. We know virtually nothing about the behavior to be expected of this solid. Its situation will differ in several ways from that of the liquid portion of the blanket. Some speculations about the approximate magnitudes of these differences follow.

Let us assume that the 0.5 mm-thick frozen layer resides within the blanket for 60 days. Let us further assume that all neutronic products formed within the film remain within the film. If so, the concentration of ^{233}U within the film will be markedly higher than that within the liquid, as will

the fission rate, and both will be functions of the neutron flux within the blanket. How large is this effect? Assume the film is laid down from "equilibrium" salt with 1.32×10^{-5} g-mol ^{233}U and 5.56×10^{-5} g-mol $^{233}Pa/cm^3$. Assume that 1.65×10^{-11} g-mol $^{233}U/cm^3\ s^{-1}$ is generated uniformly throughout the solid volume. Assume that 3 moles of ^{233}U (of 858 moles total) fission per day and that this rate (0.25% per day) is a function only of ^{233}U concentration. If so, at the end of 60 days, each cubic centimeter of the film will contain (on the average) 8.80×10^{-5} moles ^{233}U. This is some 6.7 times the nominal concentration (1.32×10^{-3} moles/cm^3) in the liquid, and the average fission rate after 60 days will exceed that in the liquid by a similar factor. The ^{233}U concentration in the film exposed to the highest neutron flux will be moderately higher, and the fission rate there will be considerably higher. We do not know what power generation level will melt the film; certainly the highest power levels (near the first wall) are the best cooled and vice versa. Maybe this situation is not terribly distressing, especially since, during the 60-day interval, some of the ^{233}U may be lost to the liquid by recoil and by diffusion.

The discussion immediately above hardly represents even a "zeroth" approximation of the real situation, which depends upon the flux distribution, time temperature, geometry, etc. A careful, detailed, and difficult task of computer modeling of the system must be completed to establish what the key parameters are and what compromises must or can be made.

Let us examine the situation (again on the average) insofar as generation of TF and He is concerned. We assume that the deposited film contains 71 mol% LiF with 1% of the Li as ^6Li, that all TF is generated from ^6Li, and that the neutron flux is uniform within the volume; this latter assumption is manifestly incorrect.

The overall generation of tritium within the blanket, with 1% ^6LiF, is to be 5.4×10^{-3} g T/s, corresponding to 2.77×10^{-11} moles TF (and He) produced/$cm^3\ s^{-1}$ of salt. Since each cubic centimeter contains 3.157×10^{-4} g-mol of ^6Li (at 1% of the Li as ^6Li) the fraction of ^6Li consumed each second is 8.77×10^{-9}, on the average over the entire blanket. This ^6Li will be replenished in the liquid on a relatively short time cycle (1 day?). Assuming that the ^6LiF from the liquid is ignored and that TF generation is proportional to the ^6Li remaining, the fraction (on the average) of ^6Li remaining in the solid will be about 0.635. This may be tolerable, although the ^6Li will be depleted more than this in the high-flux regions.

We have no information about how the generated TF and He will behave in this solid. Except by (presumably slow) diffusion from the liquid, we cannot replenish UF_3 in the solid; this UF_3 will presumably be consumed within a few hours, and no mechanism will exist for reduction of the TF to T_2. We have no knowledge about what the energetic T^+ and F^- ions as well as the He, will do in the solid. Some fraction (unknown) will presumably leave the solid by recoil or by diffusion in one direction or the other. If we assume that all the He and all the T^+ and F^- remain in the solid and that the solubilities of TF and He are the same in the solid as in liquid Li_2BeF_4, the effective pressures of TF and He in the solid after 60 days would be (on the average) 16 atm and nearly 2000 atm, respectively. Such figures suggest strongly that, unless diffusion of TF and He (or some other escape mechanism) is very rapid, the generated gases will blow the film from the wall after a relatively short time. Since the film would be rapidly replenished, such blow-off may be beneficial.

However, since we do not know, we could assume that the He and TF diffuse readily from the film and do not spall it off. Diffusion of He to the liquid would seem to pose no problem; its diffusion to the metallic wall would seem to generate bubbles at high pressure and cause blow off of the frozen layer. Diffusion of TF to the liquid permits its reduction by the UF_3 there, with no particular problems. But diffusion to the metal wall results in reudction of the metal by the steel (i.e., corrosion) and results in generation of T_2 at the wall, the T_2 readily diffusing through the wall, how serious is this corrosion possibility? Assume that the film lasts 60 days and is replenished after that interval. During each 60 days each 1 cm^3 of film generates (on the average) 1.159×10^{-4} g-mol of TF or, during a 4-year wall lifetime, each cubic centimeter of frozen salt generates 2.82×10^{-3} g-mol of TF. Each cubic centimeter of 0.5-mm thick film corresponds to a 5.2-cm length of 1/2 in. tube. Such a 5.2-cm length of tubing contains 1.08 cm^3 of metal or about 8.36 g. Assume it to be Fe; if so, some 0.15 g-mol of metal are involved. Assume half of the TF (1.41×10^3 moles) diffuses to the metal wall and reacts as follows:

$$2\ TF + Fe \rightarrow FeF_2 + T_2 \quad .$$

If so, some 7.05×10^{-4} moles of Fe would be converted to FeF_2. This is less that 0.5% of the Fe wall, again on the average. If the attack were uniform, which it probably would not be, such corrosion would not seem to be devastating.

However, as we have said several times in the foregoing, we have no real information about how radiation, fission, and transmutation occur in a frozen wall and no real notion as to how the products behave. A very large and difficult reasearch program will be required.

Concerning the fraction of tritium that will penetrate the frozen-salt film: A diffusion coefficient of 2×10^{-4} cm^2/s has been used for tritium in the frozen-salt film at 500°C (assumed to be 0.5 mm in thickness). This value is equal to that of hydrogen in molten FLINAK at 500°C, the only measured value[3-19] we know of that could possibly be relevant.

Intuition says that the diffusion coefficient for tritium in solid $LiF-BeF_2-ThF_4$, with a much higher freezing point, will be less (possibly much less) than this. This diffusion coefficient must certainly be measured: If the value for $LiF-BeF_2-ThF_4$ is markedly lower, the estimate of 12% of the tritium diffusing through the 0.5-mm film is too high. However, for a pipe length of only 20 m, we assumed a flow rate through the pipe of 1 m/s. To meet these conditions would require that we process at least 65 m^3 of salt each 20 seconds (50,000 gallons per minute); such a feat seems essentially impossible. We apparently require a considerably lower processing rate (probably by 25-fold). Accordingly, in any reasonable scenario, unless the $LiF-BeF_2-ThF_4$ film is much more resistant to diffusion than assumed, a large fraction of the tritium will permeate to the helium coolant.

2.8. TECHNOLOGY OF TUNGSTEN PERMEATION BARRIERS

A frequently used and commercial deposition process for coating and lining substrates is the hydrogen reduction of a gaseous halide, particularly in the case of tungsten and other refractory metals.[2-15] Tungsten hexafluoride is readily available and transported in containers approved by the Department of Transportation for toxic materials. It is a liquid at usual atmospheric conditions, and its vapor pressure can be usefully and easily manipulated for ready dispensing with simple feed systems. Virtually no

partial reduction problems are experienced, i.e., formation of solid subfluorides. Its present commercial cost, in 100 lb. containers, from domestic manufacturers (Air Products and Chemicals, Inc., Mountain View, Ca) is about $50/lb. for the commercial grade commonly used for producing thin layers or free-standing shapes having properties comparable to powder-consolidated, arc-cast, wrought tungsten.

Tungsten may be deposited on heated substrates in accordance with the following reaction over a wide range of conditions:

$$WF_6 + 3H_2 \rightarrow W + 6HF \quad .$$

The reactants are continuously injected into a chamber, and the products of reaction are continuously removed. The process is conducted in an anhydrous and anaerobic environment, frequently at subatmospheric pressure. Important controllable variables affecting deposition rates are temperature, pressure, molal ratio WF_6/H_2, and gas-flow rates.

Measurable deposition rates yielding dense deposits are obtained at temperatures as low as 250°C. Sound deposits can be made at temperatures exceeding 1000°C at a rate of approximately 25 μm/min. System pressure may vary from fractions of a torr to atmospheric and is easily controlled with aspirators and mechanical vacuum pumps. If need be, blower-type vacuum pumps are used for cases requiring high throughput of feed gases at low and moderate subatmospheric pressures. Hydrogen/WF_6 molal-mixture ratios from 0.5 to several hundred produce satisfactory deposits and substantial inert gas diluents to the feed gas may be used. Thick deposits, i.e., 25 μm or more, are highly oriented, with a preferred orientation of 100. Deposits of 10 μm thickness would be expected to still remain in a relatively random orientation; because, at this point in growth, the nucleated grains with the fastest growing directions have not yet completely taken over to predominate all growth.

Deposition from an alternate source, tungsten hexachloride, which is carried out in a similar manner but at about 400°C higher than the fluoride process, generally results in a different preferred orientation, i.e, 110. But, again, at 10 μm the grain orientations are still largely randomized.

Thus, no distinct advantage would be obtained if it were experimentally demonstrated that preferred grain orientation had the beneficial effect of inhibiting tungsten dissolution and mass transfer from cold to hot regions during lifetime operation. We expect that resistance of tungsten to corrosion by the molten-flouride salt is at least equivalent to stainless steel if not better. Should mass transfer occur, some measurable difference over long time periods may be evidenced between the fluoride and chloride tungsten; definitive experiments on this need to be done. Another point of concern here is that tungsten deposited from the hexachloride is generally very low in residual chlorine (i.e., 2 ppm), whereas tungsten deposited from the flouride may contain from 2 to 100 ppm residual fluorine, which is somewhat dependent on deposition temperature (i.e., high flourine at low temperature and low flourine at higher temperature).

No inherent negative effects are anticipated with regard to heat removal from the salt by the 10-μm tungsten that lines the inner wall of the steel tubing. Tungsten is a good heat conductor and is about six times better than stainless steel, so its influence would be positive.

A well known difficulty in applying tungsten to steel is the achievement of adherence by means of a good metallurgical bond. Both naturally protective oxide and the reaction between iron and halide to form a stable compound act essentially to produce parting layers that are detrimental to the adherence of tungsten on steel. Generally, flash nickel coating (one thousand angstrom or less) is applied to steel surfaces before chemical-vapor deposition of tungsten, as it has been found this effectively circumvents the difficulty. With the likely generation of helium in nickel, a degenerate bond may ensue as a result of helium bubble formation at one or both dissimilar metal interfaces. The use of an electroplated copper flash is the best alternative here. AT LLNL tungsten is often applied on critical copper assemblies that need high conductivity and resistance to certain high-temperature corrosives. Reliance on a strictly mechanical bond (no bonding layer present) may also be a viable alternative. The greater thermal contraction of the steel on cooling from the tungsten-deposition temperature would force a compression state onto tungsten, thereby benefitting intimate dissimilar metal contact. The Chemical Vapor Deposition (CVD) process temperature selected would substantially exceed the operating temperature of the tube wall so such a favored condition for tungsten, with or without a

flash-bonding layer would always be maintained. The deposition of a 10 μm tungsten liner on individual straight or circularly shaped 11-m-long pipes should not offer any particularly difficult fixturing situations. Straight tubes with an internal deposit of tungsten can be formed to shape at 300°C or above, if necessary, to facilitate deformation in tungsten above its ductile-brittle temperature. Induction, furnace or self electrical-resistance heating might be employed as all have been used commercially on tubing. Considerable production of relatively thick internal deposits with somewhat more difficult metal depositions (i.e., Nb-1%Zr alloy, Ta) have been used commercially on common and stainless steel (Refs. 2-16 to 2-18). Serpentine passages of the order of 0.5 m in length and a small diameter (0.5 mm) have been lined with films of tungsten on massive substrates at Bendix, Kansas City, Mo. (Ref. 2-19). Most such products have employed periodic, alternate gas flows to achieve thickness uniformity, varying no more than 10% from end to center of length.

The major difficulty is thought to be in joining individual tubes to manifolds and headers while still maintaining, in the joint vicinity, a coating of high integrity and good mechanical properties. For this reason, we should pursue a serious investigation, perhaps in discrete stages, into the prospect of lining the tubing and manifold walls with tungsten as a semifabricated integral unit, before shrouding and loading with reflectors and moderators. The vent valves included at the top of each pipe loop to aid gravity drainage of salt may be used for ingress or egress of feed gas to coat individual loops, headers, and manifolds. The desirability of such an approach and accomplishment would be the benefit of ensured liners over the entire wetted surface, including joints. For CVD, furnace sizes approaching those needed here are used in coating large pipe and reaction vessels (Ref. 2-18). A company concentrating on chemical-vapor deposition and capable of accomplishing the task is Chemetal (Div. of Dart Ind.) in Poicoima, CA. Another company is Ultramet. To provide the source material for lining the tubes and manifolds, the major material procurement cost is for 65,000 lbs. of WF_6 at $50/lb. The estimated material cost (WF_6 + H_2) is $4M.

REFERENCES Section 2.0.

2-1. J. D. Lee et al., Feasibility Study of a Fission Suppressed Tandem Mirror Hybrid Reactor, pp. V-41 to V-63, Lawrence Livermore National Laboratory, UCID-19327 (1982).

2-2. D. H. Berwald et al., Fission-Suppressed Hybrid Reactor--The Fusion Breeder, Lawrence Livermore National Laboratory, UCID-19638 (1982).

2-3. L. G. Miller et al., Special Topics Report for the Reference Tandem Mirror Fusion Breeder: Beryllium Lifetime Assessment, Lawrence Livermore National Laboratory, UCID-20166, Vol. 3 (1984).

2-4. M. A. Abdou et al., "Blanket Comparison and Selection Study," Chapter V, Argonne National Laboratory, ANL/FPP-83-1 (1983).

2-5. M. A. Abdou et al., Blanket Comparison and Selection Study, Argonne National Laboratory, ANL/FPP-83-1, October 1983.

2-6. W. H. McAdams, Heat Transmission, (McGraw-Hill, NY, 1954), 3rd ed., p. 272.

2-7. H. Fenech, Heat Transfer and Fluid Flow in Nuclear Systems, (Pergamon Press, NY, 1981).

2-8. M.A. Hoffman, Magnetic Field Effects on Heat Transfer of Potential Fusion Reactor Coolants, Lawrence Livermore National Laboratory, UCRL-73993 (June, 1972).

2-9. P.J. Gierszewski, B. Mikic, and N.E. Todreas, "Natural Circulation in Fusion Reactor Blankets," ASMA/AIChE National Heat Transfer Conference, Orlando, Florida, July 1980.

2-10. C. F. Baes, Jr., "The Chemistry and Thermodynamics of Molten Salt Reactor Fuels," J. Nucl. Mater. 51 (1), 149-62 (1974).

2-11. J. W. Koger, Alloy Compatibility with LiF-BeF_2 Salts Containing ThF_4 and UF_4, Oak Ridge National Laboratory, ORNL/TM-5286, (December 1972).

2-12. J. R. Keiser, J. H. DeVan, and E. J. Lawrence, "Compatibility of Molten Salts with Type 316 Stainless Steel and Lithium," J. Nucl. Mater. 85 & 86 (1979) 295-98.

2-13. W. F. Grimes, "Chemical Research and Development for Molten Salt Breeder Reactors,", Oak Ridge National Laboratory, CF-66-7-41 (1966), pp 45-55.

2-14. W. R. Grimes and S. Cantor, "Molten Salts as Blanket Fluids," The Chemistry of Fusion Technology, ed. D. M. Gruen (Plenum, New York, 1972).

2-15. C. F. Powell, J. H. Oxley, and J. M. Blocher, Jr., Vapor Deposition (John Wiley & Sons Inc., NY, 1966).

2-16. F.A. Glaski, "Survey of Refractory Composites Formed by Chemical Vapor Deposition Techniques," 12th Refractory Composites Working Group Meeting, Denver, CO, Oct. 17-19, 1966.

2-17. F. A. Glaski, "A Report on the Current Role of Chemical Vapor Deposition as a Manufacturing Process," Proc. Conf. Chemical Vapor Deposition of Refractory Metals, Alloys, and Compounds, Gatlinburg, TN, Sept. 12-14, 1967.

2-18. F. A. Glaski, "Bonded CVD Tantalum Coatings on Steel Substrates," Fourth Intn. Conf. Chemical Vapor Deposition, Boston, MA, Oct. 8-11, 1973.

2-19. J. G. Gowan and R. A. Hamil, Corrosion Resistant Laser Mirror Heat Exchanger," U. S. Patent 4,387,962 (1982).

3.0. TRITIUM PERMEATION AND RECOVERY

SYNOPSIS

Design concepts are presented to control tritium permeation from a molten-salt helium-cooled fusion breeder reactor. This study assumes tritium to be a gas dissolved in molten salt, with TF formation suppressed. Tritium, which permeates readily through the hot steel tubes of the reactor and steam generator, will leak into the steam system at the rate of about 1 g/d in the absence of special permeation barriers. This assumes that 1% of the helium-coolant flow rate is processed for tritium recovery at 90% efficiency per pass. Tritiated water in the steam system is a personnel hazard at concentration levels well below 1 ppm. This level would soon be reached without costly isotopic processing. Alternatives, including a combination of permeation barriers on reactor and steam-generator tubes and molten-salt processing, are estimated to reduce the leak rate into the steam system by over two orders of magnitude. For the option with the lowest estimated leak rate, 55 Ci/d, it may be possible to purge the steam system continously to prevent tritiated-water buildup. At best, isotopic separation of dilute tritiated water may not be necessary, and for higher leak-rate options the isotopic processing rate can be reduced.

The proposed permeation barrier for the reactor tubes is a 10-μm layer of tungsten, which in principle will reduce tritium-blanket permeation by a factor of about 300 below the bare-steel rate. A research and development effort is needed to prove feasibility or to develop alternative barriers. The partial pressure of tritium gas dissolved in molten salt is high, easing the recovery process for which a flash separator has been chosen. A 1-mm aluminum sleeve is proposed to suppress permeation through the steam generator tubes. Relative to bare steel, this gives a calculated reduction factor of more than 500, including a factor of 30 due to an assumed oxide layer.

The permeation equations are developed in detail for a multilayer tube wall, including a frozen-salt layer and two fluid-boundary-layer resistances. Conditions are discussed for which Sievert's or Henry's Law materials become flux limiters. An analytical model is developed to establish the tritium split between wall permeation and reactor-tube flow. Nomenclature used in Section 3.0 is given in Table 3-1.

Table 3-1. Nomenclature and symbols for Section 3.0.

Symbol	Definition	Unit
a	Inner radius of frozen salt layer	m
A	Total reactor-tube area	m^2
A_j	Area for helium/steam-heat exchanger j	m^2
b	Inner radius of steel-reactor tube	m
c	Outer radius of steel-reactor tube	m
C_i	Tritium concentration in material i	Ci/m^3
d	Outer radius of coating (permeation barrier) or oxide layer	m
D_i	Diffusion coefficient for tritium in material i	m^2/s
D_{lm}	Diffusion coefficient (molecular, not eddy) for tritium in molten salt	m^2/s
f	Tritium flux, referred to inner tube radius b	$Ci/(s \cdot m^2)$
f(r)	Tritium flux at radius r	$Ci/(s \cdot m^2)$
g	Fraction of helium flow rate that is processed	
G	Tritium volumetric generation rate	$Ci/(s \cdot m^3)$
H_i	Henry's Law coefficient for tritium in material i	$Ci/(m^3 \cdot Pa)$
i	Subscript denoting material (see Fig. 3-2)	
I_i	Inventory of tritium in material i	Ci or g
j	Subscript denoting helium/steam heat exchanger type	
k_i	Boundary-layer mass-transfer coefficient for tritium in fluid medium i	m/s
K_{He}	Sievert's Law leak-rate coefficient through helium/steam-heat exchanger tubes (see Eq. (58))	$Ci/(s \cdot Pa^{1/2})$
K_{MS}	Sievert's Law leak-rate coefficient through molten-salt reactor tubes (see Eq. (52))	$Ci/(s \cdot Pa^{1/2})$

Table 3-1 (cont.)

Symbol	Definition	Unit
K'_{MS}	Henry's Law leak-rate coefficient through molten salt reactor tubes (see Eq. (54))	Ci/(s•Pa)
ℓ	Length of reactor tube	m
L_{He}	Tritium-permeation (leak) rate from helium system (see Eq. (57))	Ci/s or Ci/d
L_{MS}	Tritium permeation (leak) rate from molten-salt reactor (see Eq. (49))	Ci/s
p	See p(z)	
p(z)	Tritium partial pressure in molten salt at axial location z	Pa
p_i	Tritium partial pressure in material i	Pa
$p_i(r)$	Tritium partial pressure at radius r in material i	Pa
p_{max}	Maximum tritium partial pressure in molten salt at tube outlet (see Eq. (36))	Pa
Q_5	Flow rate of recirculating helium gas	m^3/s
r	Radial position in reactor tube	m
S_i	Sievert's Law coefficient for tritium in material i	$Ci/(m^3 \cdot Pa^{1/2})$
T	Absolute temperature in kelvins	K
U	Mass-average velocity of molten salt in reactor tube	m/s
V	Total irradiated molten-salt volume	m^3
W_j	Steel wall thickness of helium/steam heat exchanger j	m
y(z)	Dimensionless tritium partial pressure at z (see Eq. (41))	
z	Axial location in reactor tube, measured from fluid inlet	m
α	Fraction of generated tritium that permeates reactor tube wall	--

Table 3-1 (cont.)

Symbol	Definition	Unit
ϵ	Partial-pressure drop ratio (see Eq. (23)); also, dimensionless wall-loss parameter (see Eq. (44))	--
η	Fractional recovery per pass through molten-salt processor	--
η_5	Fractional recovery per pass through helium slipstream processor	--

3.1. INTRODUCTION

This section deals with tritium permeation and recovery from a molten-salt/helium-cooled fusion breeder reactor. The design concept assumes that tritium is present as a gas dissolved in the molten salt and that TF formation has been suppressed by reduction with UF_3. These states are both a blessing and a curse. On the blessing side, tube-wall corrosion from TF is suppressed, and the very high partial pressure of dissolved T_2 gas makes recovery relatively easy. Moreover, the desired fuel (rather than an undesired and corrosive fluoride compound) is recovered directly. On the negative side, tritium gas tends to permeate quite easily through steel walls at elevated temperatures, and a high tritium partial pressure worsens the situation.

The production rate of tritium is 0.35 kg/d,* perhaps better expressed from a safety and environmental perspective as about 3 megacuries/day (MCi/d). To keep environmental losses low, say 30 Ci/d, requires a "5-nines" recovery, i.e., a recovery fraction of 0.99999! This cannot be accomplished from the molten salt alone and requires staged recovery, processing, at least the molten salt and the intermediate helium coolant and, probably, the steam/water system also.

To keep process rates down, distributed permeation barriers are needed to impede permeation between the fluid systems. Assuming the need to use stainless steel tubes for strength, permeation barriers will likely be applied as a coating or cladding on the steel tube walls. Tritium permeates through all metals and, to a lesser extent, through ceramics. We will focus here on the low-permeability metals.

Figure 3-1 shows the temperature variation of the permeation coefficient of various low-permeability metals, including representative data for austenitic stainless steels for comparison.[3-1] A recent steel-alloy data survey[3-2] recommends an equation for PCA (316 SS), which agrees with Ref. 3-1 within 10 to 20% in the temperature range of interest. Table 3-2 gives the permeation-equation coefficients and literature references for Fig. 3-1, together with a numerical comparison of the permeation coefficients at 540°C. A dramatic improvement is seen in going down the list from steel

*The appropriate tritium consumption rate for 3000 MW of fusion power is 0.46 kg/d. We used 0.35 kg/d in this section. The leakage by permeation can be kept the same by increasing the barrier thickness somewhat. Also, the salt volume is 77 m^3 rather than the 65 m^3 used in this section.

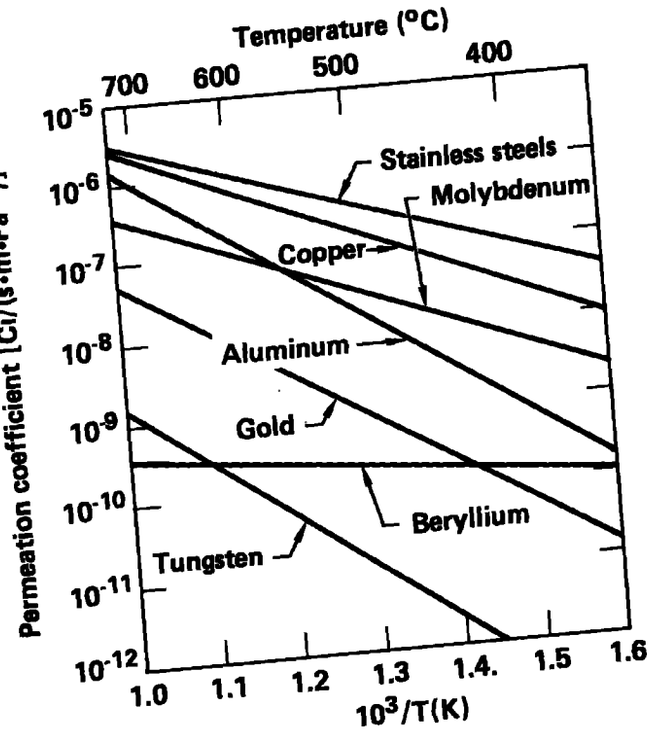

Figure 3-1. Permeability of various materials.

Table 3-2. Equations representing tritium permeation data in metals. Most data are for hydrogen or deuterium permeation, corrected by the square-root-of-mass ratio.[a]

Metal	Permeation equation constants[b] A [Ci/(s•m•Pa$^{-1/2}$)]	B 1/K	Permeation coefficient[c] at 540°C Ci/(s•m)Pa$^{-1/2}$)]	Lit. reference
St. steels	4.00×10^{-3}	7200	5.71×10^{-7}	3-1-2-3
Copper	2.82×10^{-2}	9310	3.01×10^{-7}	3-4
Molybdenum	2.53×10^{-3}	8760	5.30×10^{-8}	3-5
Aluminum	5.98	15200	4.56×10^{-9}	3-6
Gold	5.41×10^{-2}	13800	2.31×10^{-9}	3-4
Beryllium	3.37×10^{-9}	2200	2.25×10^{-10}	3-7
Tungsten	2.60×10^{-2}	16600	3.54×10^{-11}	3-8

[a]Conversion from mass to curies of tritium is based on a specific activity of 9.62×10^{6} Ci/kg.

[b]Empirical constants are listed for the equation $\phi = A \exp(-B/T)$, where T is in kelvins.

[c]The permeation coefficient is defined by $\phi = DS$, where D is diffusivity and S is solubility.

towards tungsten, with the reduction exceeding four orders of magnitude for tungsten. There is some disagreement in permeation equations in the literature, especially for materials of lower permeability, and a recent review cites alternate literature sources.[3-3] Beryllium is an exception; there can be no disagreement since there seems to be only one reference.

There are two reasons for wanting to keep tritium out of the steam system: first, any tritium leakage from there becomes a low-level environmental pollutant. This is a matter for concern, even though some consider it to be mainly a public-relations hazard. Second, tritiated water in the steam system, at seemingly low concentrations, can definitely be a personnel hazard as will be discussed in the next section.

In subsequent sections, we develop the permeation mathematics at some length. Our purpose is to show the somewhat subtle consequences that follow from combining the solubility laws of Sievert and Henry and from the competing effects of permeation and forced convection.

A wide range of exploratory design options are then considered. These will need to be pruned down, assuming feasibility, based on considerations of safety, ALARA, cost, etc. The intent is to show that there are many choices in tritium handling for this reactor concept. It is probably too early to focus on one favorite.

3.2. TRITIUM TOXICITY

Some years ago, in an invited paper on the history of tritium, Willard Libby[3-9] referred to tritium as a "very benign isotope." His reasons were, first, that the 5.7-keV, mean, beta-decay energy is "one of the softest radiations known" and, second, the 12.3-year half-life is short enough so that "we do not permanently contaminate the landscape." He then went on to express concern for tritium pollution from fusion power plants in which the time scales of interest are less than the half-century or so needed for radioactive decay.

The words "benign" and "soft" are relative and can perhaps be misleading. Tritiated water vapor is readily absorbed by the human body by means of respiration or skin contact. A one-Curie intake gives a whole-body dose of

approximately 82 rem,[3-10], half of which is delivered in the first week or two. Since pure T_2O contains over 3000 Ci/cm^3, it can be argued that a drop of water constitutes a lethal dose. So T_2O is certainly not "soft" water and Libby's friendly words do not apply, nor did he intend them to, until we dilute the tritium to trace levels with ordinary water.

On the other hand, tritium gas is virtually nontoxic, at least as long as you can hold your breath. Even if inhaled, disintegrating gas atoms deliver a relatively mild dose to lung tissue, and most of the rest are exhaled with only about 0.01% retained as tritiated water[3-10]. So perhaps tritium gas might fairly be called "benign." An important question is how fast tritium gas converts to water in the presence of water vapor and oxygen. Unfortunately, there is no simple answer. The conversion half-time can range from seconds on a catalytic surface[3-11] to years[3-12] in a Pyrex flask.

Tritium that is not recovered by processing in the molten-salt and helium-coolant loops will enter the steam system where it will tend to accumulate as tritiated water. Will this water be benign or hazardous? For permeation scenarios to be discussed below, we might expect HTO concentration to rise to, say, 1 Ci/litre. This corresponds to less than 1 ppm and could be considered a low level of contamination by ordinary standards. Let us assume a confined working area where a small amount of water leaks from the steam system and reaches equilibrium with water vapor in the air at 25°C. A worker breathing this air will be exposed at the rate of about 3 rem/h (based on equilibrium HTO-vapor concentration of 0.023 Ci/m^3 and a dose conversion factor[3-10] of 130 rem/h/Ci/m^3) (i.e., that person will reach the 1 rem annual occupational dose limit in only 20 minutes). Any leakage from a 1 Ci/litre tritiated-water system is definitely going to represent a serious personnel hazard. For this reason alone, it is desirable to design permeation barriers and to process so that the tritium input into the steam loop will be minimized. In contrast, a small amount of leakage from the helium-coolant loop will not be as hazardous to personnel, assuming that tritium present there is mainly in the hydrogen-gas form.

3.3. TRITIUM-PRESSURE DISTRIBUTION IN MULTILAYER CYLINDRICAL WALLS

Figure 3-2 shows the permeation geometry near the wall of a molten-salt reactor tube in radial cross section. One might approximate the radial geometry with a slab; instead we solve the problem exactly and then introduce approximations. Five material regions are included: (1) molten salt in the central region of the tube; (2) a frozen salt layer at the inner wall of the tube; (3) the stainless steel tube itself; (4) a coating or oxide layer at the outer wall; and (5) helium gas outside the tube. In addition, we allow boundary layers of finite mass-transfer resistance, but with negligible thickness, at the two fluid/solid interfaces. These represent the mass-transfer analog of a thermal-boundary layer in heat flow. Boundary-layer thickness must, of course, be finite and will depend on fluid properties, mainly the Reynolds Number. The mass-transfer coefficient incorporates the boundary-layer thickness, since it is, like the heat-transfer coefficient, a lumped parameter.

3.3.1. PERMEATION EQUATIONS FOR STEADY-STATE WITHOUT AXIAL FLOW

Assume that tritium is generated at a constant rate G per unit volume in Regions 1 and 2 and that the mass flow is radial and at steady state. Neglect radioactive decay compared to production. The time constant to reach steady state is about an hour for steel tube at 500°C and roughly a day at 300°C. Assume Fick's Law diffusion in Regions 1 to 4 and assume the helium in Region 5 is well-mixed from turbulent flow. We will eventually examine the mixing in the molten-salt region; for now, assume a finite diffusivity in Region 1.

For simplicity, we write the equation for mass conservation in the same form for Regions 1 to 4:

$$r^{-1}d[D_i r(dC_i/dr)]/dr + G_i = 0 \quad (i = 1, 2, 3, 4) \quad , \tag{1}$$

where

$$G_i = \begin{cases} G, & i = 1, 2 \\ 0, & i = 3, 4 \end{cases} \tag{2}$$

Reactor tube

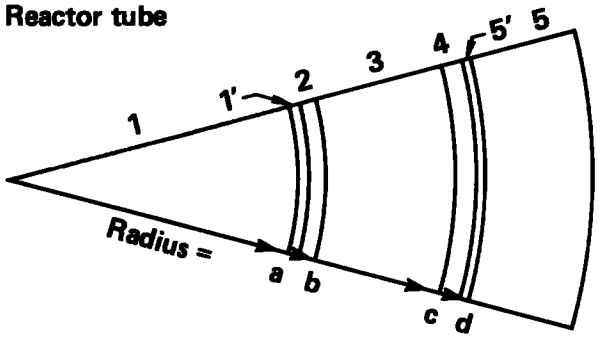

1 Molten salt
1' Molten salt boundary layer
2 Frozen salt
3 Stainless steel tube
4 Permeation barrier (tungsten)
5' Helium gas boundary layer
5 Helium gas

Steam generator tube

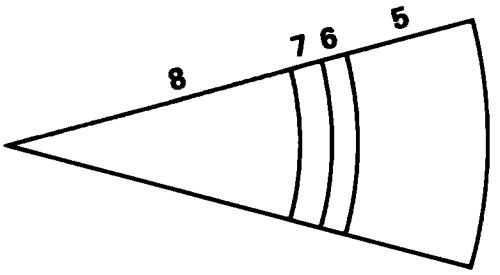

5 Helium gas
6 Permeation barrier (aluminum)
7 Stainless steel tube
8 Water/steam

Figure 3-2. Permeation geometry and materials.

$C_i = C_i(r)$ is the tritium concentration in region i at radius r. Diffusivity D_i is a function of temperature and, therefore, implicitly is a function of radius through the steady-state temperature profile, $D_i = D_i[T(r)]$. One can define an appropriate average D_i by means of the first integral of Eq. (1), and we will interpret D_i in this averaged sense.

The four constants that arise from the first integral of Eq. (1) are found by applying the following boundary conditions: the concentration gradient is zero at the center of the tube, and the flux $-D_i[dC_i/dr]$ is continuous at radius a, b, and c. The interface fluxes turn out to be:

$$f(a) = Ga/2 \ , \tag{3}$$

$$f(b) = Gb/2 \ , \tag{4}$$

$$f(c) = bf(b)/c \ , \tag{5}$$

$$f(d) = bf(b)/d \ , \tag{6}$$

and the concentration profiles may be written:

$$C_1(r) = C_1(a) + G(a^2 - r^2)/(4D_1), \ 0 \leq r < a, \tag{7}$$

$$C_2(r) = C_2(b) + G(b^2 - r^2)/(4D_2), \ a < r < b, \tag{8}$$

$$C_3(r) = C_3(c) + Gb^2 \ln(c/r)/(2D_3), \ b < r < c, \tag{9}$$

$$C_4(r) = C_4(d) + Gb^2 \ln(d/r)/(2D_4), \ c < r < d. \tag{10}$$

The result, so far, is the same as the solution to the steady heat-flow problem. If we were considering heat flow, we would next assume local thermal equilibrium at material interfaces and equate interface temperatures. For diffusion, we instead assume local chemical equilibrium at interfaces and equate the chemical potentials of the diffusing substance. Since chemical potential is linear in the logarithm of partial pressure for an ideal gas, we can equate interface partial pressures:

$$p_i = p_{i+1} \ , \qquad i = 1,2,3,4. \tag{11}$$

If tritium remains a diatomic gas upon dissolving in a particular material, then the equilibrium concentration is related to the gas phase partial pressure by Henry's Law:

$$C_i = H_i p_i \ , \tag{12}$$

where H_i is a temperature-dependent solubility constant and p_i is tritium gas partial pressure. This linear relation between concentration and partial pressure always holds at low concentrations, provided that dissociation or other chemical reaction does not occur.[3-13] For example, the solubility of hydrogen and deuterium in molten Li_2BeF_4 obeys Henry's Law.[3-14] In contrast, the solubility of hydrogen isotopes in metals obeys Sievert's Law,

$$C_i = S_i \sqrt{p_i} \ , \tag{13}$$

where S_i represents Sievert's constant. This square-root relation follows from thermodynamic arguments if gas-phase tritium is completely undissociated and solid-phase tritium is completely dissociated into atoms. Intermediate cases of partial dissociation in the gas-phase[3-15] and in the condensed-phase[3-16] have been considered, and the relation between concentration and partial pressure is not as simple as in the limiting case of Henry's or Sievert's Law.

We assume Henry's Law applies for tritium in molten and frozen salt, and also in helium, while Sievert's Law applies in steel and the coating or oxide layer on the steel. Note that solubility constants, in general, for each material. This implies a discontinuity in concentration at material interfaces, even those without fluid-boundary layers. Across a boundary layer we have an additional concentration change,

$$\Delta C_i = f/k_i \ , \tag{14}$$

where f represents the local mass flux, and k_i is a mass transfer coefficient. By means of Eqs. (11) to (14), we can solve for the four unknown interface concentrations in Eqs. (7) to (10). Expressing the results, for convenience, as interface partial pressures gives,

$$p_1(a) = f(a)/(k_1H_1) + G(b^2 - a^2)/(4D_2H_2) + p_2(b) \ , \tag{15}$$

$$p_2(b) = [Gb^2 \ln(c/b)/(2D_3S_3) + \sqrt{p_3(c)}]^2 \ , \tag{16}$$

$$p_3(c) = [Gb^2 \ln(d/c)/(2D_4S_4) + \sqrt{p_4(d)}]^2 \ , \tag{17}$$

$$p_4(d) = f(d)/(k_5H_5) + p_5 \ , \tag{18}$$

where p_5 represents tritium partial pressure in well-mixed helium gas.

Finally, the tritium partial-pressure profile at any radial position follows from Eqs. (7) to (10) as,

$$p_1(r) = p_1(a) + G(a^2 - r^2)/(4D_1H_1) , \qquad 0 \leq r < a, \tag{19}$$

$$p_2(r) = p_2(b) + G(b^2 - r^2)/(4D_2H_2) , \qquad a < r < b, \tag{20}$$

$$p_3(r) = [\sqrt{p_3(c)} + Gb^2 \ln(c/r)/(2D_3S_2)]^2 , \quad b < r < c, \tag{21}$$

$$p_4(r) = [\sqrt{p_4(d)} + Gb^2 \ln(d/r)/(2D_4S_4)]^2 , \quad c > r > d. \tag{22}$$

The set of eight equations listed above constitutes a formal solution to the problem of steady-state radial diffusion through four material regions having different properties, with generation in the two innermost regions, and with boundary-layer resistance at the two fluid/solid interfaces.

3.3.2. MASS TRANSFER RESISTANCES IN MOLTEN SALT

Since the solid regions will have thin walls, the radial dependence given by Eqs. (20) to (22) will not be needed for most calculations. Equation (19), on the other hand, applies to molten salt over the entire central region of the tube from centerline to the boundary layer at radius a. It is of interest to estimate the partial-pressure change across this region and compare it with the drop across the boundary layer. Define ε as a ratio of partial-pressure drops,

$$\varepsilon = [p_1(0) - p_1(a)]/[p_1(a) - p_2(a)] . \tag{23}$$

Using Eqs. (3), (15), (19), and (20), it follows that

$$\varepsilon = ak_1/(2D_1) . \tag{24}$$

We know intuitively that in highly turbulent flow the molten salt will be well mixed, which amounts to saying that the effective diffusivity, D_1, must be large and that ε will be a small number. Even in the absence of axial flow, we expect some natural convection because of the high heat generation and associated temperature gradients in the molten salt. Suppose, conservatively, that the natural circulation velocity is small and generates only a lazy, laminar flow. For this case, the mass-transfer coefficient is

$$k_1 = 2D_{1m}/a , \tag{25}$$

where D_{lm} represents the molecular diffusivity of T_2 in molten salt. Equation (25) is equivalent to a heat-transfer Nusselt number of 4, a value which is correct to one digit for laminar flow.[3-17] For D_l, we use the laminar-flow axial dispersion coefficient

$$D_l = D_{lm} + (Ua)^2/(48D_{lm}) \quad , \tag{26}$$

where U is the mean flow velocity.[3-18] We do not know of any measurements of T_2 diffusivity in molten Flibe, with or without a ThF_4 loading. However, Katsura and Furukawa[3-19] have measured the diffusivity of H_2 in molten Flinak, and we use their result:

$$D_{lm}[m^2/s] = (7.0E\text{-}06)\exp(-4530/T[K]) \quad . \tag{27}$$

With a 1/2-inch tube at 600°C and with an assumed velocity of 1 mm/s, the pressure drop ratio ε turns out to be 2×10^{-3}. For all practical purposes, we can assume the tritium partial pressure in the molten salt is uniform from the tube centerline out to the fluid/solid boundary layer where there is a sudden discontinuity. Equation (19) has now served its purpose, and the four interface Eqs. (15) to (18) are all we need for calculations.

3.3.3. PRESSURE PROFILES IN ABSENCE OF MOLTEN SALT

To make use of the results of the last section, a large number of parameters must be estimated. Many of these are temperature sensitive, especially diffusivity and solubility that depend exponentially on temperature. We first establish the thermal profile for a tube with given heat generation rate, outside helium temperature, etc. Table 3-3 shows the calculated results for three reactor tubes located at 1.5, 1.8, and 2.1 m from the plasma centerline, where the local heat generation rates are 60, 20, and 6 MW/m^3, respectively. Calculated temperatures and frozen-salt layer thickness are sensitive to tube location. Other parameters, such as the helium boundary-layer film coefficient, can also change the results. Table 3-3 is based on a 1/2-inch tube. Tailoring the tube size to radial position may be a useful way to adjust the thermal profile and frozen-layer thickness.

Table 3-3. Thermal regime for molten-salt reactor tube. Calculated[a] mean temperatures and frozen-salt-layer thickness for specified heat-generation rate and outside helium temperature.

Heat generation rate (MW/m^3)	Outside helium temp. (^oC)	Calculated mean temperature (^oC)				Thickness of frozen-salt layer (mm)
		Helium boundary layer	Stainless steel tube	Frozen salt layer	Molten-salt boundary layer	
60	285	394	504	536	916	0.0805
20	470	506	543	554	682	0.0875
6	550	561	572	572	604	0.0

[a]Calculations based on a 1/2-inch o.d. tube with a 20-mil wall thickness; a helium-side film coefficient of 7.4×10^2 $W/m^2 \cdot K$ based on a packed-bed Reynolds number of 3000; stainless steel conductivity of 20 W/(m•K); frozen salt conductivity of 0.24 W/(m•K); salt melting point of 565 C; salt-side film coefficient of 2.5×10^{-2} $W/m^2 \cdot K$) based on a molten-salt Nusselt number of 4; and well-mixed salt (infinite conductivity) in the central region of the tube.

Table 3-4 shows tritium permeation calculations based on the thermal profiles established in Table 3-3, and without axial flow so that all generated tritium permeates through the wall. The frozen-salt layer is assumed to have the same diffusion and solubility parameters as molten salt, D_1 and D_2 being given by Eq. (27) and Henry's Law solubility[3-14] expressed by

$$H_1[Ci/(m^3 \cdot Pa)] = H_2 = 1.19 \times \exp(-3530/T[K]) \quad . \tag{28}$$

The molten-salt boundary-layer mass-transfer coefficient, k_1, is estimated by means of Eq. (25) (i.e., based on laminar flow). A nominal 1-μm tungsten coating is used for Region 4. Permeation coefficients for tungsten and steel are as given in Table 3-2. The helium boundary-layer mass-transfer resistance turns out to be negligible at an assumed Reynolds number of 3000.

The main point of Table 3-4 is to show that, for a fixed-tube geometry, the tritium partial-pressure distribution can be significantly altered by tube location because of changes in the generation rate and the temperature distribution. The change of the relative permeation resistance of different portions of the multilayered wall is also interesting. This behavior is unlike relative thermal resistances in heat flow, which are nearly independent of the flux. If we had chosen to use, say, a 10-μm tungsten coating rather than a 1 μm, then the tungsten barrier would have been the dominant permeation resistance under all conditions. Note that neither the steel tube nor the frozen-salt layer offer very much help, while the molten-salt resistance can be significant based on the small mass-transfer coefficient in laminar flow. We may have understated the frozen-salt-layer resistance, since one would expect the solid to have a lower diffusivity than the liquid. The diffusivity of tritium in both solid and liquid Flibe will certainly need to be measured as this reactor concept is developed. Even if the frozen-layer diffusivity was much smaller, it seems unwise to count on a dynamic layer that is sensitive to thermal alteration and disruption for other reasons, e.g., periodic blowoff from helium buildup.

For design calculations below we will, therefore, consider only two simple extremes where the permeation resistance is dominated either by molten salt alone or by a tungsten barrier. Also, the material temperatures in Table 3-3 for the intermediate tube at 1.8 m from the plasma centerline (20 MW/m^3)

Table 3-4. Tritium permeation from molten-salt reactor tubes without axial flow.[a]

Parameter	Three design options		
	#1	#2	#3
Distance of tube from plasma centerline (m)	1.5	1.8	2.1
Heat generation rate (MW/m^3)	60	20	6
Tritium:			
Generation rate ($Ci/s \cdot m^3$)	1.24	0.414	0.124
Partial pressure in molten salt (Pa)	6.31×10^4	3.03×10^3	1.27×10^3
Partial-pressure drop (% of total):			
Molten-salt boundary layer	1.7	62.6	98.2
Frozen salt layer	1.2	7.1	0.0
Stainless steel tube wall	3.6	2.0	0.2
Tungsten coating (1 μm)	93.5	28.3	1.6
Helium-gas boundary layer	0.0	0.0	0.0

[a]Calculated values based on data in Table 3-3. Tritium generation rate is scaled to the heat-generation rate for the tube. We assume 100% permeation through the tube walls (no axial flow). Tritium partial pressure is assumed to be 10^{-2} Pa in helium coolant.

will be taken as representative for design calculations, because the tritium generation rate for this tube is not far from the reactor mean-generation rate, G = 0.596 Ci/(s•m^3).

We should emphasize two important messages gained from Tables 3-3 and 3-4:

- Although we know the reactor mean tritium generation rate, we do not have a corresponding mean tube-wall temperature distribution such that permeation from a representative tube will represent the correct integrated average over the whole assembly.
- Even if we did, the change in relative importance of wall resistance terms for tubes at different locations implies that exploratory calculations for a "representative" tube should be scaled to other conditions with caution.

3.3.4. RADIAL FLUX EQUATION FOR TRITIUM

If molten salt is flowing in the reactor tube, then the radial tritium flux is not proportional to production rate G, as in Eqs. (3) to (6), and instead depends on the local tritium concentration in molten salt and other system parameters. We will focus on the flux at b, the inner radius of the steel tube, and from now on denote f(b) as f. We will assume the local tritium concentration is well mixed as previously discussed and denote $p_1(a)$, the tritium partial pressure in the salt, as p. From Eqs. (15) to (18), replacing G by means of Eq. (4), we can write

$$p = fa/(bk_1H_1) + f(b^2 - a^2)/(2bD_2H_2) +$$

$$+ [fb\ln(c/b)/(D_3S_3) + fb\ln(d/c)/(D_4S_4) + \sqrt{fb/(dk_5H_5) + p_5}]^2 \ . \qquad (29)$$

Equation (29) cannot be solved explicitly for f. This is typical of realistic permeation conditions with multiple layers where Henry's-Law and Sievert's-Law regions are coupled.

Consider two simplified cases: (1) where the permeation resistance is dominated either by the molten salt or (2) by the coating. For the case of molten-salt resistance only, neglecting p_5 and assuming thin walls, solving Eq. (29) for f gives

$$f \simeq [2D_{1m}H_1/b]p \ , \qquad (30)$$

where we have assumed the laminar-flow approximation of Eq. (25) for k_1. For the case of coating resistance only, the flux is given by

$$f \simeq [D_4 S_4/(d-c)]\sqrt{p} \quad . \tag{31}$$

Note that the tritium flux is directly proportional to partial pressure when the material with the limiting permeation resistance has a Henry's-Law solubility, while the flux is proportional to the square root of partial pressure for a Sievert's-Law material. The net effect is to make the Sievert's-Law material the flux limiter if tritium partial pressure is high and the Henry's-Law material the flux limiter at low partial pressures. Table 3-4 illustrates these two extremes as well as the intermediate case where both materials serve to impede the flux.

3.4. TRITIUM SPLIT BETWEEN WALL-PERMEATION AND REACTOR-TUBE FLOW

We want to remove most of the tritium before it permeates through the reactor tube walls into the helium coolant. To do this, the molten salt must be circulated rapidly through an external process unit where tritium can be recovered. For now, we will assume a recovery system can be designed and will focus on the required permeation characteristics and recirculation rate needed to guarantee that only a small fraction of generated tritium will permeate the tube walls.

3.4.1. MODEL ASSUMPTIONS AND MASS-BALANCE INTEGRAL

As discussed earlier, tritium tends to mix well in the molten salt because of natural convection. Good mixing is reasonable on a length scale of the order of the tube size. To model the behavior of flow in a long tube, we assume that tritium is well-mixed radially while the partial pressure changes continuously in the axial direction z, that is,

$$p = p(z) \quad . \tag{32}$$

Let U represent the mean velocity along the z axis. As before, G is the volumetric generation rate, f is the local permeation flux, and H_l is Henry's constant for molten salt. A mass balance on a differential volume element, as sketched in Fig. 3-3, yields:

$$-UH_l dp/dz - 2f/b + G = 0 \quad . \tag{33}$$

Steady state is assumed, and axial diffusion has been neglected on the grounds that it is small compared to the bulk transport. Rearranging Eq. (33) and integrating over the tube from the molten salt inlet at zero to the outlet at ℓ gives,

$$H_l \int_{p(0)}^{p(\ell)} [G - 2f/b]^{-1} \, dp = \ell/U \quad . \tag{34}$$

This expression can be integrated numerically to find outlet pressure $p(\ell)$ for the general case, discussed in the last section, where f is not a simple function of the tritium partial pressure. The tube inlet pressure p(0) is related to $p(\ell)$ by

$$p(0) = (1-\eta)p(\ell) \quad , \tag{35}$$

where η represents the single-pass recovery fraction in the molten-salt processing loop. For the limiting case of perfect containment, we can calculate the maximum tritium pressure at the tube exit by integrating Eq. (34). Let's call this pressure p_{max}:

$$p_{max} = G\ell/(\eta H_l U) \quad . \tag{36}$$

We are interested in the escape fraction α, which represents the fraction of tritium generated in the tube that escapes through the wall before leaving the tube. An overall mass balance tells us that

$$\alpha = 1 - p(\ell)/p_{max} \quad . \tag{37}$$

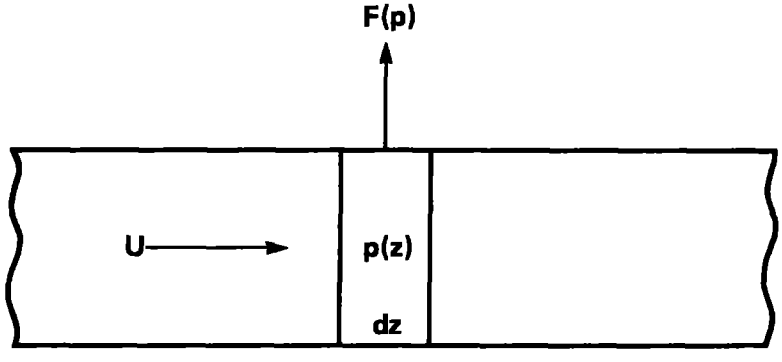

Figure 3.3. Model for tritium split in reactor tube. Molten salt flows at velocity U and is well mixed radially. Local tritium partial pressures at z, p(z) drives the radial permeation flux F(p).

3.4.2. A HENRY'S LAW BARRIER AS FLUX LIMITER

For the special case of the linear flux-pressure relation in Eq. (30) with only molten-salt resistance, the result of integrating Eq. (34) and then solving for the escape fraction by means of Eq. (37) is

$$\alpha = 1 - (\eta/\nu)[1 - \exp(-\nu)]/[1 - (1-\eta)\exp(-\nu)] , \tag{38}$$

with parameter ν defined as

$$\nu = 4D_{lm}b^{-2}\,\ell/U \quad . \tag{39}$$

If the permeating fraction is to be small, then we must have $\nu << 1$, in which case the exponentials can be expanded, and then α is simply

$$\alpha = \nu[1/2 + (1-\eta)/\eta] + \ldots . \tag{40}$$

The ratio of tube length to mean velocity, ℓ/U, that appears in parameter ν represents the residence time of fluid passing through a tube, in other words, the ratio of fluid volume to volumetric flow rate for that tube. If we neglect variations in tube length at different radii and possible variations in tube diameter, then tube residence time also represents the ratio of total molten-salt volume to total volumetric flow rate. Nominal tube length varies from 9 to 13 m, with an average of, say, 12 m. There will be additional manifolding length, which we will neglect, since it will not be part of the 65 m^3* design-basis volume of molten salt in the reaction zone. We pick a velocity of 0.1 m/s, which corresponds to a tube Reynolds number of about 3×10^2. The tube residence time, on this basis, is 2 minutes and the total volume flow rate of molten salt is 0.54 m^3/s (8600 gal/min. Assuming a recovery fraction of 0.9 and calculating molten-salt diffusivity based on a temperature of 680°C gives $\nu = 0.86$. If we use the exact analytical solution for α, since ν is not small in this case, the fraction of generated tritium that escapes through the tube walls is 0.37. This 37% loss

*The salt volume in the rest of the report is 77 m^3 rather than 65 m^3 used here.

could be reduced to a 15% loss by increasing the velocity by a factor of 3. The processing rate would then be 1.6 m^3/s (26,000 gal/min), which is starting to be uncomfortably high.

3.4.3. A SIEVERT'S LAW BARRIER AS FLUX LIMITER

Define a normalized pressure y(z) at any position z along the tube axis,

$$y(z) = p(z)/p_{max} \ . \tag{41}$$

We assume that the coating-resistance term dominates in the general flux relation, Eq. (29), in which case the wall flux is given by

$$f = D_4 S_4 \sqrt{p}/[b\ell n(d/c)] \ . \tag{42}$$

This equation reduces to Eq. (31) in the thin-wall approximation, a step that will be deferred for now since one might wish to consider a wide range of coating thicknesses. After substituting flux Eq. (42) into the integral in Eq. (34), the resulting integral equation can be written as follows:

$$\int_{(1-\eta)y(\ell)}^{y(\ell)} [1 - \varepsilon \sqrt{y}]^{-1} \, dy = \eta \ , \tag{43}$$

where the dimensionless wall-loss parameter ε is defined by

$$\varepsilon = 2D_4 S_4 \sqrt{p_{max}}/[b^2 \ell n(d - c)G] \ , \tag{44}$$

and all other symbols have been defined. Note that the operational parameter of direct interest to us, i.e., the tritium escape fraction dc, is related simply to $y(\ell)$ by:

$$\alpha = 1 - y(\ell) \ . \tag{45}$$

The point in writing Eq. (43) in the particular form given above, is as follows. First of all, we note that it can be integrated exactly but the

result is transcendental in $y(\ell)$ and thus rather opaque for computational purposes. So we resort to a series expansion of the integrand followed by term-by-term integration. We proceed by noting that ε is a small number, generally much less than unity for the low-permeability materials of interest to us. The varible y is also less than unity, and so we can expand the integrand of Eq. (43) in the form

$$[1 - x]^{-1} = 1 + x + x^2 + \ldots \quad . \qquad (46)$$

Keeping only the first two terms, integrating, and solving for the tritium escape fraction, we obtain

$$\alpha = 2[1 - (1-\eta)^{3/2}]\varepsilon/(3\eta) + \ldots \quad . \qquad (47)$$

We can see that ε is roughly equal to α, and since we are going to demand that α be small, it follows that our expansion to terms of order ε will be accurate.

Combining Eqs. (36), (44), and (47) gives the final working equation for the tritium escape fraction for a Sievert's Law flux limit, in terms of all the system parameters:

$$\alpha = (4/3)\eta^{-3/2}[1 - (1-\eta)^{3/2}]b^{-2}[\ell/H_1G]^{1/2}D_4S_4/[U^{1/2}\ell n(d/c)] \quad . \qquad (48)$$

The permeation coefficient D_4S_4 has the most important effect, because it varies by orders of magnitude among materials. Once the material is specified, the main variables in process design are wall thickness, velocity, and process recovery efficiency. Although it's a little hard to see in Eq. (48), the product ηU is nearly constant at fixed α, and so a decrease in process efficiency can be compensated for by a corresponding increase in flow velocity.

Evaluating the above expresssion using a 10-μm tungsten coating at 540°C, with other parameters the same as the previous linear case, gives a calculated escape fraction equal to 0.08. The 10-μm tungsten barrier reduces the permeation rate below that of the 20-mil bare stainless steel tube by a factor of about 300. This is a substantial improvement, yet not so high as to defy credibility. Coatings are inevitably imperfect. Asking for a permeation reduction factor of 300 over the base metal implies that an

uncoated portion (cracks, pinholes, etc.) of only about 1 part in 1000 of the bare tube area can be tolerated without degrading performance. To do the same job with beryllium requires a 64-μm layer, based on resists of Table 3-2. Gold is next in line in permeability and is an easily applied, non-brittle coating material. Unfortunately, to match 10 μm of tungsten would require an 0.65-mm layer of gold and cost about $4 billion! The effectiveness of tungsten or other low-permeability barriers must be assessed by an experimental research and development program. Tungsten powder can be melted and applied to tube exteriors by a commercial plasma-spray process. Tungsten can also be coated on surfaces by chemical vapor deposition from the volatile hexafluoride,[3-20] which might permit the inside of the reactor tubes to be coated as well.

3.5. TRITIUM PERMEATION RATE TO HELIUM COOLANT LOOP

3.5.1 THEORY

The essential results of the last section are contained in Eqs. (38) and (48) for the tritium escape fraction in the Henry's or Sievert's Law flux limit. The leak rate (permeation rate) of tritium from the molten-salt loop is the product of escape fraction, volumetric production rate, and total molten-salt volume in the reactor tubes,

$$L_{MS} = \alpha G V \quad . \tag{49}$$

For both the Henry's and Sievert's Law cases, assuming as usual a small escape fraction, the outlet tritium partial pressure is to a good approximation given by Eq. (36), $p_{max} = G\ell/(\eta H_1 U)$. By using this relation, we can write the permeation rate in a more familiar fashion in terms of partial pressure. The total tube area A can also be introduced by recognizing that

$$A = 2V/b \quad . \tag{50}$$

For a Sievert's Law barrier as flux limiter, assuming a thin-walled tube, Eq. (49) can be written

$$L_{MS} = K_{MS} \sqrt{p_{max}} \quad , \tag{51}$$

where the Sievert's Law leak-rate coefficient from the molten-salt loop K_{MS} is

$$K_{MS} = \{(2/3\eta)[1 - (1-\eta)^{3/2}]\}D_4S_4A/(d-c) \quad . \tag{52}$$

The terms following the curly bracket are what we would expect in a permeation equation: diffusivity, solubility, area, and wall thickness. If we had ignored the axial gradient and assumed the tube was a well-mixed tank (as will be done in the helium section to follow) the result looks exactly like Eq. (52) except the quantity in the curly brackets is unity. This factor, which depends only on process efficiency, is the correction for the axial gradient arising from the tritium processor. The tritium processor recycles molten salt with a low tritium partial pressure back to the reactor-tube inlet.

Going through a similar procedure for a Henry's Law barrier as the flux limiter, we can write the leak rate

$$L_{MS} = K'_{MS}p_{max} \quad , \tag{53}$$

where Henry's Law leak-rate coefficient K'_{MS} is:

$$K'_{MS} = \{1 - \eta/2\}k_1H_1A \quad , \tag{54}$$

and again the curly-bracket factor represents the axial-gradient correction to a well-mixed-tank model.

3.5.2 DESIGN OPTIONS

We now consider a range of feasible design alternatives:

Option A. Process molten salt, restricted permeation.

Option B. Process molten salt, unrestricted permeation.

Option C. No salt processing, 100% permeation.

A 10-μm tungsten barrier [as discussed in the paragraphs following Eq. (48)] is used in Option A, while Option B and C have only the molten salt boundary-layer resistance. The process recovery fraction is 0.9 for cases A and B, while case C has no tritium recovery system for the molten salt. The

temperatures for permeation are 540 and 680° C for tungsten and molten salt, respectively. Other parameters are given in Table 3-5 along with calculated results. For case A, Eq. (51) is used for the leak rate. For case B, the leak rate is too large for Eq. (53) to be accurate, instead Eq. (49) is used, along with Eqs. (38) and (39), to obtain the exact solution to the linear problem. For case C, the tritium pressure in molten salt is obtained from Eq. (29) rather than Eq. (36). The leak rate to the helium loop is 7.6%, 37%, and 100% for Options A, B, and C, respectively.

Table 3-5. Permeation from the molten-salt loop for three design options.[a]

Parameter	Design option A	B	C
η	0.9	0.9	0.0
ℓ/U (s)	120	120	--
(d-c) (μm)	10	--	--
p_{max} (Pa)	2710	2710	3050
α	0.0759	0.367	1.000
$p(\ell)$	2500	1720	3050
L_{MS} (Ci/s)	2.94	14.2	38.7

[a]For all cases, G = 0.596 Ci/(s•m^3), V = 65 m^3, and b = 5.842 mm.

3.6. TRITIUM PERMEATION INTO THE STEAM/WATER LOOP

From the point of view of tritium permeation, the helium-coolant loop is in a crucial position between the molten salt and steam systems. Figure 3-4 shows a sketch of the three tritium processing loops. Tritium is generated at a high rate in the molten salt, and it will be difficult to recover much more than 90% of the tritium produced there. Tritium that permeates through the reactor tubes will enter the helium heat-transfer loop. Table 3-6 gives approximate figures on amounts and flow rates in the three loops. The mass of molten salt is large because of its high density. However, pumping power and equipment size and cost scale with volumetric flow rate. The bottom line on Table 3-6 shows why it is unreasonable to process for tritium recovery more than a small fraction of the helium flow, which amounts to 800 m^3/s or nearly 2 million atmospheric ft^3/min at 450° C and 60 atm.

A steady-state concentration will quickly be reached that will depend on the helium volume and helium-processing rate, assuming that processing is the main removal mechanism. There will also be a tritium permeation loss through the walls of the helium/steam heat exchanger, and perhaps some conversion of tritium gas by homogeneous-phase oxidation to water or chemical exchange with water vapor in the circulating helium. Direct conversion in the helium is an intriguing possibility. Maroni[3-22] presented the thermodynamic arguments showing that tritium gas partial pressure (and therefore the permeation loss) will be very small if a modest oxygen partial pressure is maintained and tritiated water vapor is adsorbed at a reasonable rate, assuming equilibrium prevails. Unfortunately, the kinetics are too slow without a catalyst, and a conventional catalytic converter to handle 800 m^3/s would be absurdly large. The design challenge is to get a large catalytic surface area into the helium without introducing any significant pressure drop (e.g., 10^3 Pa at 800 m^3/s requires 1 MW_e of pumping power at 80% efficiency). Perhaps very small catalytic particles could be distributed and maintained in the flowing gas. For design calculations below, we will simply use a conventional catalytic reactor in a relatively low-flow bypass loop.

3.6.1. FOR WELL-MIXED TANK MODEL

For this study, we assume that tritium entering the helium system is either recovered in a helium slipstream processor or permeates to the steam

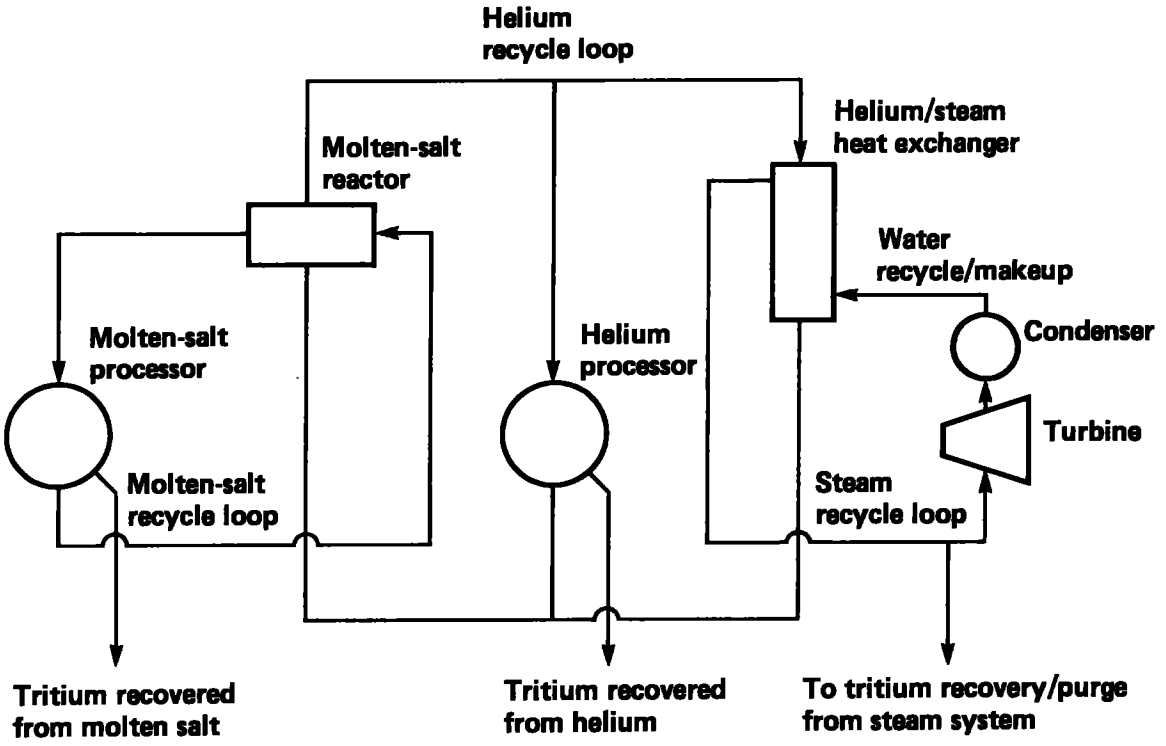

Figure 3-4. Diagram of tritium processing loops, showing principal flows only. Losses from process lines and equipment housings not shown.

Table 3-6. Size comparison of loops for molten-salt reactor, processing, and coolant.[a]

Parameter	Molten salt	Helium	Steam
Mass (kg)	4.6×10^5	1.3×10^4	3.8×10^5
Volume (m^3)	100	3200	10,000
At T (^oC)	600	450	340
At P (MPa)	5.1	6.1	8.4
Mass flow rate (kg/s)	2.5×10^3	3.2×10^3	1.6×10^3
Volume flow rate (m^3/s)	0.54	800	43

[a]Coolant loop flow-rate data from Ref. 3-21; mass and volume values are estimates.

system, in which case the mass balance reads:

$$L_{MS} = \eta_5 g Q_5 H_5 p_5 + L_{He} \quad . \tag{55}$$

The fractional efficiency of slipstream processing is η_5; the fraction of helium that is processed is g; H_5 and p_5 are the Henry's Law constant and partial pressure for tritium in helium; and L_{He} is the permeation rate out of the helium system. The assumption of a well-mixed tank is implicit in the above equation. Assuming that $L_{He} << L_{MS}$, we neglect the second term in Eq. (55) and solve for the tritium partial pressure

$$p_5 = L_{MS}/(\eta_5 g Q_5 H_5) \quad . \tag{56}$$

The leak rate L_{He} is assumed to depend only on the helium-side partial pressure

$$L_{He} = K_{He}\sqrt{p_5} \quad , \tag{57}$$

where K_{He} is a Sievert's Law leak-rate coefficient for the helium/steam heat exchanger tubes.

Table 3-7 shows heat exchanger design data for the reactor of reference,[3-21] which we have combined with permeation data[3-1] for clean, unoxidized stainless steel to give a leak rate per unit driving force. It is interesting to note that there is a considerable difference in the mean wall temperature of the four types of exchangers shown in Table 3-7. We define the mean wall temperature as the arithmetic average of helium and steam/water inlet and outlet temperatures. As a consequence of this temperature difference, the resuperheater accounts for 46% of the leakage although it has only 15% of the wall area and, in addition, has thicker walls.

The overall leak-rate coefficient is calculated from

$$K_{He} = \sum DS_j A_j / W_j \quad , \tag{58}$$

where the sum is over each heat exchanger with specified permeation coefficient DS_j, area A_j, and wall thickness W_j.

Table 3-7. Tritium permeation through bare steel helium/steam-heat exchangers.[a] These values are based on data in Ref. 3-21 for 4480-MW_t design heat duty. Except for data in bottom row for the reactor with 12 generators, the data are for one generator set.

Type	Area (m^2)	Area (%)	Wall thickness (mm)	Mean temp. (°C)	DS[b]	Leak-rate coefficient [(Ci/(d•$Pa^{1/2}$)]	Leak-rate coefficient (%)
Resuperheater	512	(15)	2.54	488	27.1	5.46×10^3	(46)
Superheater	385	(12)	1.78	432	12.8	2.77×10^3	(23)
Evaporator	1409	(42)	1.57	355	3.66	3.28×10^3	(27)
Economizer	1017	(31)	1.57	275	0.678	0.445×10^3	(4)
1 Generator	3323	(100)		<384>[c]	<6.11>[d]	1.20×10^4	(100)
1 Reactor (x 12)	3.99×10^4					1.44×10^5	

[a]Note that 46% of the leakage goes through only 15% of the area, and 69% of the leakage goes through only 27% of the area.

[b]Permeation coefficient for clean steel (no oxide) at the specified temperature (Ci•mm/d•m^2•$Pa^{1/2}$).

[c]Permeation mean temperature calculated from weighted-mean permeation coefficient (DS).

[d]Weighted-mean DS = $\Sigma(DS_j A_j/W_j)/\Sigma(A_j/W_j)$.

3.6.2. PERMEATION RATES FOR RANGE OF DESIGN OPTIONS

Two design alternatives are considered for the helium/steam-heat exchanger system:

- Option 1. Restrict permeation with a 1-mm aluminum sleeve.
- Option 2. Unrestricted permeation.

Unrestricted permeation (see Fig. 3-2) means that the only resistance comes from the stainless steel tube wall (Material 6 present, Material 7 absent), while restricted permeation implies that the aluminum permeation barrier (Material 7) is present and is the tritium flux limiter.

For Option 2, a steel tube leak-rate coefficient of 1.44×10^4 Ci/(d•Pa$^{1/2}$) is used. This is obtained from the temperature- and area-averaged coefficient given in Table 3-7 by dividing by a factor of 10 to allow for an oxide layer on the steam side. This is believed to be a conservative oxide-factor "credit." Much higher factors have sometimes been reported, but the effective permeation reduction by thin oxide layers is rather uncertain. We have ignored fluid boundary-layer resistances for these heat exchangers.

For Option 1, we use a 1-mm aluminum sleeve as permeation barrier with the sleeving, for simplicity, assumed to enclose the steel tubes of Option 2. Aluminum has a larger thermal expansion coefficient than steel, and there may be less degradation of heat-transfer performance if the aluminum tube can be placed inside the steel tube. The same temperatures and areas in Table 3-7 are used, as a simplifying approximation. The aluminum sleeve leak-rate coefficient is 269 Ci/(d•Pa$^{1/2}$), obtained from the Table 3-2 data after allowing a factor of 30 credit for the aluminum oxide layer. We use a factor of 30 since hydrated oxides are known to form almost immediately on a clean-scraped aluminum surface, and these are both tenaceous and self-healing.[3-23]

For both options, 8 m^3/s (1% of the helium flow rate) is processed with a 90% per-pass tritium removal efficiency. Even at 1% of the helium flow rate, 8 m^3/s (17,000 ft^3/min) requires a large gas processor.

Combining the two options above with the three cases of tritium input rate from Table 3-5 gives six representative cases of tritium permeation into the steam/water system. The calculated results are given in Table 3-8, and range from 55 Ci/day to 11,000 Ci/day. It appears that permeation barriers between the helium/steam systems are more effective than between the

salt/helium systems. This important fact follows from combining permeation-rate equations to show the dependence on leak-rate coefficients[4],

$$L_{He} \propto K_{He}(K_{MS})^{1/2} , \tag{59}$$

i.e., the permeation reduction from the molten-salt tubes (see the bottom line in Table 3-5) is suppressed by the Sievert's Law square-root effect of the next stage. This is unlike the more usual linear effect of staging multiple barriers, where the decontamination factors of each stage multiply directly to give the overall effect.

Table 3-8. Comparison of the rates of tritium permeation into the steam/water system under different design options.[a]

Design option	Description of process	L_{He} (Ci/d)
1	Process helium, 1-mm aluminum sleeve, with:	
	A. Process molten salt, 10-μm tungsten coating	55
	B. Process molten salt, fluid b.l. resistance only	120
	C. Molten salt not processed, 100% permeation	200
2	Process helium, steel tube resistance only, with:	
	A. Same as above 1A.	3,000
	B. Same as above 1B.	6,500
	C. Same as above 1C.	11,000

[a]Tritium input to the helium system is taken from Table 3-5 for processes A, B, and C. Partial pressure in helium is calculated from Eq. (56) with $\eta = 0.9$, $g = 0.01$, $Q_5 = 800\ m^3/s$, $H_5 = 6980/T(K)\ Ci/(m^3 \cdot Pa)$, and $T = 723\ K$. The results are 0.042, 0.20, and 0.55 Pa for options A, B, and C, respectively.

3.7. PROCESS CONCEPTS FOR TRITIUM RECOVERY FROM FLUID LOOPS

We briefly outline some process design concepts for recovering tritium from the three fluid systems; molten salt, helium, and water.

3.7.1. TRITIUM RECOVERY FROM MOLTEN SALT BY FLASH VAPORIZATION

An estimate of the tritium pressure at the tube outlet is given by Eqs. (36) and (37). Using the data in Table 3-5, the result comes to at least 12.9 Torr. This is a very high pressure compared to most breeder designs, and is due to a combination of very low tritium solubility in the salt, moderate wall losses, and a reasonably long residence time. A high tritium partial pressure makes recovery relatively easy and is an important fringe benefit of keeping tritium in the dissolved T_2 gas form, rather than as TF.

Figure 3-5 shows a schematic of the proposed molten-salt processing system. We chose a flash vaporization unit, similar to the concept of Johnson.[3-22] The liquid enters the vaporizer (or disengager to use Johnson's terminology) and expands through jet nozzles (essentially a showerhead) into a large disengaging tank where liquid droplets settle to a liquid sump at the tank bottom. The pressure in the tank is maintained at the desired level by an external pumping system that carries the effervescing gas out of the chamber. The desired pressure level is set by the design recovery efficiency together with the assumption that residual dissolved tritium in the tank liquid is in equilibrium with the partial pressure of gas-phase tritium. With a design efficiency of 90%, the pressure level would be 1.29 Torr, assuming the temperature in the salt loop is constant and provided there were no other evolved gases. Allowing roughly 3 moles of other gases (primarily helium) per mole of T_2 generated[3-22], the pressure level in the disengager must then be 5.2 Torr. The total gas rate leaving the disengager is essentially 4 times the T_2 generation rate, or 2.67 mmol/s. This rate corresponds to a volumetric flow rate of 12.8 ℓ/s at 600° C (3.9 ℓ/min at 20° C, 1 atm) - a very modest gas flow rate, even by tritium pumping standards. Assuming that the oxygen level is maintained at a low level with a separate slipstream processor, the 25% T_2 in He mixture is cooled to near room temperature, compressed to about 1 atm and passed over a powdered uranium bed to recover the bulk of the tritium as a hydride. The tritium-contaminated helium stream will need a final cleanup step before release, such as the

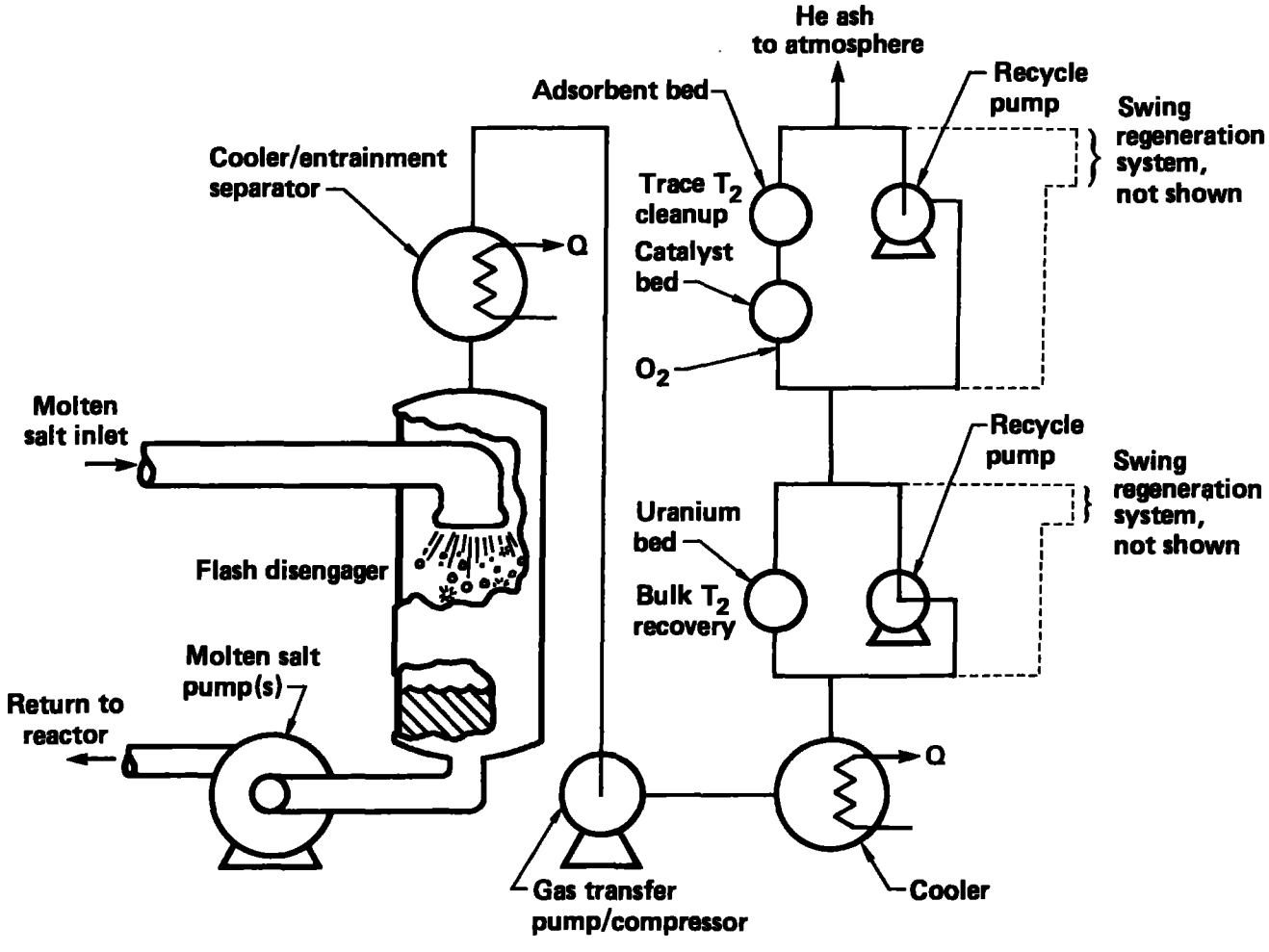

Figure 3.5. Tritium recovery-system flow sheet.

introduction of a little oxygen followed by catalysis/adsorption. The recovery beds will be paralleled, to allow cyclic operation, changeouts, etc.

Returning to the molten salt, we next estimate the pumping requirement. The flash disengager operates at near zero pressure compared to the salt tubes, which at maximum will operate at pressure balance very near to the helium heat-transfer-loop pressure of 50 atm. At 0.54 m^3/s, 50-atm pressure rise, and 70% pump efficiency, the worst-case power requirement is 3.9 MW_e (some 500 Hz). This does not seem unreasonable, leaving pump technology aside as a separate issue.

The size of the flash disengager is also reasonable at the design recirculation rate for molten salt. Allow a 3-second liquid residence time and a 50% void fraction for gas. This gives a 3.2 m^3 tank volume. With a nominal length to diameter ratio of 3, the tank has a diameter of 1.1 m and is 3.3 m high. To give some perspective, the pipe diameter for this salt recirculation loop will need to be in the neighborhood of 0.4 m in order to keep the pressure drop near 1 atm and the pump power less than 0.1 MW_e.

It may be helpful to provide the reader a "nearest-integer exponent" cost estimate. This is a very rough estimate; less refined than the back-of-the-envelope method. In our judgment, the molten-salt processor as sketched on Fig. 3-5 has a nearest-integer exponent of 6, i.e., the capital cost may range from $0.32M to $3.1M.

3.7.2 TRITIUM RECOVERY FROM HELIUM BY OXIDATION/ADSORPTION

Tritium can be removed from helium by adding a few parts per million of oxygen, converting to tritiated water in a packed-bed catalytic reactor, and adsorbing the water vapor on a zeolite molecular-sieve adsorbent bed.[3-21,-24,-25] Two adsorbent beds are required; one on-line while water is being desorbed from the other. The desorbed water then goes to an electrolysis unit for tritium recovery. At 8 m^3/s helium flow, and at 60 atm pressure, the reactor and adsorbers will be substantial vessels, larger than any now in tritium service. Nevertheless, a 90% per-pass recovery should not be difficult. We estimate a nearest-integer cost exponent of 7 for this system.

3.7.3. TRITIATED WATER PURGE OR ISOTOPIC SEPARATION

Tritium gas permeating into the steam generation loop will be converted to tritiated water by exchange with the overwhelming supply of hydrogen atoms in hot steam. According to experience with the Canadian heavy-water reactor (CANDU), most of the tritium entering their steam generator leaves as tritium oxide in boiler blowdown and less than 1% as gas or water vapor in turbine off-gas.[3-26] For simplicity, we will assume the residual HT gas partial pressure is low enough so that permeation loss through condenser-tube walls can be neglected. This means that tritiated water concentration is determined simply by a balance between tritium input and removal rates. Removal may be accomplished either by purging to the environment, as at CANDU, or by processing, as at Grenoble.[3-27]

Purge Rate and Concentration for Low Tritium-Input Rates

The CANDU purge rate is 7.5% of the steam circulation rate; or 0.06 and 0.10 m^3/s at the Pickering-A and Bruce-A reactors, respectively.[3-26] Let's suppose that 0.1 m^3/s (1600 GPM) represents a reasonable upper limit on the steam-system purge rate. For the lowest tritium input rate shown in Table 3-8 (55 Ci/d), the steady-state water concentration is 6.4 $\mu Ci/\ell$. This is about 300 times the EPA drinking water limit of 20 $\mu Ci/m^3$, which in turn is equivalent to 4 mrem/y for continuous exposure. This modest level of environmental pollution just might prove acceptable, given a long outfall pipe to a large and rapidly moving body of water.

Process Rate and Concentration for High Tritium-Input Rates

Most of the design options calculated in Table 3-8 give tritium input rates that will probably prove too high to allow environmental purging to be acceptable by present or future U.S. standards. Excepting case 1A, the range of tritium input rates is from about 10^2 to 10^4 Ci/d. If the tritium input was allowed to accumulate in the water system, assuming no losses and with the water mass from Table 3-6, a concentration level of 1 Ci/ℓ would be reached in only 38 days for the high end of the input range. As discussed earlier, this tritiated water level is a personnel hazard if the steam/water system has any leaks.

Suppose we process water from the steam system at a modest rate of 4 l/min and, by isotopic separation, remove 50% of the tritium per pass (we pick these design numbers since a process cost estimate is available). The steady-state concentration depends inversely on the tritium input rate and will be 0.03, 0.3, and 3 Ci/ℓ for 10^2, 10^3, and 10^4 Ci/d input, respectively. The cost to extract tritium from Savannah River heavy-water reactors, using the Grenoble Sultzer Process[3-27] and for the process conditions above, is about $130M according to the Savannah River Reactor "high spot" estimate.[3-28] This process involves catalyzed hydrogen gas/water vapor exchange followed by cryogenic distillation of tritium-enriched gas. Since 3 Ci/ℓ tritiated water is very hazardous, as discussed earlier, it may be desirable to increase the process rate for the worst case input to prevent the system from reaching the 3 Ci/ℓ level. This will cause a corresponding increase in process cost. Moreover, the time constant to reach steady state, for the proposed process rate, is only about 4 months.

3.8. TRITIUM INVENTORY IN FLUID SYSTEMS AND TUBE WALLS

Inventory estimates are summarized in Table 3-9 for the fluid systems and steel tube walls. The basis for the numbers is discussed below.

Tritium inventory in the molten-salt tubes is calculated from

$$I_1 = VH_1p_1 \ , \tag{60}$$

where p_1 is an integral average partial pressure along the length of a reactor tube. We take the average to be $[p(0)+p(\ell)]/2$, use Eq. (35) for $p(0)$ and the $p(\ell)$ values from Table 3-5. Equation (28) is used for H_1, tritium solubility at 680°C in molten salt. Calculated inventories amount to only a fraction of a gram for options A, B, or C. The numbers are small because of the low estimated solubility of tritium in molten salt.

The estimated tritium inventory in the helium system is also small for the three options. Tritium inventory in the water system can range from negligible to large (120 g) over the wide range of tritium input and of process rates discussed in Sections 3.3.1 and 3.3.2 above.

Tritium inventory in the reactor tube walls is calculated from

$$I_3 = V[(c/b)^2 - 1]S_3\sqrt{\bar{p}_3} \ , \tag{61}$$

Table 3-9. Tritium inventory in fluid systems and in steel tube walls.

System	Tritium inventory (g) for options: A	B	C
Molten-salt system[a]	0.4	0.3	0.6
Helium-gas system[b]	0.1	0.6	1.8
Steel walls of molten-salt reactor tubes[c]	200	2.4	4.0
Steel walls of steam-generator tubes[d]	5.1	11	19
[Tritium input rate (Ci/d) to steam/water system]	(10^2)	(10^3)	(10^4)
Water system[e]	1.2	12	120

[a]For options A and B, a 100-m^3 salt volume is used to allow for the process loop, while option C uses a volume of only 65 m^3.

[b]We used the helium volume as shown in Table 3-6 and the tritium partial pressures given in footnote to Table 3-8.

[c]Data is for 1/2-inch o.d. tubes with 20-mil-thick walls; tritium solubility at 540°C is from Ref. 3-1; partial pressures are from Tables 3-5 and 3-8.

[d]The tube sizes and temperatures are from Table 3-6 (weighted according to $\sum A_j W_j S_j$); tritium partial pressures are given in footnote to Table 3-8. Values given are for options 1A, 1B, and 1C; divide by 2 for 2A, 2B, and 2C.

[e]Data are based on Table 3-6. Water volume and tritiated water concentrations are given in Sections 3.3.2. For the low-input purge case of 3.3.1, the inventory is only 2.5×10^{-4}.

where p_3 is a radial, average, tritium partial pressure. The solubility of tritium in steel[3-1] is calculated from:

$$S_3[Ci/(m^3 \cdot Pa^{1/2})] = (1.04 \times 10^4 \exp(-705/T[K]) \quad . \tag{62}$$

The amount of tritium contained in the steel reactor tubes for option A is a large number (200 g) for several reasons. The permeation barrier is on the outside of the tube wall, which keeps the tritium partial pressure in the steel essentially equal to the axial, mean, molten-salt partial pressure, which is quite high. In addition, tritium solubility in steel is exceptionally high. It is too early in the design cycle to consider this to be a real problem, especially since the whole issue goes away if we put the low-permeability barrier on the inside of the tube.

Options B and C have much lower inventories, since there is no tungsten layer and the partial-pressure drop is taken across the molten-salt boundary layer, leaving the steel at the relatively low tritium partial pressure in helium.

The steam generator tubes will store a moderate amount of tritium, somewhat larger than the reactor tubes for options B and C mainly because of the larger wall thickness.

3.9. SUMMARY AND RECOMMENDATIONS

Tritium in the form of tritiated water is a personnel hazard at concentration levels well below 1 ppm, and steam-generator water will reach the 1 ppm level within a few months of reactor operation unless a combination of permeation barriers and processing are employed.

To gain a better understanding of permeation effects, equations describing steady-state tritium permeation without axial flow have been derived for a multilayer tube wall within the blanket region. A layer of frozen salt is included, along with fluid boundary-layer resistances. Calculations of the partial-pressure distribution show significant differences for tubes irradiated at different power densities. Molten-salt boundary-layer resistance can be important in the absence of a good permeation barrier, or for a low-power tube coated with a nominal 1-μm tungsten barrier. This nominal permeation barrier will dominate the flow resistance, however, for medium or high power-density

tubes closer to the first wall. Examination of the radial flux equation shows a complicated dependence on upstream partial pressure, which reduces to a linear dependence at low pressures where Henry's Law materials become flux limiters and a square-root dependence at high tritium partial pressures where Sievert's Law materials are flux limiting.

An analytical model was developed to establish the tritium split between wall permeation and reactor-tube flow. The tritium fraction escaping through the tube walls has been quantified for limiting cases of Henry's Law and Sievert's Law barriers as flux limiters. All parameters of design interest are explicitly included: tritium generation rates and solubility in salt, tube geometry, barrier permeation parameters, and molten salt processing rate and recovery efficiency.

The intermediate, helium, heat-transfer loop has been treated as a well-mixed tank for analytical purposes, with input from the reactor, partial tritium recovery in a slipstream process loop, and Sievert's Law permeation loss to the steam system.

A combination of effective tritium permeation barriers are required on both blanket and steam-generator tubes (together with substantial process rates for molten salt and helium systems) in order to hold tritium permeation into the steam system to 55 Ci/d, according to case 1A. If this can be done, it may be feasible to simply purge the steam system of incoming tritium with only minor environmental impact and personnel hazard from steam leaks, and without the necessity of costly and hazardous isotopic processing to separate tritiated and ordinary water.

A surprisingly thin (10 μm) tungsten coating will, in principle, provide a good permeation barrier on the blanket tubes. The feasibility of, in fact, reducing tritium blanket permeation by a factor of 300 or so below the bare steel tube rate for some 1×10^4 m^2 of tube area will require a research and development effort. Other materials or alloys may prove to be superior, probably at the price of greater thickness of coating.

A relatively thick 1-mm aluminum sleeve was selected to suppress permeation through the steam-generator tubes. This gave a calculated reduction factor of more than 500 relative to bare steel and including a factor of 30 because of an assumed oxide layer. This is essentially a brute force approach that may well be improved upon by the development of more sophisticated permeation barriers.

Although we have focused attention on a tungsten barrier because of a remarkably low tritium permeability, beryllium and other low-permeability materials such as ceramics and cermets should be considered in a barrier-development problem.

The diffusivity of tritium gas dissolved in molten salt will need to be measured, especially to verify whether or not the fluid-boundary-layer barrier of Option B is realistic.

Finally, some definitive experimental work is called for on the kinetics of tritium gas conversion to tritiated water at low concentrations in helium. Popular opinion has oscillated over the last decade from an initial optimism that thermodynamics would reduce the gas concentration to nil, to a current pessimism that predicts no gas conversion at all in the main helium loop. The critical experiments remain to be done, both with "clean" walls and particulate-free helium as well as in the presence of catalytic surfaces or other reaction promoters. The challenge is to demonstrate a method of drastically reducing tritium gas partial pressure in the intermediate helium loop and thus suppress permeation into the steam system.

REFERENCES SECTION 3.0.

3-1 M. R. Louthan, Jr. and R. G. Derrick, Corrosion Sci. 15, 565 (1975).

3-2 A. M. Hassanein and D. K. Sze, Data Survey and Recommended Values for Permeation of Hydrogen and Its Isotopes Through Steel Alloys, unpublished report, Argonne National Laboratory (1984).

3-3 S. A. Steward, Review of Hydrogen Isotope Permeability Through Materials, Lawrence Livermore National Laboratory, UCRL-53441 (1983).

3-4 D. R. Begeal, J. Vac. Sci. Technol., 15, 1146 (1978).

3-5 J. W. Guthrie et al., J. Nucl. Mater., 53, 313 (1974).

3-6 W. Eichenauer and A. Pebler, Z. Metallkd. 48, 373 (1957).

3-7 P. M. S. Jones and R. Gibson, J. Nucl. Mater. 21, 353 (1967).

3-8 E. A. Aitken et al., Trans. Metall. Soc. AIME, 239, 1565 (1967).

3-9 W. F. Libby, "History of Tritium", in Tritium, A. A. Moghissi and M. W. Carter, Eds. (Messenger Graphics, Phoenix, Arizona, 1971, p. 3).

3-10 G. G. Killough, Derivation of Dose Conversion Factors for Tritium, Oak Ridge National Laboratory, ORNL-5853 (1982).

3-11 A. E. Sherwood, Catalytic Oxidation of Tritium in Air at Ambient Temperature, Lawrence Livermore Laboratory Report, UCRL-52811 (1979).

3-12 C. E. Easterly and M. R. Bennett, "Radiation Catalyzed Conversion of Tritium Gas to Tritiated Water", Proc. 5th Topical Meeting Technol. of Fusion Energy, Knoxville, Tennessee, 116, 1983; Nuclear Technology/Fusion 4, (2) (1983), part 2.

3-13 G. N. Lewis, M. Randall, K. S. Pitzer, and L. Brewer, in Thermodynamics, Chapter 19, (McGraw Hill, New York, 1961), 2nd ed.

3-14 A. P. Malinauskas and D. M. Richardson, Ind. Eng. Chem. Fund. 13, 242 (1974).

3-15 D. S. Shupe and R. E. Stickney, J. Chem. Phys. 51, 1620 (1969).

3-16 J. M. Prausnitz, Molecular Thermodynamics of Fluid-Phase Equilibria, Chapter 8 (Prentice-Hall, Englewood Cliffs, NJ, 1969).

3-17 E. R. G. Eckert and R. M. Drake, Jr., Analysis of Heat and Mass Transfer, (McGraw Hill, New York, 1972), pp. 338, 340, 731.

3-18 G. I. Taylor, Proc. Roy. Soc. London, 219A, 186 (1953).

3-19 H. Katsura and K. Furukawa, J. Nucl. Mater. 71, 375 (1978).

3-20 W. R. Holman and F. J. Huegel, Proc. Conf. Chemical Vapor Deposition Refractory Metals, Alloys, and Compounds, USAEC (1967), p. 127.

3-21 D. J. Bender, Ed., Reference Design for the Standard Mirror Hybrid Reactor, Chapter 9, Lawrence Livermore Laboratory and General Atomic Company Joint Report, UCRL-52478 and GA-A14796 (1978).

3-22 R. G. Mills, Ed., A Fusion Power Plant, Chapters 14 and 15 by Maroni and Johnson, Plasma Phys. Lab., Princeton University, Princeton, New Jersey (1974).

3-23 S. Steward, Lawrence Livermore National Laboratory, private communication (January 1984).

3-24 C. C. Damm, et al., Preliminary Design of a Tandem-Mirror-Next-Step-Facility, Lawrence Livermore National Laboratory, UCRL-53060 (1980).

3-25 L. A. Flanagan, D. Steiner, and G. E. Smith, Fusion Engineering Device Design Description, Vol. 2, Oak Ridge National Laboratory, ORNL/TM-7948/V2 (1981).

3-26 K. Y. Wong, et al., "Permeation of Tritium Through Steam Generator Tubes at CANDU Stations," 10th Symp. Fusion Engineering, Philadelphia, PA, (1983).

3-27 H. K. Rae, Ed., Separation of Hydrogen Isotopes, Am. Chem. Soc. Series 68, Washington, D.C. (1978), p. 163.

3-28 J. Maienschein, Lawrence Livermore National Laboratory, private communication (June 1984).

4.0. MOLTEN-SALT REPROCESSING

We have selected the fluorination process to remove ^{233}U from the salt slipstream. We find it unnecessary to use the more complex reductive extraction of fission products. Molten-salt reprocessing applied to the fusion breeder is well discussed in Ref. 4-1.

A study of three levels of molten-salt reprocessing was carried out recently.[4-2] The simplest level is fluorination only, which removes ^{233}U but not protactinium or many fission products. The next level is both fluorination and reductive extraction in which both uranium and proctactinium are removed along with small amounts of fission products. The final level is the addition metal-transfer treatment, which removes most of the rare earth fission products.

Employing the second and third levels of reprocessing had negligible effects on breeding rates and decay afterheat, except months after reactor shut down. Therefore, our choice of employing only the fluorination process was reaffirmed.

REFERENCES SECTION 4.0.

4-1 J. D. Lee, et al., Feasibility Study of a Fission-Suppressed Tandem Mirror Hybrid Reactor, Lawrence Livermore National Laboratory, UCID-19327 (1982), Section VIIB, "Molten-Salt Fuel Reprocessing" by Warren Grimes.

4-2 F. A. Patterson-Hine, J. W. Davidson, and D. E. Klein, "Contributions to the Thermal Power of Continously Processed TMHR Molten-Salt Blankets," Proc. IEEE 10th Symp. Fusion Engineering, Dec 5-9, 1983, Philadelphia, PA, p 988.

5.0. BALANCE-OF-PLANT CONSIDERATIONS

A brief discussion of the balance-of-plant (BOP) aspects of the Molten Salt Fusion Breeder Plant is presented here. These aspects include: general plant arrangement with special reference to the Fusion Island*, blanket heat-transport system with special reference to the piping and equipment designs, and steam-generator system with special reference to tritium permeation consideration through steam-generator tubes.

5.1. GENERAL PLANT ARRANGEMENT

The major BOP buildings are shown in the Key Plan (Fig. 5-1). The buildings that constitute the Fusion Island are reactor building, steam generator building, molten-salt processing building, tritium processing building, and hot cell. The plant arrangement takes full advantage of the linear nature of the tandem mirror concept. One side of the reactor building is open for rapid construction access, which will impact favorably on plant construction schedule. For the sake of simplicity all the buildings are shown contiguous. Further analysis may favor separation of some of the buildings for safety and cost effectiveness.

The reactor building, steam generator, and molten-salt processing buildings enclose the entire molten-salt and helium-coolant system. The Fusion Island buildings provide a leak-tight confinement for the radioactive materials and radiation protection for operating personnel and the public at large. These buildings are reinforced concrete structures capable of withstanding credible natural and accidental conditions such as earthquake, tornado, or accidental tritium release.

The reactor vessel (including end cells) and its associated structural supports are located in the reactor building. The helium-cooling loops are located partly in the reactor building and partly in the steam-generator building. The steam generators and helium circulators (one of each in each

*Fusion Island consists of the following systems and components and the buildings in which they are located: the reactor, steam generators, molten-salt processing system, tritium processing system, and the hot cell.

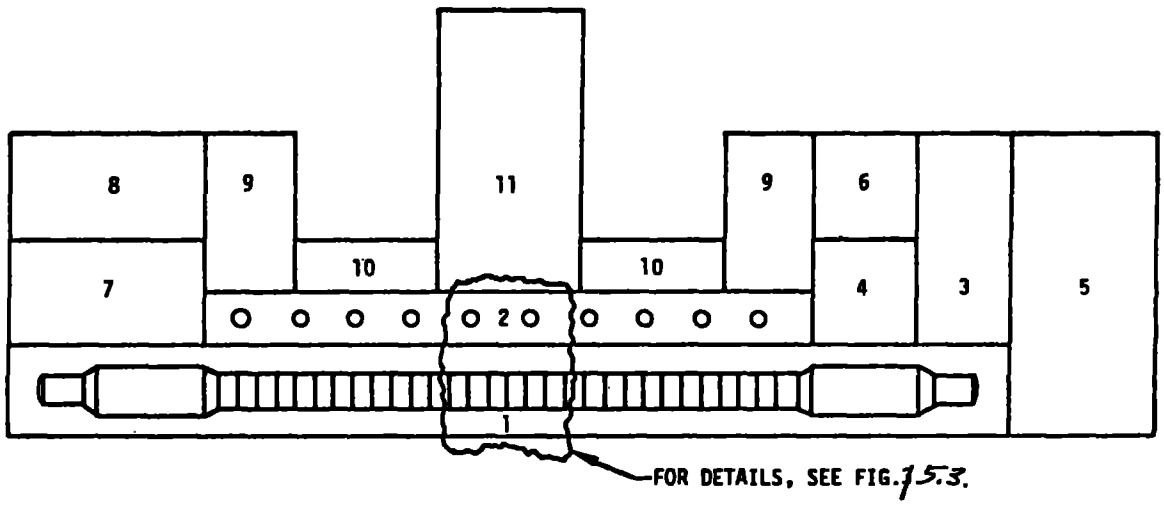

Fig. 5-1. Diagram of plant arrangement: (1) Reactor building, (2) steam generator building, (3) tritium processing building, (4) molten salt processing building, (5) hot cell, (6) radwaste building, (7) component cooling building, (8) plant auxiliary building, (9) power supply building, (10) cryogenics building, and (11) turbine building. Buildings 1 through 5 constitute the Fusion Island.

cooling loop) are located in the steam-generator building. The tritium-processing building primarily houses the equipment for processing plasma exhaust to recover tritium. The molten-salt processing building houses the equipment for processing molten salt to recover uranium and tritium. The hot cell, which is provided for maintaining radioactive components, consists of a hot cell and a warm cell. The warm cell is provided for limited hands-on maintenance operations.

In molten-salt fusion breeder plants all the Fusion Island buildings contain radioactive materials and are thus safety-related structures. According to current fission-industry practice, these buildings are required to be nuclear-grade structures. In addition to meeting many industry codes and standards, nuclear-grade structures are required to meet very stringent Nuclear Regulatory Commission (NRC) criteria. These NRC criteria make structures very expensive. Nuclear-grade structures are used in fission plants for high-pressure-containing (500 to 600 kPa) reactor containment building and its contiguous buildings for safety purposes primarily to contain, in case of an accident, the releasable radioactive materials. However, in the molten-salt fusion breeder plant, there are no such pressure-containment structures, and in addition, the after heat generated is much less than in fission plants.

In light of these unique safety features of fusion, a relevant question may be asked: Can the Fusion Island buildings be constructed to criteria that are less stringent than nuclear standards? In essentially all the fusion conceptual studies it has been assumed that all NRC regulations applicable to fission plants will also be applicable to fusion plants. It is too premature to determine whether this will indeed be the case. In the meantime the question raised here is an attempt to utilize fusion's safety features and to find ways to reduce fusion plant cost. Thus we propose that a new set of criteria be developed for fusion breeders. These new "safety" criteria will retain all NRC safety philosophy; systems and structures built to these standards will meet all NRC radiation-exposure criteria.

Another phenomenon observed in the fission industry indicates that, based on historical cost data, some nonnuclear-grade facilities cost more than comparable facilities on conventional (fossil) power plants. This is primarily because the nonnuclear-grade facilities are often

unnecessarily constructed to nuclear-grade requirements. Many builders find it convenient to build most facilities at one site to one set of standards. However, because of high costs of current fission plants, a trend is developing within the fission industry to build safety-related structures to nuclear-grade standards and nonsafety-related structures to commercial-grade standards. A similar approach is proposed here for the molten-salt fusion breeder plant as indicated below:

- Fusion safety-grade standards:
  - Reactor building
  - Molten-salt processing building
  - Tritium-processing building
  - Steam-generator building
  - Hot cell
  - Radwaste building

- Commercial-grade standards:
  - Component cooling building
  - Turbine building
  - Power-supply building
  - Plant-auxiliary building
  - Cryogenics building
  - Other miscellaneous buildings

5.2. BLANKET HEAT TRANSPORT

The parameters for the blanket heat-transport system are listed in Table 5-1; schematic diagram is shown in Fig. 5-2; and the piping and equipment arrangements are given in Figs. 5-3 and 5-4.

Table 5-1. Heat-transport system of blanket.

Thermal power:	
Total blanket	3,840 MW_t
Added by helium circulator	110 MW_t
Blanket modules (no.)	30
Steam generators (no.)	10
Helium circulators (no.)	10
Thermal power of each steam generator	395 MW_t
Helium temperature:	
Blanket outlet/steam-generator inlet	545°C
Blanket inlet/helium-circulator outlet	300°C
Steam-generator outlet/helium-circulator inlet	293°C
Helium pressure:	
At circulator outlet	5,000 kPa
At circulator inlet	4,875 kPa
Helium pressure drop:	
Blanket	55 kPa
Steam generator	50 kPa
Piping	20 kPa
Total	125 kPa
Helium pumping power:	
Total	110 MW_e
Per circulator	11 MW_e (15,000-hp motor)
Helium flow rate:	
Total	3,000 kg/s
Per module	100 kg/s
Per circulator	300 kg/s
Steam-outlet temperature	510°C
Steam-outlet pressure	16.9 MPa
Feedwater-inlet temperature	193.3°C
Feedwater-inlet pressure	19.0 MPa
Steam flow-rate per steam generator	159 kg/s

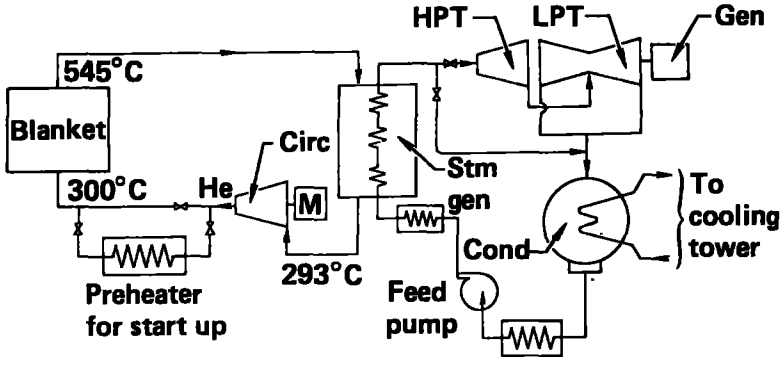

Fig. 5-2. Schematic of heat-transport and power-conversion systems of blanket.

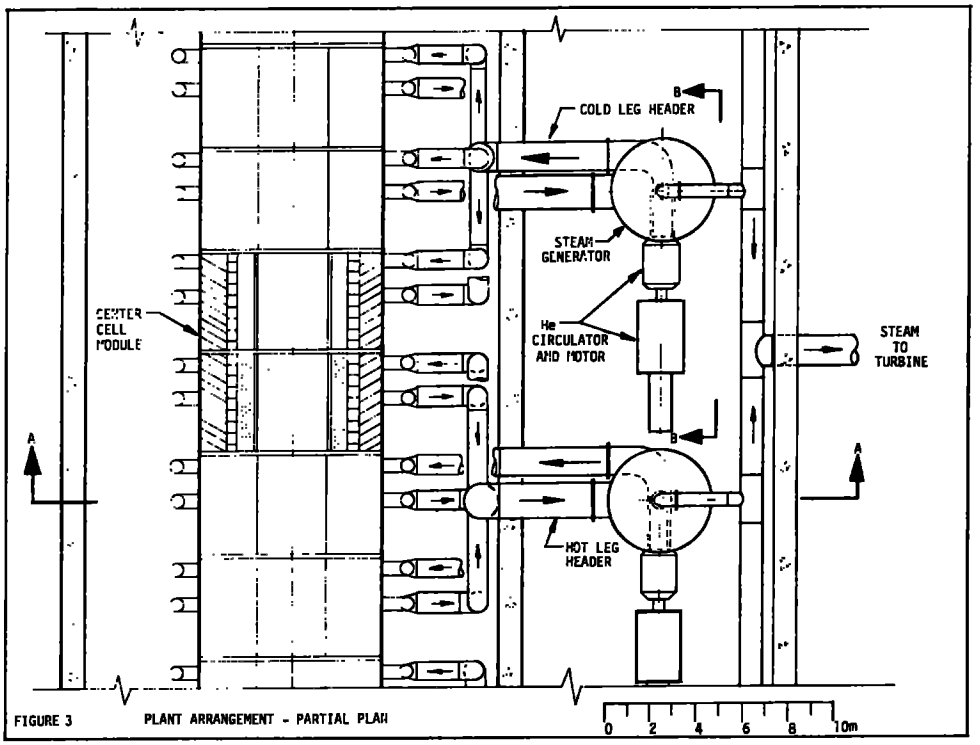

Fig. 5-3. Heat transport system, showing piping and equipment arrangement (overhead view).

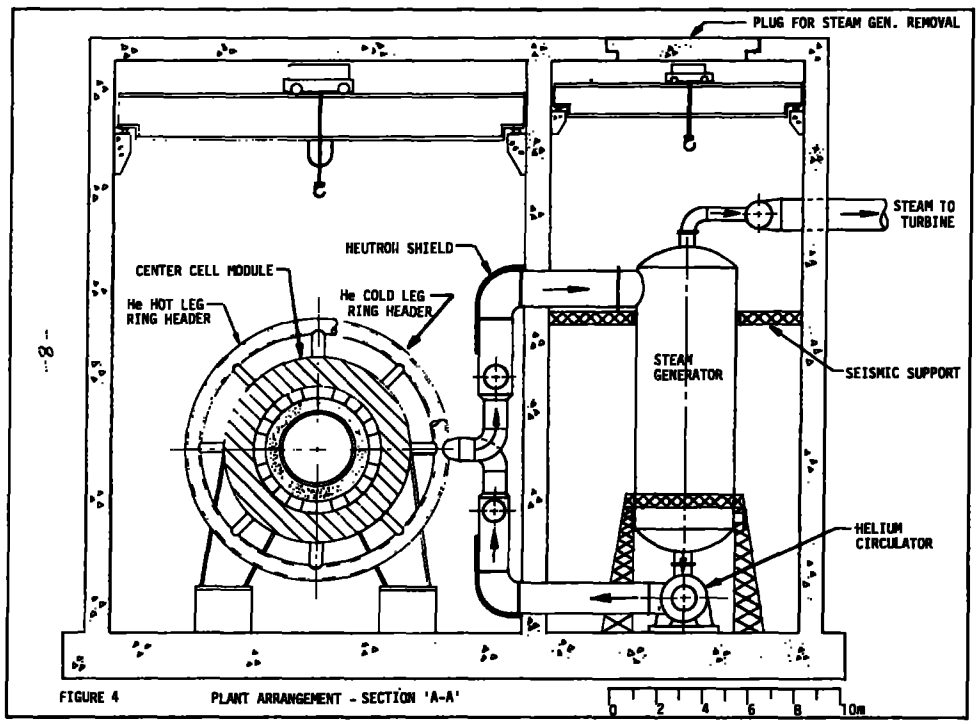

Fig. 5-4. Heat transport system, showing piping and equipment arrangement (sideview).

For the blanket configuration considered, the entire central cell (127-m long) is divided into 30 modules. The size of each module is based on considerations for shop fabrication, transportation, handling, and maintenance. To transport blanket thermal energy, each module is provided with a cold-helium ring header and a hot-helium ring header. Radial supply and return lines connect these headers to the blanket "pods" (see Fig. 3-2 in Section 3.0).

The central cell modules are grouped such that one steam generator serves three modules, which results in ten steam generators each having a capacity of 395 MW_t. Each generator is coupled with a helium circulator to supply cooled helium to the blanket at 5 MPa and 300°C.

The steam generators proposed here are based on design features similar to those already operating in the Fort Saint Vrain high-temperature-gas reactor (HTGR) plant near Denver, Colorado, and also as proposed for the gas-cooled fast reactor (GCFR) demonstration plant.[5-1,5-2] However, the steam generators proposed in this study are located in steel pressure vessels, whereas the Fort Saint Vrain steam generators are located in monolithic prestressed concrete pressure vessels (PCRV). A steel pressure vessel for steam generators is also proposed for modular HTGR concepts currently being considered.[5-3]

In the steam generators proposed for fusion hybrids, hot helium (545°C) enters at the top of the steam generator, flows downward on the shell side of the tube bundle and gives up heat to water and steam, and exits at the bottom (293°C). The water enters through a feedwater tubesheet located at the bottom, flows upward inside the tubes and exits at the top through a superheater tubesheet. An elevation view of the factory-assembled once-through steam generator along with some representative tube details is shown on Fig. 5-5. An internal view of the steam generator used at Fort Saint Vrain plant[5-4] is also given on Fig. 5-5. Figure 5-6 shows an internal view of a steel vessel steam generator considered for the modular HTGR concepts. The pictures and sketches presented here demonstrate the current trends in steam-generator design.

As seen in Figs. 5-4 and 5-5, the steam generator is supported at the bottom on a support structure and is provided with a lateral seismic restraint at the top. A flow-distribution device at the inlet ensures uniform helium flow. Helical coiled tubes, which make up the heat-transfer section of the steam generator, are threaded through perforated tube-support plates, which

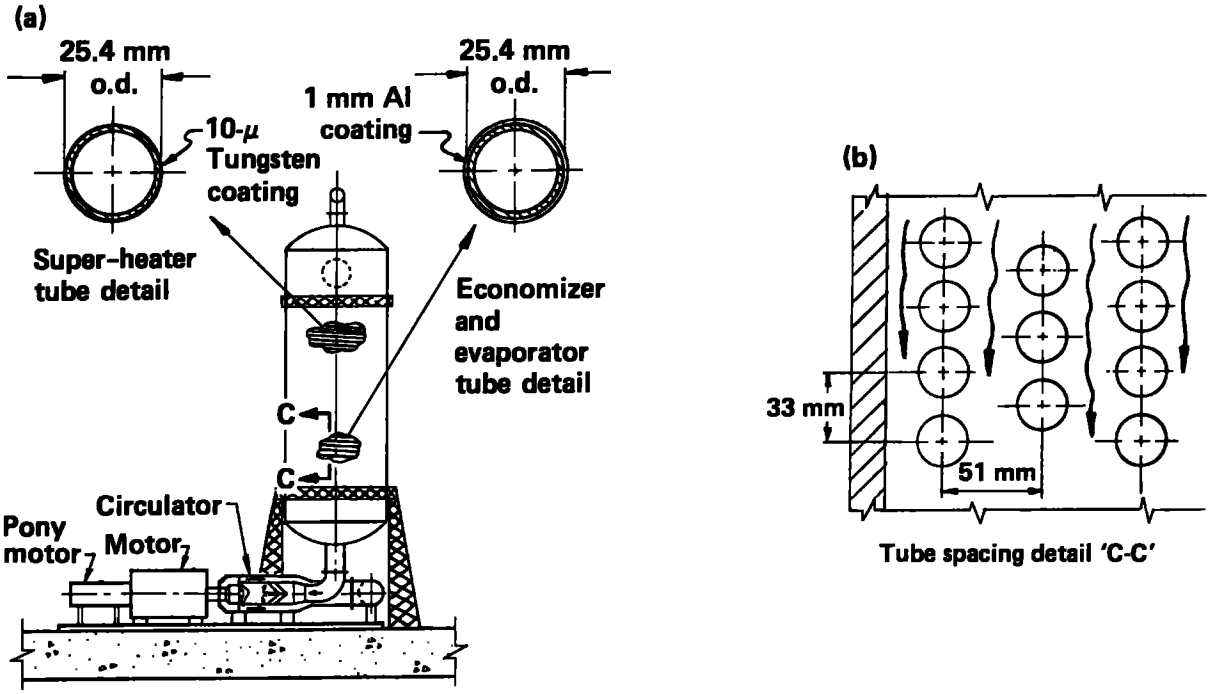

Figure 5.5. Steam generator arrangement. (a) Section 'B-B', (b) Typical tube sparing detail, (c) Fort Sait Vrain steam generator.

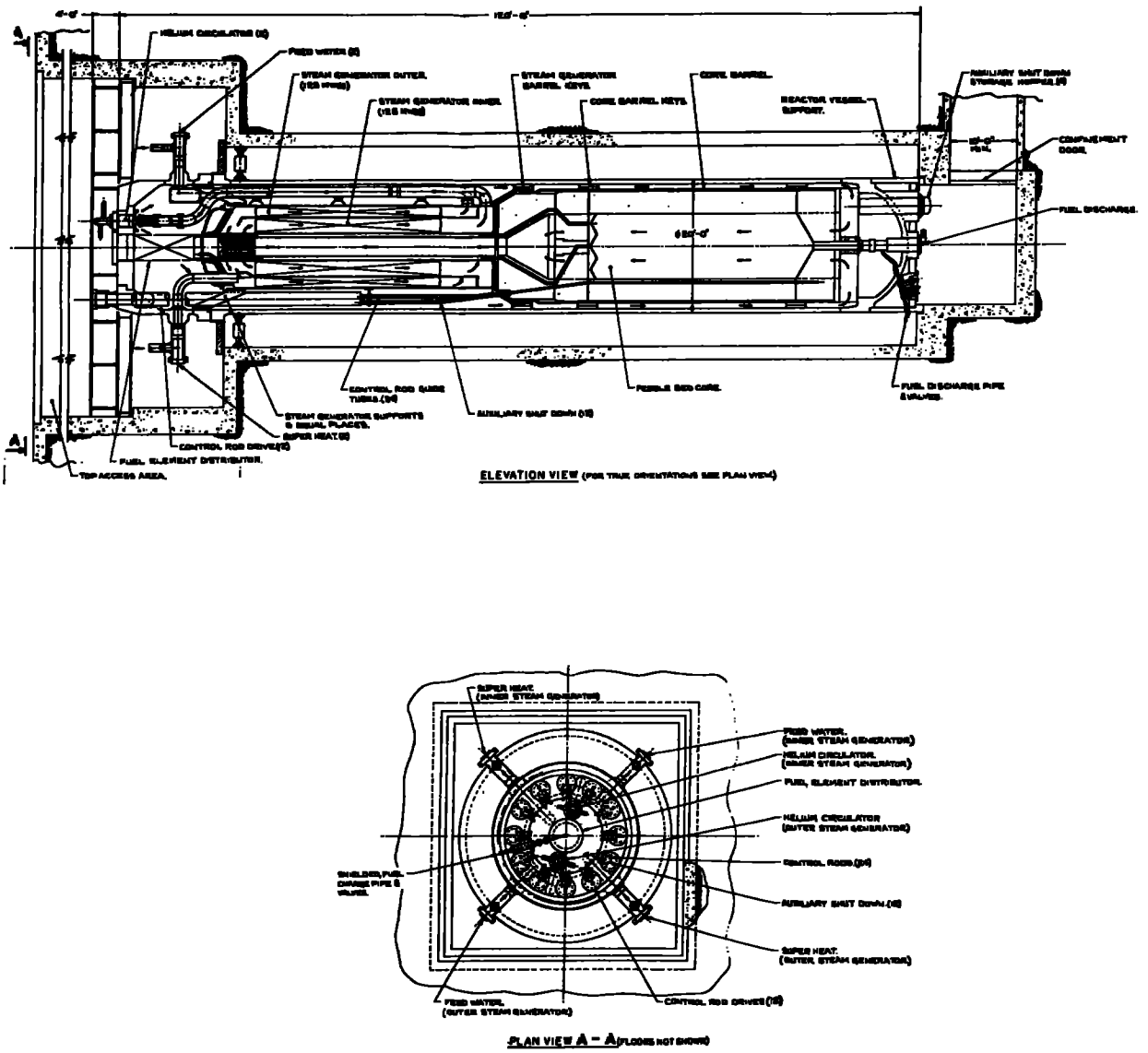

Figure 5-6. Steel vessel steam generator for a high-temperature gas reactor (HTGR).

transmit dead weight and seismic loads to the supporting shrouds. The heat-transfer section of each steam generator is about 4 m in diameter, 8 m long, and is made up of tubes, 2.54-cm o.d.

The entire steam-generator assembly, which can accommodate in-service inspection and in-place tube plugging, is capable of being removed and reinstalled, if required, through a shielded opening plug in the roof of the steam-generator building.

As mentioned earlier, the steam-generator capacity selected for this study is 395 MW_t. This capacity is dictated by two major factors:

- Physical size of steam generator.
- Pipe size for transporting helium.

The largest practical size of steam generator is, in turn, dictated by factors such as thermal load, temperature and pressure of helium, log mean temperature difference (LMTD) across the heat transfer area, temperature and pressure of steam and temperature gradient across the tube. Induced stresses (thermal and pressure) in the tubes, tubesheets, and vessel walls put practical limits on the amount of heat-transfer area that can be accommodated in a single steam generator. The largest capacity currently being considered for steel vessel steam generators for modular HTGR application[5-3] is 250 MW_t. For this HTGR, helium conditions are 688°C and 8.7 MPa, and steam conditions are 541°C and 17.3 MPa, with an overall LMTD of about 98°C. In the molten-salt fusion breeder plant, the helium conditions are 545°C and 5 MPa, the steam conditions are 510°C and 16.9 MPa, and the overall LMTD is approximately 62°C. Thus, the largest capacity steam generator (equivalent to modular HTGR) would be about 160 MW_t. In view of the time frame of fusion deployment, which is some years away, an extrapolation in size by a factor ranging from two to three is considered reasonable. A capacity of 395 MW_t capacity thus falls within this anticipated range.

As an example of the impact of helium pressure and temperature on steam-generator design, let us consider the superheater section. In this section peak helium temperature and pressure are 545°C and 4.945 MPa. For a vessel with an outside-diameter of 4 m, the wall thickness required is about 20 cm. This unusually heavy thickness is required because the allowable stress in the vessel material (2 1/4 Cr, 1 Mo) at 545°C is only about 48 MPa (ANSI B31.1). In the economizer section, on the other hand, the lowest helium temperature is

293°C and the allowable stress is 118.6 MPa. The vessel-wall thickness required is about 9 cm.

Two potential alternatives may be considered to reduce wall thickness in the hotter sections of the steam generator vessel. First, the helium flow paths inside the steam generator may be arranged so that the vessel wall is in contact with the cooler helium (see Fig. 5-6). This may require slightly larger diameter vessel to accommodate the annular passage for the cooler helium. This method is used in the modular HTGR steam-generator design.[5-3] Second, for this potential alternative, the inside surface of the vessel wall may be lined with a thermal insulation such that the metal temperature is maintained at or below 340°C to take advantage of the maximum allowable stress (118.6 MPa, see ANSI B31.1). In this case, however, the inside surface of the thermal insulation must be lined with steel to avoid contamination of helium by the insulating material.

Helium pipe size may also put a limitation on the steam-generator capacity. A larger steam generator requires a larger helium flow through pipe headers connecting the steam generator with the reactor. High temperature and pressure of helium put practical limitation on pipe sizes. The largest pipe size considered in this study is 1.5 m o.d. A discussion on pipe size selection is given in the following paragraphs.

The piping system connecting the reactor and the steam generators constitutes an important element of the heat transport system because of its cost and its impact on the building size and helium pumping power. The piping arrangement shown in Figs. 5-3 and 5-4 is developed with a view to reducing these impacts. Pipe sizes are selected for reasonable flow velocities (50 to 70 m/s) to limit pressure drop in the piping system to a reasonable level (20 kPa, which is about 15% of the total pressure drop in the heat transport loop).

Selection of pipe size is generally based on a cost trade-off between initial cost of pipe and operating cost due to pumping power. A larger pipe has a lower pressure drop, which results in lower pumping power. This implies higher initial cost of pipe but lower operating cost of pumping. A smaller pipe has an opposite effect. In the present study, results of existing design studies[5-2,5-4] are used instead of a trade-off study. Helium pumping power for the entire heat-transport loop is generally limited to 2.5% to 3% of total thermal power. Using this criterion and knowing pressure drop through blanket and steam generator[5-5], we target the pressure drop in the piping system to

Table 5-2. Parameters for hot-leg header of helium-transport loop.

Parameter	Value
Pipe	
Outside diameter, D_o	1.50 m
Wall thickness	0.08 m
Inside diameter, D_i	1.34 m
Internal flow area	1.41 m^2
Pipe material	Alloy carbon steel (2 1/4 Cr, 1 Mo)
Helium	
Temperature	545°C
Pressure, P	4.945 MPa
Density, ρ	2.9455 kg/m^3
Viscosity, μ	3.92×10^{-4} poise (g/cm•s) = 3.92×10^{-5} kg/m•s (Ref. 5-6)
Flow rate, m	300 kg/s (total for three modules) = 102 m^3/s
Flow velocity, V	flow rate/flow area = 102/1.41 = 72 m/s
Reynold's number, $Re = \rho VD/\mu$	$2.9455 \times 72 \times 1.34 / 3.92 \times 10^{-5} = 7.25 \times 10^6$
Friction factor, f (Ref. 5-6)	0.01
Pressure drop	
Per meter of pipe length	$fV^2\rho/2D_i = \frac{0.01 \times 72 \times 72 \times 2.9455}{2 \times 1.34}$ $\sim$ 60 Pa
Total in 20-m-long header (including 50% allowance for losses in the bends)	1.5 kPa

approximately 15% of the total loop pressure drop. The pipe sizes thus estimated result in the flow velocities between 50 and 70 m/s, which are generally used in the industry. As an example, let us consider the hot-leg header having the parameters shown in Table 5-2. Pressure drop in all segments of the piping system can be similarly evaluated. Alloy carbon steel (2 1/4 Cr, 1 Mo) is assumed for all helium piping.

The largest pipe sizes for helium flow between a steam generator and three central-cell modules combined are estimated to be 150 and 130 cm o.d. for the hot leg and the cold leg, respectively. The operating conditions in these pipes require large wall thicknesses. In the hot leg, for example, the 545°C and 5 MPa (approx.) operating conditions lower the allowable stress to about 48 MPa (7,000 psi) requiring 8-cm wall thickness. These unusually heavy pipes, which truly may be characterized as pressure vessels, are very expensive. In addition, their seismic support and thermal expansion requirements will have adverse impact on the building sizes and costs. Several alternatives for alleviating these adverse impacts, such as the following, will be considered:

The pipes may be internally insulated so that the steel wall is subject to much lower temperature. A steel liner on the surface of the insulation and in contact with helium is required to maintain purity of helium and possibly to reduce tritium permeation. The liner may be so provided that it is not subject to stress. A similar method is used in the steel industry, although there the hot gas is at much lower pressure (0.1 to 0.2 MPa).

In contrast to a large single pipe, three smaller pipes may be provided, each serving a module. The economics of the two approaches need to be evaluated. One major disadvantage of the three-pipe over the single-pipe approach is the need for three times as many penetrations through the reactor building wall. This may degrade the leak-tightness of the building, and more shielding will be needed to prevent neutrons escaping through the penetrations.

The steam generators may be located in the reactor building very close to the reactor to minimize the pipe lengths. This arrangement exposes the steam-generator components to low-level neutron radiation and, consequently, makes the steam-generator and reactor maintenance more difficult. Future studies should focus on which of these alternatives is most cost effective.

Each of the helium circulators is rigidly mounted horizontally on the floor below the steam generator. Each is driven by an 11-MW_e (15,000-hp) electric motor, also mounted horizontally. Helium leaving the steam generator

enters the circulator and is accelerated by a centrifugal impeller, passes into a series of pipe diffusers and then discharges into a plenum surrounding the circulator. Helium from this plenum then flows through the cold-leg header (Fig. 5-3) to the cold-leg ring header (Fig. 5-4) and is then distributed radially inwards into the blanket 'pods'.

The helium circulators are of single-stage radial-flow type. A variable frequency (thyristor type) controller provides for variable-speed operation of the circulator to provide the required cooling flow for part-load and full-load operation. In addition, the circulators are capable of performing under emergency conditions. Independently powered pony motors (low-capacity motors) provide circulation for decay-heat removal.

The pumping power requirement for each circulator is estimated by using the following expression:[5-7]

$$\text{Power} = m \frac{k}{k-1} P_1 V_1 \left[(P_2/P_1)^{(k-1)/k} - 1 \right] / n_c, \ MW_e ,$$

where m = helium flow-rate per circulator (kg/s), k = ratio of helium specific heats (C_p/C_v); P_1, P_2 = inlet and outlet pressures (MPa); v_1 = specific volume of helium at inlet (m^3/kg); and n_c = overall compression efficiency.

If m = 300 kg/s,
k = 1.667,
P = 4.875 MPa,
P = 5.0 MPa,
ρ = 0.2383 m^3/kg (at 4.875 MPa and 293°C),
n_c = 0.8,
then power = 11 MW_e (15,000-hp-rated motor).

Steam power-cycle parameters, listed in Table 5-1, are dictated by a large number of factors. The most important of them are hot and cold helium temperatures, steam-generator design (i.e., available technologies for its structural and thermal design), and steam-generator cost. A detailed discussion of the steam-generator design is not the purpose of this report. However, if helium is proposed for fusion reactor designs, it is important to pay serious attention to its impact on fusion plant design and economics.

With the general objective of optimizing steam-cycle efficiency for a given hot-helium temperature, one likes to get as high a steam temperature as possible. However, a higher steam temperature implies a smaller log-mean-temperature difference (LMTD), and as we know, a smaller LMTD implies a larger steam generator. Thus the added steam generator cost needs to be weighted against the added benefits from a higher steam cycle efficiency. For comparison, note that current helium steam-generator designs employ superheater LMTD's of about 160°C[1,5-1] whereas the design in this study employs a superheater LMTD of about 65°C. Thus, for the same MW_t requirement, a much larger superheater section (about 2.5 times as much heat transfer area) is needed. Similar considerations also apply to the evaporator and economizer sections of the steam generator. The cost of this larger steam generator needs to be determined in future work.

The effect of pinch point also needs to be considered in selecting steam cycle parameters. The pinch point is the smallest temperature difference between helium and water which occurs in the evaporator section. The average value of pinch point commonly used in industry is about 30°C[5-1]. However, if desired, smaller values may be used with higher heat-transfer area.

The helium and steam parameters at various stages in the steam generators are presented in Fig. 5-7. Standard steam and feedwater conditions that are currently in use in industry are assumed. Superheater-outlet steam conditions are 16.9 MPa and 510°C, and feedwater-inlet conditions are 19 MPa and 193.3°C. The diagram in Fig. 5-7 is also used to make a rough estimate of the heat transfer area needed. The following expression is used to estimate the heat transfer area:

$$Q = U\ A\ (LMTD) \quad ,$$

where Q = heat transferred (W); U = overall heat-transfer coefficient across the steam-generator tube from the helium side to steam/water side ($W/m^2 \cdot °C$); A = heat transfer area (m^2); LMTD = log-mean-temperature difference in °C. The above expression is applied to each section of the steam generator and an approximate heat-transfer coefficient, 1135 $W/m^2 \cdot °C$, is assumed for the purpose[5-8]). The following approximate heat-transfer areas are estimated for each steam generator: Economizer - 2,315 m^2, Evaporator - 1,810 m^2, Superheater - 1,715 m^2. All the steam generator tubes are 25.4 mm o.d. Estimated tube-wall thicknesses are 4 mm in the economizer and evaporator sections and 5 mm in the superheater section.

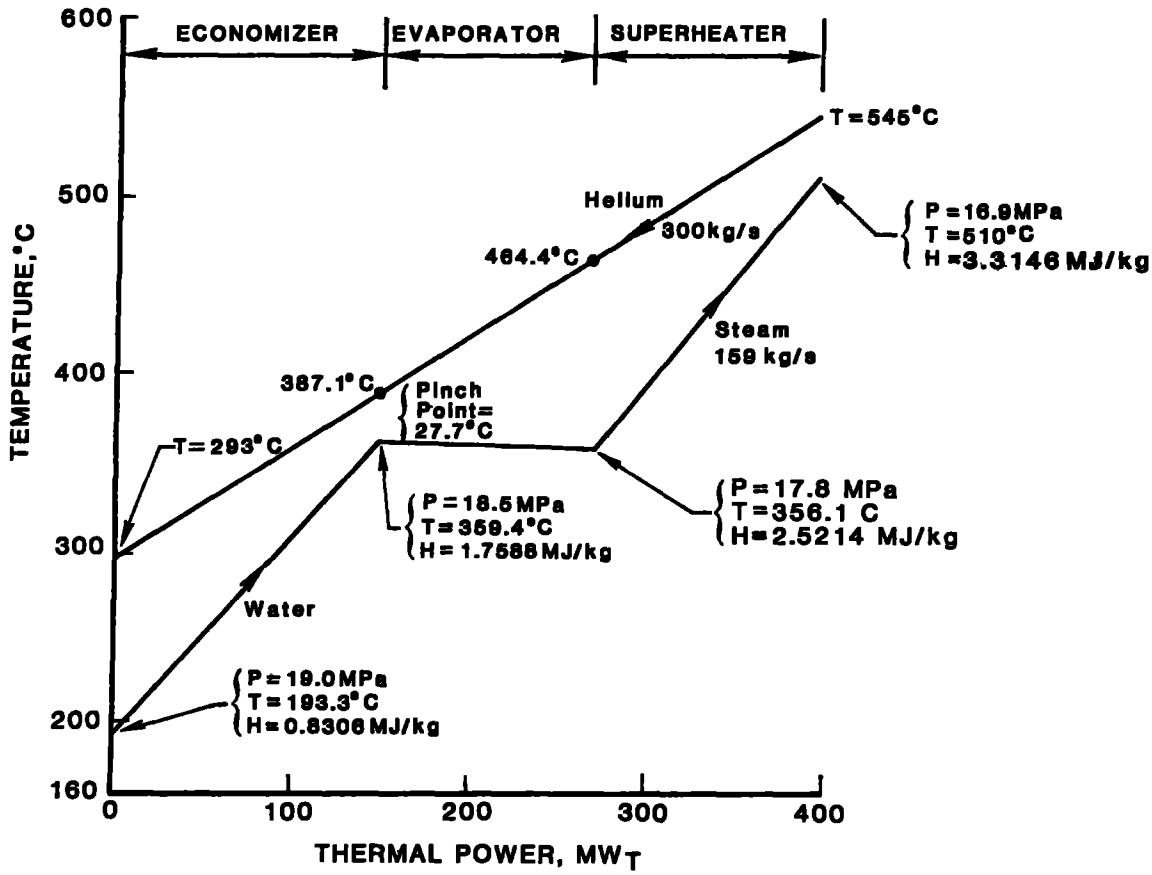

Figure 5.7. Temperature profile for steam generator.

5.3. TRITIUM PERMEATION IN STEAM GENERATORS

As previously discussed in Section 2.4, tritium permeation from helium to steam through steam-generator tubes is a major safety and economic concern. That permeation can be reduced by a factor of 300 by providing a permeation barrier on the tube surfaces also was mentioned in that section. The stated reduction factor can be achieved by either a 10-μm tungsten or a 1-mm aluminum coating on the tube surface. We discuss the selection of the proposed barrier in the following paragraphs (also see Refs.).[5-9 to 5-13]

The permeation barriers may be provided either on the inside or on the outside surface of the tubes. Two potential problems are associated with the inside barriers. First, high-temperature steam (510°C) in contact with aluminum results in unacceptable corrosion problems. Second, several problems are associated with the use of tungsten. Although technology exists for making tungsten-coated (internally) pipes, it may be difficult to ensure complete internal coverage. Incomplete coverage results in unacceptable tritium permeation, for example, loss of coverage occurs when tubes are prepared for welded joints. Flaking of tungsten off the tube wall may cause serious damage in the turbine components. Thus, in view of the above potential problems, internal barriers are not proposed in this study. However, the choice should be revisited in the future as these problems may be overcome by improvement in design and/or technology. External barriers are proposed, as discussed below.

Several processes are available for providing an aluminum barrier on the outside surface of a steam-generator tube wall. First, a method known as 'cold extrusion' may be used to form a duplex tube. Although technology exists, this specific combination (aluminum over alloy steel) has not been tried. Another method is to use two separate tubes, one steel and one aluminum. The aluminum tube is heated to a high temperature and pushed over the cold steel tube. The major uncertainty in the two above methods is the performance of the as-formed tube at operating temperature. Aluminum, with a coefficient of thermal expansion higher than that of steel, may tend to separate, thus greatly lowering the heat-transfer coefficient. A third and relatively new process known as 'Alonizing' is also available.[5-14] This is a diffusion process in which gaseous alumina (Al_2O_3) is allowed to diffuse into the tube wall. Alumina concentrations up to about 40% and to a depth of up to about 1 mm may be obtained. However, it is not known if this will meet

the tritium barrier requirements. Further information regarding diffusion bonding between aluminum and steel may be obtained from Ref. 5-15.

Tungsten coating, as a barrier, can also be applied in a number of ways. First, a process similar to 'Chromizing' may be employed. This is done by placing the tube in contact with tungsten powder, heating it to a high temperature, and keeping it there for a long time in a reducing environment. This is a diffusion process. The major uncertainties in this process are the achievable concentration and depth of tungsten on the tube wall. Another and more readily applicable process is plasma spraying or flame spraying. However, exfoliation (flaking off) at high temperature is a major concern. This may reduce effectiveness of tungsten as a tritium barrier and may cause damage to the helium circulator impeller. Another method is chemical vapor deposition as proposed for the salt-carrying tubes where WF_6 is reduced by H_2 at 550 to 640°C. This process application is discussed in Section 2.7.

In light of the above discussion, aluminum coating in the form of a duplex tube is proposed. However, in the superheater section of the steam generator, helium operating temperature (545°C) is close to the melting point of aluminum alloy 6061-T6 (582°C). Thus, it is proposed that tungsten coated tubes (using plasma spraying or flame spraying) be used in the superheater section and aluminum-coated tubes elsewhere (economizer and evaporator sections).

It is evident from the above paragraphs that the tritium barriers proposed are not entirely satisfactory because of the problems associated with them. Aluminum coating in the form of duplex tube may degrade the heat-transfer coefficient and is not suitable in the superheater section. Exfoliation of tungsten coating in the superheater-section tubes may cause damage to the helium circulator and may degrade the quality of tritium barrier. 'Alonizing' may be a potential solution to these problems. Since aluminum forms an alloy with steel, it is suitable in the superheater section and does not degrade the heat=transfer coefficient in the manner that an external sleeve does. Also exfoliation is not a problem with alonized steel. The major uncertainty, however, is its effectiveness as a tritium barrier. Thus, it is important to further investigate, both theoretically and experimentally, the effectiveness of alonized steel as a tritium barrier and to find methods for improving resistance to tritium permeation.

As indicated earlier (Section 3.0.), tungsten is a better tritium barrier than aluminum by a factor of about 100. Thus diffusion bonding of tungsten and steel (similar to 'Chromizing') should also be investigated.

REFERENCES SECTION 5.0.

5-1 J. King, GA Technologies, San Diego, CA, private communication (Oct. 1984).

5-2 Gas-Cooled Fast-Reactor Demonstration-Plant Design Description, Helium Breeder Associates, Feb. 1980).

5-3 Interim Evaluation Report - 4X250 MW_t HTGR Plant Vertical-Inline Steel Vessel Concept, Gas-Cooled Reactor Associates, Report No. BNI/GCRA 84-006 (Sept. 1984).

5-4 D. E. Davis and J. M. Krase, Fort St. Vrain Nuclear Generating Station--Nuclear Components, Nuclear Engineering International, December 1969.

5-5 C. P. C. Wong, GA Technologies, San Diego, CA, private communication (April 1984).

5-6 Flow of Fluids, Crane Co., Technical Paper No. 410 (1974).

5-7 Kent's Mechanical Engineers' Handbook, Power Volume, Twelfth Edition, Page 1-42 (December 1954).

5-8 D. Carosella, GA Technologies, San Diego, CA, private communication (Oct. 1984).

5-9 Y. Chung, Bechtel Group, Inc., San Francisco, CA, private communication (Oct. 1984).

5-10 D. Roberts, GA Technologies, San Diego, CA, private communication (Oct. 1984).

5-11 M. Gold, Babcock & Wilcox, Barberton, Ohio, private communication (Oct. 1984).

5-12 A Blazewicz, Babcok & Wilcox, Barberton, Ohio, private communication (Oct. 1984).

5-13 D. Schluderberg, Babcock & Wilcox, Lynchberg, Virginia, private communication (Sept. 1984).

5-14 W. A. McGill and M. J. Weinbaum, "Aluminum Diffused Steels Resist High Temperatures in Hydrocarbon Environments," Metal Progress (Feb. 1979).

5-15 P. D. Calderon, Evaluation of Diffusion Bonded Aluminum Alloys to Stainless Steel, M. S. Thesis, University of California, Davis, CA; also Lawrence Livermore National Laboratory, UCRL-53428 (July 1983).

6.0. INTEGRATED PERFORMANCE AND ECONOMICS

6.1. OVERVIEW

In this section, the overall performance and cost figures for the molten-salt fusion-breeder reactor are estimated and are combined with similar data for ^{233}U-burning LWR fission reactors. We can then estimate the costs of electricity and bred fuel for a symbiotic, electricity-generation system consisting of the fusion breeder, its LWR clients, and the associated fuel cycle facilities. Throughout the discussion, the results for the molten-salt fusion breeder are compared with those for a reference case, the liquid-lithium-cooled fusion breeder design of 1982.[6-1] Derived quantities (such as the plant capital cost, the plant net electricity and fissile-fuel production, the cost of bred fuel, and the symbiotic cost of electricity) are compared on a consistent basis for tandem mirror fusion breeders with the same fusion power but with different blanket designs and fuel cycles. The performance parameters used to describe the molten-salt fusion breeder are given in Table 6.1.

Table 6.1. Performance parameters.

F_{net}	0.6
M	1.6
$P_{wall\ load}$	2 MW/m^2
P_{fusion}	3000 MW
$P_{blanket}$	3840 MW
$P_{nuclear}$	4440 MW
$P_{electric}$ [a]	1380 MW_e
Production rate[b]	6380 kg of ^{233}U per full-power year
Cost	$4867 M

[a]Assuming Q = 15, direct conversion efficiency = 50%, thermal conversion = 33%, and P_{max} = 30 MW_e.
[b]At a capacity factor of 80%.

In addition to comparing the two fusion-breeder options, each option is compared with that of an alternative LWR that is fueled with mined uranium and benefits from the full recycle of all fissile uranium and plutonium isotopes (i.e., fuel reprocessing is assumed to be available and to be economically advantageous). The latter comparison provides some indication of the potential economic viability of the fusion breeder under government or utility ownership and operation.

6.2. SYMBIOTIC ECONOMICS

Since the fusion breeder produces two principal products (fissile fuel and electricity), a method of economic assessment that equitably balances the cost of producing each must be established. The conceptual basis for one such method is shown in Fig. 6-1. Specifically, an imaginary line is drawn that encloses the fusion breeder, its LWR clients (enough of them to consume all of the bred fuel), and the associated fuel-cycle facilities. Then it is possible to construct an electricity-generation system that has no net fuel production or consumption and that produces only one net product, electricity. Knowing the annual capital, operating, and fuel-cycle costs for both the breeder and its LWR clients and assuming that the fusion breeder and LWRs sell electricity at the same price, we can estimate the cost of symbiotic electricity on an annual basis. Further, a consistent unit cost of bred fissile fuel in any year of operation can be estimated by subtracting the electricity-production revenue of the breeder (as derived above) from its overall annual operating cost (including all components) and dividing by the net fissile-fuel production. It can be shown that LWRs consuming fuel at this cost will also produce electricity at the same cost as the fusion breeder.

A detailed description of the methods of economic analysis used in developing the above cost estimates is beyond the scope of this section but is provided in Ref. 6-1. A list of the general financial input data used in this analysis is presented in Table 6-1.

For the fusion breeder, both government and utility ownership were considered. Government ownership may be the more likely option for several reasons. First, fusion breeders effectively are a fissile enrichment technology, which (with fuel reprocessing) will eventually replace existing

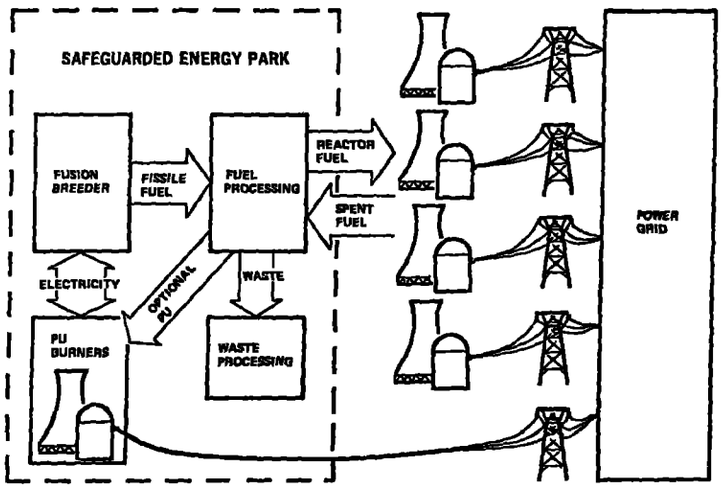

Figure 6-1. A fusion-fission electricity-generation system. Such a system would have only one net product--electricity.

Table 6-2. Comparison of financial input data for breeder and light-water reactors (LWR).

Financial input	Utility-owned breeder	Gov't-owned breeder	Utility-owned LWR
Plant construction period (yr)	10	Same	Same
Plant lifetime (yr)	30	Same	Same
Inflation rate (%/yr)	5	Same	Same
General escalation rate (%/yr)	5	Same	Same
Bond finance fraction (%)	55	100	55
Tax-exempt bond rate (%/yr)	8.2	Same	Same
Stock finance fraction (%)	45	N/A	45
Taxable stock rate (%/yr)	10.25	N/A	10.25
Net discount rate (%/yr)	9.12	8.2	9.12
Income tax rate on stocks (%)	50	N/A	50
Property tax rate (%)	1.45	0	1.45
Annual depreciation (%)	3.3	N/A	3.3
Misc. fixed charge and ins. rate (%)	0.25	0	0.25
Decommissioning cost (% of original)	5	Same	Same
Net total fixed charge rate (%/yr)	15.05	9.05	15.05
Fixed charge rate on fissile inventory (%/yr)	7.9	3.0	7.9
Net operation and maintenance cost (%/yr)	1.8	Same	Same

N/A indicates not applicable.

and advanced fissile-enrichment technologies as conventional uranium resources become scarce and expensive. Enrichment facilities have historically been government owned and have been operated under government contract.

Second, to achieve economics of scale, fusion breeders will be large and expensive. Since one fusion breeder will serve 15 to 20 LWRs of equivalent thermal power, it is likely that most utilities would prefer to look to the federal government as a continual provider of fissile fuel.

Third, by controlling the production and processing of fissile fuel, the government can best implement a system of technical and institutional safeguards to prevent the illicit diversion of fissile materials. If the bred fuel is ^{233}U (the preferred option) a diversion resistant product can be provided to LWR operators by denaturing the ^{233}U with ^{238}U and/or spiking, etc. The small quantities of plutonium produced from LWR neutron capture in the ^{238}U could be designated for consumption at an "approved" LWR site, burned in LWRs co-located within the safeguarded, fuel cycle center (as shown in Fig. 6-1) or disposed of.

Referring to Table 6-1, note that inflation and escalation rates of 5%/yr are assumed in all cases. Also, plant construction periods and lifetimes of 10 and 30 years, respectively, are also assumed in all cases. For government financing, 100% debt financing at 3% above the inflation rate (i.e., 1.05 x 1.03 = 1.082) is assumed. In this case, no federal, state, or local taxes, or insurance, or miscellaneous costs are applied, and the resulting net total fixed-charge rate of 9.05%/yr is 6%/yr lower than the 15.05%/yr cost of money for a utility. Consequently, the economics for government ownership will result in a marked advantage relative to those for utility ownership of the fusion breeder. In all cases the client LWRs are assumed to be utility owned and operated.

Prior to presenting the results for symbiotic electricity-generation systems, we will develop a consistent electricity-cost estimate for an alternative LWR fueled by conventional uranium with full fissile recycle and reprocessing. An understanding of the cost of electricity for the above option will provide a means to better understand the potential economic advantages for a fusion breeder.

As shown in Table 6-3, it is assumed that the LWR capital cost in 1982 dollars is \$467/kW_t (or \$1.4B/GW_e). This value, used throughout the

*Higher LWR costs would increase the cost of electricity but also would make the fusion breeder more attractive as a supplier of fuel.

Table 6.3. Market penetration analysis of economics for a U_3O_8-fueled LWR with reprocessing (1982 U.S. dollars).

LWR capital cost ($/$kW_t$)	467
Total fixed charge rate (%/yr)	15.05
Fuel cycle	Full recycle
^{235}U consumption ($g/kW_t \cdot yr$)	0.194
Avg. burn-up (MW•d/tonne of heavy metal)	30,400
Reprocessing cost ($/kg heavy metal)	558
Fabrication cost ($/kg heavy metal)	554
Enrichment cost ($/kg heavy metal product)	130
Transport and disposal cost ($/kg heavy metal)	97
Year-one cost of U_3O_8 ($/kg)	55
Year-one cost of elec. (mil/kW_ehour)	47.3
U_3O_8 escalation rate (%/yr)	7.1
Avg. PV cost of elec. (mil/kW_ehour)	31.0
Avg. PV cost of U_3O_8 ($/kg)	76

analysis, anticipates a stable nuclear economy and is consistent with long-term planning assumptions rather than with recent experience.* The fuel cycle costs shown in the table were taken from Reference 1, but were originally adapted from the results of the NASAP study.[6-2] The U_3O_8 escalation rate of 7.1%/yr (2%/yr above general inflation) is used to model the increasing cost of mined uranium over the 30-year life of an alternatively fueled LWR which operates during the time frame of conventional uranium depletion (e.g., beginning in the year 2020) but is not fueled by the fusion breeder. Specifically, U_3O_8 is assumed to cost \$55/kg (\$25/lb) in the first year of operation, \$59/kg in the second, and \$402/kg in the thirtieth year. However, accounting for the 5%/yr inflation rate, the year-one worth (i.e., 1982 dollar value) of 402 dollars in year 30 is only $402/(1.05)^{29}$ = \$98, or about a 75% uranium cost increase in constant dollars over 30 years. The average cost of U_3O_8 during this period is \$76/kg in 1982 dollars.

The results shown in Table 6-3 indicate that the U_3O_8-fueled LWR would produce electricity for 47.3 mil/kW_e•h during its first year of operation. The average present value cost of electricity over the 30-year operating life, 31.0 mil/kW_e•h, is lower than the year-one value because the annual cost of electricity from the LWR increases less quickly than general inflation. The latter behavior is a well-known feature of all capital-intensive power-production options -- they are expensive to build but pay off in later years because of low operating costs.

6.3. COMPARISON WITH REFEFENCE CASE

For purpose of illustration, the performance and economics results for the molten-salt blanket fusion breeder are compared with those for a reference fusion breeder.[6-1] The reference breeder would utilize the liquid lithium-cooled blanket shown in Fig. 6-2, but the fusion-driver components would be identical to those for a fusion breeder with a molten-salt blanket. This choice of the fusion driver allows a consistent comparison of the two blanket types accounting for any differences in the areas of cost, breeding, power production/conversion, and fuel processing.

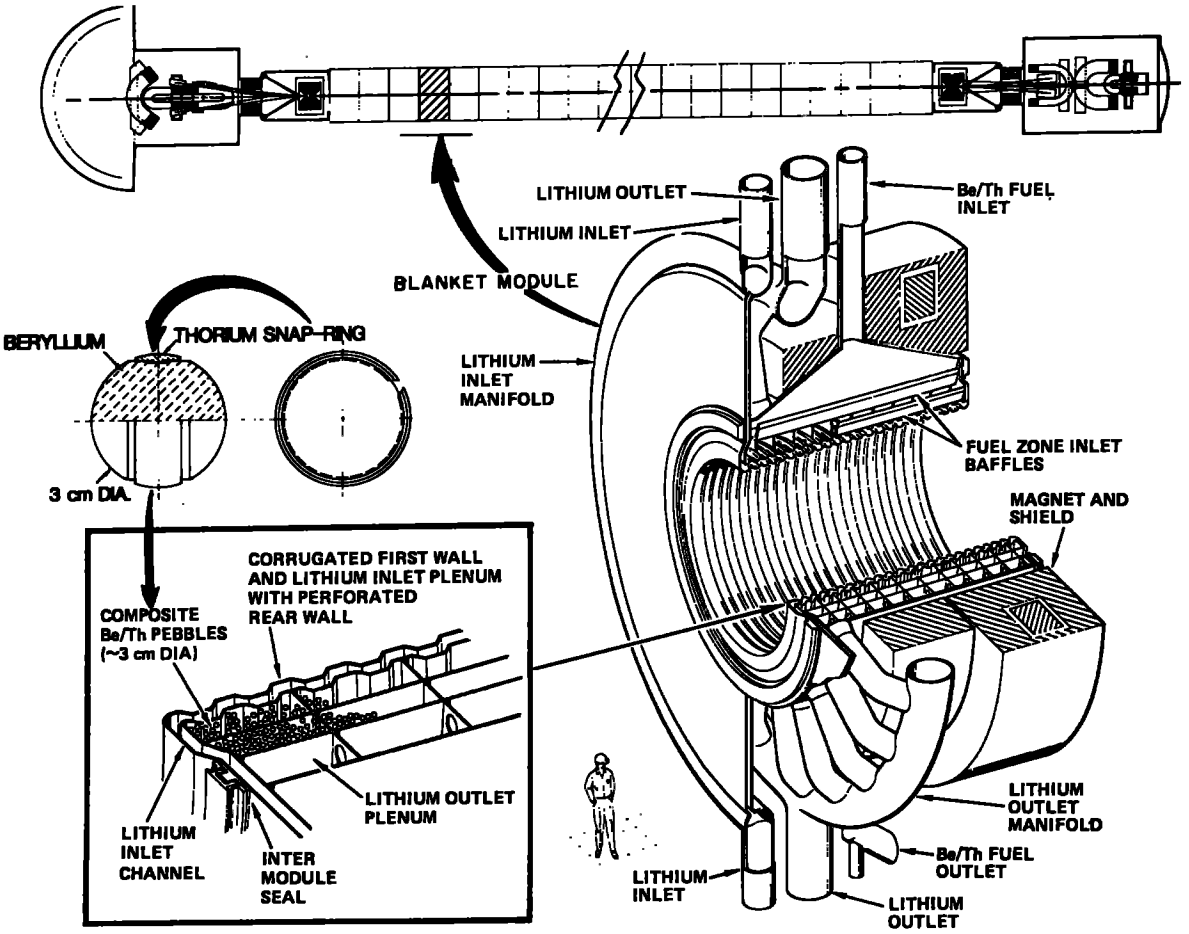

Figure 6-2. Schematic of reference fusion breeder with liquid-metal cooled blanket.

6.3.1. MOLTEN-SALT ADVANTAGES

Several features of the molten-salt blanket can be expected to positively impact system economics. Most importantly, replacing aqueous THOREX-fuel reprocessing with direct fluorination of the molten salt gives the following advantages:

- Lower cost for fuel-reprocessing plant.
- Elimination of thorium-metal fuel-fabrication plant.
- Lower blanket-energy multiplication.
- Zero blanket-energy swing.
- Lower in-core and ex-core fissile inventories.
- Higher plant-capacity factor.

The first of these is well known. As shown in Table 6-4, despite the added burden of maintaining a much lower fissile-discharge concentration, the molten-salt reprocessing plant is expected to cost about an order of magnitude lower than that of the THOREX plant.[6-3]. The elimination of the requirement for a thorium-metal fuel-fabrication plant (and the remote operation of same) also represents a direct benefit of molten-salt reprocessing.

Because the molten salt is maintained at a constant and low fissile concentration, the other important advantages listed above also result. The lower blanket-energy multiplication can result in an enhanced fissile-fuel production per unit thermal power (i.e., higher support ratio). Although not an economics advantage per se, it is expected that fusion breeders with the lower blanket-energy multiplication will have higher safety margins and will also be institutionally favored, because less electrical power will be generated within the remote fuel-cycle center.

Because the fissile concentration can be easily controlled in the molten-salt blanket, it is also possible to operate the blanket at higher than the minimum blanket-energy multiplication. For example, a blanket-energy multiplication of 2.5 rather than 1.6 (the lowest possible value) could be achieved by maintaining a slightly higher ($\sim$0.5%) ^{233}U concentration in the salt. Given that such an increase would not severely impact fissile production (i.e., by requiring a larger number of smaller tubes), that blanket safety is not adversely impacted, and that the additional electricity can be sold at its

Table 6-4. Typical reprocessing economics (1982 U.S. dollars).

Economic factors	THOREX	Molten salt
Throughput (tonne/yr)[a]	510	5100
Fissile discharge, assay (at.%)	1.10	0.11
Plant capital cost ($M)	516[b]	61.5[c]
Cost of capital ($M/yr)[d]	93	9.3
Plant operating cost ($M/yr)	38[b]	2.0[c]
Total annual cost ($M/yr)	131	11.3
Reprocessing cost ($/kg heavy metal)	257	2.2
Unit cost ($/g)[e]	23.4	2.0
Av. PV of unit cost ($/g)[f]	15.3	1.2

[a]At 5635 kg/yr of ^{233}U.

[b]Based on 1982 General Atomic Co. assessment of Bechtel design.

[c]Presumed to be conservative on basis of 1981 assessment of Oak Ridge National Laboratory.

[d]Utility ownership.

[e]First year.

[f]PV factor ∿ 0.51 times fixed-charge rate.

equilibrium market value (see above), it then follows that higher blanket multiplication can be economically advantageous.

Specifically, nearly all of the incremental cost of the additional electricity generation would be associated with components other than the expensive fusion driver. If we consider only the incremental costs, the cost of additional electricity generation is, most likely, less expensive than the capital-cost component of the client LWR electricity with which it competes. A decision on the optimal blanket-energy multiplication requires further consideration, but cases for M = 1.6 and M = 2.5 are presented in the next subsection.

In addition to better control of the average ^{233}U concentration to lower levels than possible with the liquid-metal-cooled reference design, the molten-salt breeder also benefits from the lack of a swing in the ^{233}U concentration. That is, in a batch-fueled blanket such as the reference design, the blanket power increases over the fuel-residence time. There are methods to limit the power swing,[6-1] but in all cases a situation arises such that the plant must be sized and costed for an end-of-cycle (EOC) power level that is significantly higher than the average power level. This situation is avoided in molten-salt breeders that are subject to continuous reprocessing.

Another benefit of continuous (as opposed to batch) fuel reprocessing is the potential to achieve a slightly higher plant-capacity factor. In the case of batch reprocessing, periodic shutdowns are required to load and unload fuel. Typically, these operations would occur about three times per year for about one week each but could often be combined with other required maintenance functions (e.g., turbine maintenance, blanket-structure replacement) which occur on an annual or semiannual basis. Nevertheless, a molten-salt breeder with continuous fuel reprocessing would have a modest ($\sim$2 to 4%) advantage in this respect.

It is important to note that design features other than the use of molten-salt reprocessing also impact the performance and cost differences between the molten-salt and reference fusion breeder designs. One such design feature, the use of a helium rather than lithium coolant eliminates the cost of an intermediate heat-transfer loop and is expected to result in a lower overall capital cost. Because the molten-salt blanket also operates at a higher neutron wall

loading (2 vs 1.3 MW/m^2), the first-wall radius decreases and the blanket/magnet/shield costs decrease. This is partly compensated for by the thicker blanket and larger beryllium inventory in the molten salt blanket. The longer expected life of beryllium in the molten-salt design is expected to lower beryllium recycle costs.

6.3.2. FUSION BREEDER PERFORMANCE AND COST COMPARISON

The performance and cost of tandem mirror fusion breeders with the following three blanket types were estimated using the Tandem Reactor Systems Code (TMRSC) developed by TRW[6-4]: the reference lithium-cooled blanket, an M = 1.6 molten-salt blanket, and an M = 2.5 molten-salt blanket. The results are shown in Tables 6-5 and 6-6.

As shown in Table 6-5, despite having the same fusion power, the three breeder options differ widely in net electrical-power outputs. These can be attributed to the molten-salt blanket fuel-management features discussed in the previous section. Note also that the helium-coolant loop pump-power requirement imposes an extra burden on the two molten-salt blankets. Nevertheless, the M = 2.5 molten-salt breeder has the highest electricity production, 17% higher than the reference breeder and 55% higher than the M = 1.6 molten-salt breeder.

The net fissile production of the three breeders is similar, but slightly higher for the molten-salt breeders. For the M = 2.5 molten-salt breeder, it is assumed that higher blanket energy multiplication does not adversely impact breeding. This assumption is in general agreement with previous design work and analysis.[6-1]

The fissile inventories for the molten-salt breeders are substantially lower than for the reference breeder. This occurs for two reasons. First, the average in-core fissile enrichment is lower because of fissile recovery at a much lower concentration (i.e., 0.11% vs 1.1%). Second, the ex-core inventory is lower because the batch practice of holding the entire discharge product (i.e., ^{233}U + ^{233}Pa) for ~6 months to allow for ^{233}Pa decay to ^{233}U ($T^{1/2}$ = 27d) prior to reprocessing is avoided.

As shown in Table 6-6, the reference lithium-blanket breeder is the most expensive. Comparing the reference breeder with the M = 2.5 molten-salt

Table 6-5. Fusion breeder performance comparison.

Parameter	Blanket Type		
	Lithium (reference)	Molten Salt (M = 1.6)	Molten Salt (M = 2.5)
Fusion power (MW)	3000	3000	3000
Blanket energy multiplication			
Minimum	1.25	--	--
Maximum	2.50	--	--
Average	1.88	1.6	2.5
Gross nuclear power (MW)[a]	5100	4440	6600
Gross electric power (MW)[a,b]	2226	1895	2710
Driver recirculating power (MW)	325	325	325
Additional recirculating power (MW)	180	280	380
Net electric power (MW)[a]	1720	1290	2005
Net fissile production (kg/yr)[c]	5635	5810	5810
Fissile inventory (kg)[c]	3995	775	825
In-core[a]	1180	105	155
Post discharge[d]	2815	670	670
Plant capacity factor[a]	70.0	72.2	72.2

[a]Average over cycle.

[b]Includes direct conversion.

[c]Includes average plant-capacity factor.

[d]Assumed to be a half-year's average production for the liquid-lithium blanket and 1/12 year's full-power production for the molten-salt blanket.

Table 6-6. Fusion breeder cost comparison (1982 U.S. $M).

Facilities and equipment	Blanket Type		
	Lithium (reference) ($M)	Molten Salt (M = 1.6) ($M)	Molten Salt (M = 2.5) ($M)
Land and land rights	$ 6	$ 6	$ 6
Structures and site facilities	536	422	461
Fusion driver components[a]	822	679	805
First wall/blanket shield[b]	475	400	558
Heat transport components[c]	478	250	356
Misc. reactor equipment	285	285	285
Turbine plant equipment	352	258	350
Electrical plant equipment	150	223	295
Misc. plant equipment	18	11	18
Fuel cycle facilities	364	46	46
Total direct cost	3486	2580	3180
Contingency	697	516	636
Indirect cost	1414	1046	1290
Total plant cost	6577	4867	6000

[a]Includes magnets, heating systems, and direct convertor.

[b]Includes beryllium, lithium, and molten salt.

[c]Includes circulators for molten-salt helium loops.

[d]Includes reprocessing, beryllium fabrication, and thorium fabrication.

breeder (same thermal power rating), the largest cost differences occur in the following:

	Reference breeder
• Structures and site facilities	75 $M more
• First wall/blanket/shield	83 $M less
• Heat-transport components	122 $M more
• Electrical-plant equipment	145 $M less
• Fuel-cycle facilities	318 $M more

The larger structures and site facilities and heat-transport component costs can be attributed to differences between the lithium and helium coolants (e.g., the expensive intermediate loop for lithium). The savings in the blanket/shield cost can be attributed to a lower requirement for expensive beryllium in the lithium blanket. The savings in the electrical plant equipment cost can be attributed to the cost of the molten-salt breeder electrical bulks (which is conservatively taken to be directly proportional to the recirculating electrical power). Finally, the large fuel-cycle-facility cost for the lithium-blanket breeder reflects the cost of dedicated THOREX and thorium-metal recycle plants.

6.3.3. ECONOMICS OF SYMBIOTIC ELECTRICITY-GENERATION SYSTEMS

We merged the performance and cost results (presented in the previous section) with similar data for LWRs and their fuel cycles to predict the symbiotic cost of electricity and the cost of bred fuel on a year-by-year and on a 30-year average present-value basis. The economics methodology used in the analysis is described in Ref. 6-1.

Table 6-7 shows the results of this analysis for the reference lithium-blanket fusion breeder in symbiosis with ^{233}U-burning LWRs operating on a denatured thorium-fuel cycle.[6-1] The breeder cost per unit thermal power is about 2.8 times that of the LWR. However, the effective capital cost of the breeder decreases to 1.6 times the LWR cost when adjustments for government ownership of the breeder are made. As shown, this difference has only a minor effect on the cost of electricity. Because most of the electricity ($\sim$ 95%)

is generated in LWRs that dominate the symbiotic system, the symbiotic cost of electricity is always quite insensitive to perturbations of the breeder cost and/or performance.

Nevertheless, slight changes in the cost of electricity represent large changes in the cost of bred fuel. This can be easily understood if one notes that at the current price of U_3O_8 (~$55/kg), the cost of mined uranium is typically only about 3% of the overall cost of LWR electricity. Thus, an electricity cost increase of 6% would about triple the allowed cost of U_3O_8. Table 6-7 indicates a similar result -- a 12% electricity-cost differential represents a 130% ^{233}U-cost differential.

Table 6-7. Comparison of utility ownership and government ownership for the lithium/beryllium reference fusion breeder.

Cost data	Utility owned	Government owned
Total plant capital cost ($M)	6580	6580
Breeder/LWR cost ratio[a]	2.76	2.76
Total fixed-charge rate on capital for breeder plant ($/yr)	15.05	9.05
Effective Breeder/LWR capital cost ratio	2.76	1.60
Year-one cost of elec. (mil/$kW_e \cdot h$)	54.1	48.5
Avg. PV[b] cost of elec. (mil/$kW_e \cdot h$)	33.0	30.2
Year-one cost of ^{233}U ($/g)	109	46.9
Avg. PV cost of ^{233}U ($/g)	61.6	30.0

[a] LWR cost = $467/$kW_t$ (1982).

[b] PV = Present value.

In Table 6-8, we compare the results of the previous table with those for the U_3O_8-fueled LWR of Section 6.2. In comparison with the conventionally fueled LWR, the symbiotic system produces electricity more expensively during the first year of operation.

If the fusion breeder is utility owned, its cost of electricity does not become equal to that of the conventional LWR until the twenty-fourth year of operation, the 30-year average present value of the cost of electricity is higher than that of the conventional LWR by 2.0 mil/kW_e•h, and a 30-year cumulative loss of 8.5 billion dollars results. Although this case does not indicate market penetration under the assumed conditions (i.e., $55/kg of U_3O_8 at the start of operation), further studies indicate a thirty-year breakeven (i.e., zero benefit) if the starting price of U_3O_8 is $110/kg, or about twice the current price. Higher U_3O_8 costs would lead to a net benefit for the fusion breeder.

In the case of government ownership, a year eight breakeven is achieved and an average 0.8 mil/kW_e•h benefit accrues over the entire fusion-breeder operating life. This results in an integrated benefit of $3.5 billion over a 30-year period.

Table 6-9 shows results for symbiotic electricity-generation systems that utilize M = 1.6 molten-salt breeders. Compared with the reference system, the molten-salt breeder results show marginal electricity cost advantages but a substantial reduction in the cost of fissile material. Although utility ownership is more attractive in this case, there is a substantial benefit for government ownership.

Results are summarized in Table 6-10. If the molten-salt breeder is government owned (Case 3), the electricity cost breakeven occurs during the first year of operation and an $8 billion benefit per fusion breeder accrues over its 30-year operation. If the molten-salt breeder is utility owned (Case 4), breakeven occurs in the fourteenth year and the integrated benefit is only $200 million.

The Case 5 results indicate that a 20% increase in predicted fissile breeding gives an ∿50% increase in the integrated benefit. The Case 6 results indicate that a 20% decrease in the predicted fissile breeding gives an ∿ 20% decrease in the integrated benefit. The latter result indicates that the beryllium multiplier might be replaced with a less exotic option (e.g., lithium or lead) without proaucing an intolerable economic impact.

Table 6-8. Comparison of cost data for a symbiotic system, including a liquid-lithium blanket fusion breeder, and a U_3O_8-fueled LWR.

Cost data	Utility owned (Case 2)	Government owned (Case 1)
Delta year-one cost of elec. (mil/$kW_e \cdot h$)[a]	6.8	1.2
Breakeven year[b]	24	8
Delta avg. PV cost of elec. (mil/$kW_e \cdot h$)[a]	2.0	-0.8
Integrated benefit ($M)[c]	-8500	3500

[a]Delta = Symbiotic system minus conventional system.

[b]Year in which Delta = 0.

[c]Pv Present-value (PV) benefit per fusion breeder over 30 years.

Table 6-9. Molten-salt fusion-breeder cost data.

Cost data	Utility owned (Case 4)	Government owned (Case 3)
Total plant capital cost ($M)	4867	4867
Breeder/LWR cost ratio	2.35	2.35
Total fixed-charge rate (%/yr)	15.05	9.05
Effective breeder/LWR cost ratio	2.35	1.41
Year-one cost of elec. (mil/$kW_e \cdot h$)	50.8	46.9
Avg. PV cost of elec. (mil/$kW_e \cdot h$)	31.0	28.9
Year-one cost of ^{233}U ($/g)	72.5	29.2
Avg. PV cost of ^{233}U ($/g)	38.6	15.6

Table 6-10. Comparison of data for lithium-blanket or molten-salt reactor type and ownership.

Case	Govt./Util. owned	Reactor type[a]	Breakeven year	Present Value		Benefit $B
				Elec.	Fuel	
1	Govt.	Lithium	8	30.2	30.0	3.5
2	Util.	Lithium	24	33.0	61.6	-8.5
3	Govt.	MS/1.6	1	28.9	15.6	8.0
4	Util.	MS/1.6	14	31.0	38.6	0.2
5	Govt.	MS/1.6/F + 20%	1	28.7	13.5	11.8
6	Govt.	MS/1.6/F - 20%	1	29.15	18.5	6.5
7	Govt.	MS/2.5	1	28.2	7.8	12.5

[a]MS = molten salt; M = labor 2.5; F = fissile breeding ratio.

Finally, Case 7 shows the potential advantage for an M = 2.5 molten-salt blanket. With government ownership, the high-power molten-salt breeder achieves the highest potential benefit of the cases considered. A comparison of Cases 5 and 7 indicates that the economic value of 50% higher blanket-energy multiplication is roughly equivalent to the economic value of an ~20% higher fissile-fuel production. Because the energy multiplication of molten-salt blankets is easily adjusted in this range (see Section 6.2 discussion), the above trade could be quite valuable in defining the optimal system.

6.4. CONCLUSIONS

We conclude the following from the described modeling of the potential economic performance of fusion breeders:

- As an advanced enrichment facility, the reference Li/Be fusion breeder with government ownership could be economical at today's price of U_3O_8.
- In the above case and with utility ownership, U_3O_8 must initially cost $110/kg for a 30-year breakeven.
- The molten-salt fusion breeder could be economical at today's price of uranium regardless of ownership.
- With government ownership, the molten-salt fusion breeder could break even in year one and produce a multibillion dollar benefit over its operating lifetime.
- Bigger benefits accrue for the molten-salt fusion breeder operation at higher breeding and/or higher blanket-energy multiplication.
- A 20% breeding decrease is clearly tolerable
- Some issues yet to be addressed include the potential impacts of lower LWR separative work unit costs, higher LWR fuel-reprocessing costs, and the like.

REFERENCES SECTION 6.0.

6-1. D. H. Berwald et al., Fission Suppressed Hybrid Reactor - The Fusion Breeder, Lawrence Livermore National Laboratory, UCID-19638 (1982).

6-2. U.S. Department of Energy, Non-Proliferation Alternative Systems Assessment Program, DOE/NE-0001 (1980).

6-3. J. D. Lee, et al., Feasibility Study of a Fission-Suppressed Tandem Mirror Hybrid Reactor, Lawrence Livermore National Laboratory, UCID-19327 (1982).

6-4. R. H. Whitley, Tandem Mirror Reactor Systems Code Manual, contact author at TRW, 1 Space Park, Redondo Beach, CA.

7.0. TECHNICAL ISSUES

7.1. TRITIUM MANAGEMENT

Permeation barrier development and demonstration is the critical R & D need. Tritium will need to be removed from both molten salt and helium loops. Recovering tritium from molten salt is yet to be domonstrated but should be manageable since the partial pressure is high. Process technology is known for recovering tritium from helium, although a large increase in scale will be required. The key is to have good permeation barriers both on salt tubes and steam-generator tubes, thus easing requirements for both salt and for helium process systems. Single-pass process efficiencies can be moderate, and only a small fraction of the circulating helium must be processed. Failure to develop effective barriers shifts the burden of processing tritium into the steam/water system. Isotopic processing of tritiated water then becomes a high priority R & D requirement. Isotope separation will be more difficult and costly, and the steam system must be kept leak-free to avoid personnel hazards from tritiated water vapor. A successful barrier development effort could avoid both the need for water processing and the hazards that accompany tritiated water systems.

7.2. BERYLLIUM FEASIBILITY

Beryllium-beryllium self-welding and beryllium-steel welding at the contact points are issues needing experimental investigation. This is the objective of a planned set of capsule tests at ORNL. The ability of the beryllium balls to stand up under neutron radiation is maximized by design (their small size); however, irradiation data are needed. Some of this can be done in fission reactors; for example, the tests carried out in EBR-II and the planned neutron radiation induced-creep tests.

7.3. MATERIAL COMPATIBILITY

We predict the steel (type 316) will have a long lifetime in contact with the salt, if it is kept in a reducing state. Corrosion tests with molten salt in a flowing loop would prove the predicted compatibility. Irradiation tests in a fission reactor should be carried out to verify the chemical compatibility of salt and steel.

7.4. REPROCESSING

Removal of uranium by fluorination is fairly well understood but needs demonstrating at a reasonable scale. From a neutron economy point of view, removal of fission products is known to be unnecessary. From a safety point of view, removal of fission products would be desirable but only partially effective. Removal would entail salt/metal pyrochemical reduction processing to be scaled up from small batch tests to larger continuous processing and would require developing refractory metal piping. We do not believe this is necessary. Therefore, development and demonstration of a continuous fluorinator is the only important reprocessing R & D need.

7.5. NEUTRON ECONOMY

The breeding performance of the molten-salt design is very sensitive to parasitic absorption in structural material (principally iron). This is due to the low concentration of thorium in the salt (only 7% of the salt atoms are thorium). The neutronic calculations in this report include pipe walls but do not include other needed structural material; however, too much first-wall material was used which might provide sufficient compensation. We must make better calculations of the nuclear performance and emphasize designs that minimize structure material. Alternatives to steel should be considered. Finally, experimental verification of tritium and fissile breeding should be carried out with a point 14-MeV neutron source.

4358t & 4359t/0020t,
4360t/0021t
DB/RP

U. S. Government Printing Office: 1985/5-587-002/24074